

Single cell plasticity and population coding stability in thalamic circuits upon associative learning

Inauguraldissertation

zur

Erlangung der Würde eines Doktors

der Philosophie vorgelegt der

Philosophisch-Naturwissenschaftlichen Fakultät

der Universität Basel

von

James Alexander Taylor

2022

Originaldokument gespeichert auf dem Dokumentenserver der Universität Basel

edoc.unibas.ch

Genehmigt von der Philosophisch-Naturwissenschaftlichen Fakultät

auf Antrag von

Jan Gründemann

Rainer W. Friedrich

Daniel Huber

Basel, 14/12/2021

Prof. Dr. Marcel Mayor

Table of Contents

Acknowledgments.....	iv
List of figures.....	v
List of abbreviations	vii

Abstract.....	1
----------------------	----------

Chapter 1. Introduction

1.1. Background.....	2
1.1.1. Associative learning.....	2
1.1.2. Fear conditioning	3
1.1.3. The auditory thalamus	5
1.1.4. Sensory coding in auditory thalamus	6
1.2. Aims and outlines of the thesis.....	8
1.3. Disclosures	8

Chapter 2. The multisensory medial geniculate body, an ideal candidate for sensory plasticity

2.1. Introduction	9
2.2. Miniscope imaging in freely moving animals	9
2.3. Individual cells respond to tones and footshocks.....	11
2.3.1. Response to CS and US.....	11
2.3.2. US response not solely due to movement.....	12
2.3.3. US response not solely due to self-generated sounds	13
2.4. Spatially intermingled unisensory and multisensory cells.	15
2.5. Discussion	15

Chapter 3. The medial geniculate body: a center for associative learning

3.1. Introduction	17
3.2. Fear conditioning paradigm.....	17
3.3. MGB is necessary for fear learning	18
3.4. Intraday US plasticity	20
3.5. Interday CS plasticity	20
3.7. Plasticity in MGB's different subdivisions	24
3.8. Association of CS-US is necessary for MGB plasticity	25
3.9. Discussion	26

Chapter 4. Medial geniculate body neurons encode fear learning

4.1. Introduction	28
4.2. Neuronal responses in a high fear state	28
4.3. Neuronal responses across the fear conditioning paradigm	29
4.4. Ramp-Up cells are correlated with freezing	31
4.5. Discussion	33

Chapter 5. The medial geniculate body's inputs and their role in auditory fear conditioning

5.1. Introduction	35
5.2. Cholinergic inputs to MGB modulate behavior	35
5.3. Cortical feedback is not driving the plasticity in MGB	38
5.4. Discussion	41

Chapter 6. Medial geniculate body projections to amygdala not an enriched line

6.1. Introduction	43
6.2. Anatomical distribution of MGB→BLA neurons	43
6.3. MGB→BLA plastic but not enriched.	45
6.4. Ramp-Up cells in MGB→BLA neurons	47
6.5. Discussion	48

Chapter 7. Medial geniculate body projections to amygdala are necessary for learning and for neuronal stability

7.1. Introduction	50
7.2. MGB→BLA neurons are necessary for associative learning	50
7.3. Manipulation of MGB→BLA neurons leads to changes in US adaptation	51
7.4. Manipulation of MGB→BLA neurons leads to aberrant plasticity in MGB	53
7.5. Manipulation of MGB→BLA neurons does not alter the CS+ encoding	55
7.6. Discussion	56

Chapter 8. A plastic medial geniculate body which allows for stable representation of the sensory environment

8.1. Introduction	58
8.2. Decoding of MGB population dynamics	58
8.3. Population vector distance	59
8.3.1 Transient plasticity in MGB and MGB→BLA neurons	59
8.3.2 Inhibition of cortical feedback does not affect population plasticity	62
8.3.3 Inhibition of MGB→BLA neurons reduces the transient plasticity	62
8.4. Discussion	63

Chapter 9. General discussion	65
--	-----------

Chapter 10. Methods

10.1. Animal subjects	70
10.2. Surgical procedures	70
10.3. Behavioral paradigms and analysis	71
10.4. Miniature microscope imaging	72
10.5. Image analysis	73
10.6. Ca ²⁺ data analysis	73
10.7. Sound recordings and analysis	75
10.8. Histology	75
10.9. Statistical analysis	76

References	77
-------------------------	-----------

Appendix 1: Taylor J.A., Hasegawa M., Benoit C.M. Amorim Freire J., Theodore M., Ganea D.A., Innocenti S.M., Lu T., Gründemann J.. Single cell plasticity and population coding stability in auditory thalamus upon associative learning. *Nat Commun* 12, 2438 (2021).

Acknowledgments

I want to thank Jan Gründemann for giving me the opportunity to join such a fun, dynamic lab and work on an exciting project with his full support. I feel very fortunate to have been able to perform scientific research under such a great supervisor who has helped me grow not only as a scientist but also as a person. It has really been a pleasure.

I would like to also thank all of the lab members past and present who have helped with experiments, analysis and lively scientific discussion. Thank you Lynda Demmou, Joana Amorim Freire, Masashi Hasegawa, Chloé Maëlle Benoit, Dan Alin Ganea, Marine Theodore, Sabrina Milena Innocenti, Julia Esser, Ziyang Huang and Benay Baskurt.

I want to thank all of the colleagues across the University of Basel with whom I have had the pleasure to interact. Their friendship, advice and general help made my life so much easier and my PhD a lot of fun.

I want to acknowledge past supervisors Steven Clapcote, Francesca Bernardini, Josef Kittler and James Drew for their help in setting me up for a PhD.

I would also like to thank my family for their support not only throughout the PhD but also throughout my life. Emma, Ben and Bex thank you for being great siblings on whom I can always rely on. Mum and Dad, thank you for supporting me throughout my education (and life) and for encouraging me to always be curious, inquisitive and to keep an open mind. Your education and support have allowed me to succeed in life.

Finally, I would like to thank my wonderful wife Marion. Thank you for being an inspiration for hard work and always pushing me to be better. Thank you for your support throughout the years, without you I would not be where I am now. Thank you for listening to me ramble on about MGB when you are preoccupied with treating the whole human body. You are my rock and my inspiration.

« Le fruit du travail est le plus doux des plaisirs. » Luc de Clapiers

James

List of figures

Figure 1: Imaging neuronal activity of auditory thalamus in freely moving mice.

Figure 2: Imaging of excitatory cells in MGB

Figure 3: Mixed selectivity tone CS+ and shock US coding of MGB neurons upon fear conditioning.

Figure 4: Correlation of neuronal activity and mouse movement.

Figure 5: Ca^{2+} activity of MGB neurons is weakly correlated with self-evoked sounds during the US.

Figure 6: Spatial distribution of unisensory and multisensory MGB neurons.

Figure 7: Fear conditioning paradigm and behavioral response.

Figure 8: Optogenetic inhibition of MGB neurons suppresses consolidation of fear learning.

Figure 9: Single cell US plasticity.

Figure 10: Single cell CS plasticity.

Figure 11: US response type is not predictive of CS plasticity.

Figure 12: Similar CS and US plasticity types between MGB subdivisions.

Figure 13: CS+ responses are mostly stable across days upon unpaired conditioning.

Figure 14: Multitude of neuronal responses to the CS+ when in a high fear state.

Figure 15: CS+ responses are dynamic across the fear conditioning paradigm.

Figure 16: Proportion of Ramp-up cells changes throughout the fear conditioning paradigm.

Figure 17: Ramp-up cells are correlated with freezing behavior.

Figure 18: Ramp-up cells are correlated with US response.

Figure 19: Optogenetic manipulation of cholinergic PPT fibers in MGB during fear conditioning.

Figure 20: Inhibition of cholinergic PPT fibers in MGB during fear conditioning leads to a high fear state.

Figure 21: Inhibition of cortical feedback during auditory fear conditioning.

Figure 22: Inhibition of cortical feedback does not alter behavior nor tone responses.

Figure 23: Inhibition of cortical feedback does not influence plasticity in MGB.

Figure 24: Inhibition of cortical feedback does not alter the CS+ encoding.

Figure 25: Anatomical distribution of amygdala projecting neurons in MGB.

Figure 26: MGB→BLA neurons send collaterals to auditory cortex.

Figure 27: MGB→BLA responses to CS and US stimuli.

Figure 28: Plasticity of MGB→BLA neurons.

Figure 29: MGB→BLA neurons show similar CS+ encoding to total MGB population.

Figure 30: Optogenetic manipulation of MGB→BLA neurons.

Figure 31: All-optical activity recording of MGB and manipulation of MGB→BLA neurons.

Figure 32: Manipulation of MGB→BLA neurons leads to changes in US adaptation.

Figure 33: Manipulation of MGB→BLA neurons causes aberrant plasticity in MGB.

Figure 34: MGB CS+ encoding is stable despite manipulations of MGB→BLA neurons.

Figure 35: MGB population dynamics can be stably decoded across days.

Figure 36: MGB population vector distance is stable across days.

Figure 37: CS+ to CS+ and CS- to CS- population vector distances.

Figure 38: Correlation of relative change in PVD with fear learning.

Figure 39: Inhibition of cortical feedback does not affect MGB PVD between CS and US.

Figure 40: MGB population vector distances during manipulation of MGB→BLA neurons.

List of abbreviations

ACtx – Auditory cortex	MGB→BLA – MGB neurons that project to the basolateral amygdala
BLA – Basolateral amygdala	
Ca ²⁺ – Calcium	MGBd – Dorsal subdivision of the medial geniculate body
ChAT– Choline acetyltransferase	MGBm – Medial subdivision of the medial geniculate body
CNO – clozapine-N-oxide	MGBv – Ventral subdivision of the medial geniculate body
CS – Conditioned stimulus	NT – Neutral Tone
DREADD – Designer Receptors Exclusively Activated by Designer Drugs	PFC – Prefrontal cortex
Ext. – Extinction	PIL - Posterior intralaminar thalamic nucleus
FC – Fear conditioning	PPT – Pedunculo pontine tegmental nucleus
GABA – <i>gamma</i> -Aminobutyric acid	PTSD – Post traumatic stress disorder
GCaMP – Genetically encoded calcium indicator	PVD – Population vector distance
GFP – Green fluorescent protein	ROI – Region of interest
GRIN – Gradient index	S.E.M. – Standard error of the mean
Hab – Habituation	tdTom – tdTomato
IC – Inferior colliculus	TRN – Thalamic reticular nucleus
LFH – Low frequency harmonic vocalizations	US – Unconditioned stimulus
MGB – Medial geniculate body	zS – zScore

Abstract

Cortical and limbic brain areas are regarded as centers for learning. However, how thalamic sensory relays participate in plasticity upon associative learning, yet support stable long-term sensory coding remains unknown. Using a miniature microscope imaging approach, we monitor the activity of populations of auditory thalamus (medial geniculate body) neurons in freely moving mice upon fear conditioning. We find that single cells exhibit mixed selectivity and heterogeneous plasticity patterns to auditory and aversive stimuli upon learning that is independent from cortical feedback. We identified neurons in medial geniculate body that encode for the upcoming behavior of the animal. Cholinergic inputs to the medial geniculate body modulate the associative learning. The plasticity and neuronal responses to the different stimuli are conserved in amygdala-projecting medial geniculate body neurons but there is no enhanced plasticity in these cells. Activity in auditory thalamus to amygdala-projecting neurons stabilizes single cell plasticity in the total medial geniculate body population and is necessary for fear memory consolidation. In contrast to individual cells, population level encoding of auditory stimuli remained stable across days. Our data identifies auditory thalamus as a site for complex neuronal plasticity in fear learning upstream of the amygdala that is in an ideal position to drive plasticity in cortical and limbic brain areas. These findings suggest that medial geniculate body's role goes beyond a sole relay function by balancing experience-dependent, diverse single cell plasticity with consistent ensemble level representations of the sensory environment to support stable auditory perception with minimal affective bias.

Chapter 1. Introduction

1.1. Background

1.1.1. Associative learning

Emotion can be defined as the unconscious evaluation of a situation as potentially beneficial or harmful. These emotions lead to responses as we adapt to the situation, these responses can be innate (fear of the dark) but can also be learnt (for example, not touching a hot plate). The ability to learn from past experiences is essential, not only for humans but for all animals. It allows animals to escape from predators or to know where to find food. An animal's ability to learn gives it the best chance of survival as it can adapt to changing circumstances. When the ability to learn is impaired individuals have greater life challenges. In 1992, the psychologist David Shanks described a patient, named Greg, who had a benign brain tumor removed^{1,2}. This left him amnesic, he could only remember events from his early life but could not remember experiences from later on in life and was unable to learn anything new. In 1976, Greg believed that Lyndon Johnson was still president of the United States of America (he was president from 1963 to 1969 and died in 1973). He was also unable to remember his father's death. On each occasion Greg was confronted by the information of his father's death, he was overwhelmed with grief, negatively impacting his long-term mental well-being and quality of life^{1,2}.

One of the most basic forms of learning is associative learning, whereby a new response becomes associated with a particular stimulus. For example, seeing a hot oven and not touching it or smelling the delicious aroma of cooking food and then eating it. In its broad sense associative learning can be used to describe any form of learning outside of habituation, however in its more restrictive definition it is learning that occurs through conditioning.

Conditioning is a form of learning whereby a stimulus becomes more effective in evoking a response. The most famous example comes from the Russian psychologist Pavlov³⁻⁵. In his famous experiment, when a dog was presented with food, it started to salivate. The food led to an unconditioned, innate, response: salivation. Therefore the food is termed unconditioned stimulus (US). When Pavlov then rang a bell before presenting the food, it conditioned the dog to expect food after hearing a bell ring. The ringing of the bell was a conditioned stimulus (CS) because by the end of the learning, the dog salivated upon hearing the bell.

This basic form of learning has been used in neuroscience to understand how the brain computes memory formation and retrieval. Understanding the circuitry involved in associative

learning is essential for understanding what happens in disorders where memory is hijacked into a high fear state such as post-traumatic stress disorder (PTSD) where noises, sounds, places are associated with traumatic experiences⁶. It also enables a better understanding of what happens when disorders prevent proper learning and understanding of the world around such as in schizophrenia or autism^{7,8}.

One of the most common paradigms used to study classical pavlovian conditioning is an auditory fear conditioning paradigm. In these experiments, instead of food, which made Pavlov's dog salivate, a tone CS is paired with a mild foot shock US. In the pre-conditioning state, the animal shows no fear response and in the post conditioning state, it develops a fear response in the shape of freezing, which is characterized by a complete absence of movement and is easy to track.

1.1.2. Fear conditioning

Classical fear conditioning has been widely used to understand the brain processes involved in associative learning. Using this paradigm has allowed us to understand that the amygdala, a highly connected brain region in the temporal lobe which receives inputs from the auditory cortex, auditory thalamus and many other brain regions such as the prefrontal cortex and the hippocampus^{9–12}, plays an essential role in fear conditioning. Indeed, inactivation of the amygdala through pharmacological or lesioning studies prevents the acquisition or retrieval of the fear memory underlining that neural activity in the amygdala is necessary for associative fear learning^{13–15}. It has also been shown that individual neurons in amygdala receive converging auditory CS and somatosensory US information therefore placing it in an ideal position for Hebbian learning¹⁶. Furthermore, it has been demonstrated that auditory CS neural responses in the amygdala are enhanced when the CS is paired with the US demonstrating that pairing the CS and US leads to the strengthening of the auditory inputs to the amygdala^{17,18}. With this evidence placing the amygdala at the center for associative learning, its role and circuitry has been further explored.

Findings of this amygdala research suggest that there are distinct populations of cells within amygdala which enable mice to switch between different fear states¹⁹. The micro-circuitry of the amygdala is shown to be deciphered with inhibitory interneurons controlling the fear learning through disinhibition²⁰. Different subtypes of interneurons such as somatostatin, vasoactive intestinal peptide and parvalbumin expressing interneurons have been demonstrated to play distinct roles within the amygdala microcircuit^{20,21}. It has also been shown that not only individual cells of the amygdala code for the fear learning, but that it also occurs

at the population level. Moreover, the strength of the ensemble-encoded CS-US association was shown to predict the level of behavioral conditioning in each mouse²².

Whilst the research in auditory fear conditioning has concentrated on the amygdala, it has become increasingly apparent that the amygdala is not the only brain area to play a crucial role in fear learning²³. The auditory cortex is heavily involved in the processing of sounds and has been shown to play a role in auditory fear conditioning. Auditory cortex lesions or inactivation reduce fear learning when complex sounds are used^{24–26}. Interestingly lesions of auditory cortex do not affect fear learning when the CS+ is a pure tone²⁷. In a similar way to the amygdala, a disinhibitory microcircuit controls fear learning in auditory cortex. Briefly, it was shown that layer 1 interneurons are activated by basal forebrain cholinergic inputs during the US foot shock. Layer 1 then inhibited layer 2/3 parvalbumin expressing interneurons. This led to disinhibition of layer 2/3 pyramidal neurons and an enhanced response to the complex auditory CSs²⁶.

The amygdala is known to project to the prefrontal cortex (PFC) and as such the PFC has also been well studied within the context of fear conditioning. It has been shown that inactivation of the PFC lead to reduced expression of the conditioned fear in response to an auditory stimulus. This inactivation did not have an effect on innate fear response nor on plasticity in amygdala²⁸. The PFC was activated by the conditioned stimulus but unlike the amygdala, the responses lasted several seconds mirroring the freezing output²⁸. This suggested that activity in the PFC mediates the behavioral responses during fear conditioning. This extended on the known role of the PFC in mediating the extinction of fear²⁹. Using single-unit recordings and optogenetic manipulations in behaving mice it was possible to understand how the precise temporal control of fear behavior is achieved at the level of prefrontal circuits. It was shown that inhibition of parvalbumin expressing interneurons activity disinhibited prefrontal amygdala projecting neurons and synchronized their firing which leads to fear expression³⁰.

Another cortical brain area which has been shown to be involved with associative fear learning is the insular cortex. Lesions to this brain area attenuate the fear conditioning when the US is associated with an auditory stimuli. However, fear conditioning was unaffected by the lesions when the US was associated with the context³¹. Similar results were found with pharmacological and optogenetic inhibition of insular cortex^{32,33}.

This evidence has enabled a comprehensive overview of the fear circuit and whilst the amygdala has been considered to be the center for associative learning, it is evident that many brain areas are involved in fear learning and therefore, it can be strongly argued that there is a distributed circuit for fear learning^{23,34,35}.

One of the brain areas historically considered heavily involved in fear learning but not yet discussed here is the auditory thalamus, also known as medial geniculate body (MGB). As the primary thalamus for the auditory system it is often regarded as just a sensory relay, however it has been argued that MGB is the center of fear learning and not the amygdala³⁶. We will next discuss the auditory thalamus and its role in fear conditioning.

1.1.3. The auditory thalamus

Hearing, one of the five main senses, is the perception of sound. This involves the detection of waves of pressure which leads to activation of central auditory pathways. These central auditory pathways start with the cochlear nuclei which project to the superior olivary nuclei and then to the inferior colliculi (IC) of the midbrain. Neurons in the IC project to the auditory thalamus which is the primary sensory input to auditory cortex (ACtx). The auditory thalamus therefore plays a critical role in auditory processing.

MGB is located in the dorsal thalamus and has three main subdivisions, dorsal (MGBd), ventral (MGBv), and medial (MGBm)³⁷. MGBv is considered to be the first order subdivision, receiving tonotopic inputs from the central nucleus of the IC and projecting to the primary auditory cortical areas^{38–40}. MGBv is tonotopically organized⁴¹ and receives modulatory feedback from layer 6 of the auditory cortex^{40,42}. The dorsal division (MGBd) receives inputs from the dorsal nucleus of the IC and sends outputs primarily to secondary auditory areas^{40,43}. The medial division (MGBm) receives inputs from the lateral IC and sends inputs to all areas of auditory cortex and also to the basolateral amygdala (BLA) and the dorsal striatum^{44–47}. MGBd and MGBm are considered to be the higher order nuclei of MGB. These higher order neurons are calretinin positive^{48,49}, however it is harder to distinguish between MGBm and MGBd using cell markers.

MGB not only receives input from the IC or cortical feedback but also inhibitory inputs from the thalamic reticular nucleus (TRN). The TRN receiving inputs itself from the amygdala creates a thalamic-amygdala circuit which allows the amygdala to send feedback indirectly to MGB via the TRN as well as the ACtx^{50,51}.

Being a highly connected brain area further suggests that MGB's function could well extend beyond that of a classical sensory relay. Indeed MGB is a site for CS/US multisensory information which makes it an ideal candidate for playing a role in associative learning occurring upstream of amygdala⁵². Early work has suggested that MGB's presynaptic drive to the BLA could act as a plasticity mechanism. A study in cats recorded neuronal activity in MGB whilst presenting a white noise followed by a paw shock. They found that the neuronal response of the paired tone, CS+, was enhanced during conditioning, whilst the control tone,

CS-, did not exhibit any change in neuronal activity⁵³. In another study, it was found that lesioning MGBm fully blocked fear-potentiated startle responses to an auditory cue. This behavioral response was not blocked by lesioning of primary ACTx, revealing that MGB has a role in auditory associative learning rather than solely acting as a relay⁵⁴. More recently, it has been shown that upon auditory fear learning phosphorylated CREB, a marker for neuronal plasticity, is enhanced in the higher order MGB. Over-expression of CREB led to a strengthening of fear memories⁵⁵. Inhibition of RNA-synthesis and protein expression in MGB reduces freezing levels after fear conditioning^{56,57}.

These previous studies strongly suggest that MGB is an essential part of the circuitry involved in auditory fear conditioning and associative learning. Nevertheless, the role of MGB in neuronal response plasticity upon fear learning has been debated^{36,58,59} and recent physiological studies of fear conditioning have mostly omitted this site of sensory integration and response potentiation upstream of the BLA and ACTx. This has meant that currently it is not known if individual MGB neurons exhibit complex response dynamics upon adaptive associative behaviors and how this potential heterogeneity could be balanced with reliable representations of the sensory environment.

We will next discuss how the auditory thalamus codes for the sensory environment as to better understand how MGB can code for the fear conditioning as well as the sensory environment.

1.1.4. Sensory coding in auditory thalamus

An essential function of our brain is accurate perception of the world around us, which enables us to make appropriate decisions based on accurate information. MGB, as the thalamic nucleus for audition, is a critical part in the sensory coding of our auditory environment.

To understand our auditory environment, it is important to be able to discriminate between sound frequencies. As previously discussed, MGBv is tonotopically organized and the neurons have a short response latency with sharp frequency tuning^{60–62}. The higher order areas of MGB (MGBm and MGBd) have been shown to have multi-peaked frequency response areas, meaning that they have a broader tuning range^{60,62,63}. The projection of MGBv to the primary auditory cortex allows precise frequency information to be passed on to cortical brain areas. In a similar way to the auditory cortex, frequency tuning in MGB becomes broader with increasing sound level particularly for frequencies lower than the best frequency^{64,65}.

Notably, MGB neurons show strong onset responses to tones with weaker sustained or offset responses. At the onset of a sound, a large number of neurons are responsive but if the sound

is sustained, only neurons best tuned to the sound stay responsive^{64,66,67}. This allows for MGB neurons to rapidly adjust to a changing auditory sensory environment.

Another key aspect for understanding our sensory environment is being able to localize the sound source. Early studies in cats suggested that approximately 60% of MGB neurons were responsive to stimuli to either ear and therefore that 40% of neurons were responsive only by contralateral ear stimulation⁶⁰. In anesthetized cats it was shown that sound location tuning of MGB neurons was 60° for pure tones and 40° for more complex sounds⁶⁸. As these numbers are significantly smaller than cats' actual ability to localize sounds, it suggests that MGB does not play a key role in sound localization⁶⁹. This hypothesis was strengthened by a study in rats with bilateral lesions of MGB. The study showed that the animals were still able to perform a sound localization task⁷⁰. This suggested brainstem structures were involved with sound localization perhaps via projections to motor structures.

As discussed, MGB codes for the auditory environment, but there is further evidence that this thalamic nucleus also responds to non-auditory cues. Single unit recordings in rats found cells in MGB were responsive to somatosensory stimulation of hindpaws⁵². Similar results were found in cats, with MGB cells showing responses to not only somatosensory stimuli but additionally nociceptive and visual stimuli⁷¹.

Not only does MGB encode for different stimuli but these stimuli also influence how MGB encodes the auditory environment. It has been shown that in auditory fear conditioning, when the tone is associated with the somatosensory stimuli of a mild footshock, there are short-term changes in the best frequency of MGB neurons towards the CS tone frequency^{72,73}. It was also shown that in rats many of the higher order MGB neurons increased their responses when a sound was paired with a light or a reward⁷⁴. These enhanced responses disappeared when the association was no longer present, suggesting that higher order MGB neurons integrate auditory and non-auditory inputs.

In summary, we have shown that the auditory thalamus plays a key role in coding the sensory environment, in particular the auditory environment but also integrating somatosensory and visual inputs. However, the mechanism by which MGB neurons can encode for fear learning without getting hijacked into a fear state and reliably continue to encode the sensory environment is a key question which will be further explored in this thesis.

1.2. Aims and outlines of the thesis

The aim of this thesis is to investigate the fundamental role of the sensory auditory thalamus in the formation of memories and experience-dependent plasticity across fear learning, to understand how large populations of MGB neurons encode fear learning and the role of MGB within the fear circuit. A second aim is to address the associated paradox of how sensory relays can be plastic and yet preserve stable sensory representations.

To answer these questions we start, in chapter 2, by looking at the responses of MGB cells upon tone and footshock presentations.

In chapter 3, we look at how these responses are plastic upon associative learning.

In chapter 4, we look at what is encoded in the MGB neuronal responses.

In chapter 5, we look at some of the inputs to MGB and their role in fear conditioning.

In chapter 6, we look at the responses of the amygdala projectors in MGB upon auditory fear conditioning.

In chapter 7, we look at the role of the MGB→BLA neurons in the fear circuit

Finally, in chapter 8, we answer the paradox of how the sensory relays are plastic yet allow for stable sensory representations by looking at the population coding.

1.3. Disclosures

The experiments described here were carried by me in the lab and under the supervision of Prof. Jan Grundemann. Experimental and analytical help was provided by Dr Lynda Demmou, Dr Masashi Hasegawa, Dr Dan Alin Ganea, Joana Amorim Freire, Chloe Maelle Benoit, Marine Theodore, Sabrina Innocenti.

Part of this work has been published in the following paper:

Taylor J.A., Hasegawa M., Benoit C.M. Amorim Freire J., Theodore M., Ganea D.A., Innocenti S.M., Lu T., Gründemann J.. Single cell plasticity and population coding stability in auditory thalamus upon associative learning. *Nat Commun* **12**, 2438 (2021).

Chapter 2. The multisensory medial geniculate body, an ideal candidate for sensory plasticity

2.1. Introduction

To understand the role of MGB in the formation of memories and experience-dependent plasticity, it is important to understand how large populations of MGB neurons respond to the different stimuli involved in associative learning. Previous papers have shown that single cells respond to the tone CS+ but also to the footshock US⁵². However, due to limitations of the methods, our knowledge is restricted to only a few individual cells. Here, we use a deep brain miniature microscope imaging approach to record the neuronal activity of large populations of MGB neurons across a fear conditioning paradigm allowing us to understand their responses to different stimuli.

2.2. Miniscope imaging in freely moving animals

To record the activity of large populations of MGB neurons, we established a gradient-index (GRIN) lens deep brain miniature microscope imaging approach of identified auditory thalamus neuronal populations in freely behaving mice (**Fig. 1a, b**).

For this, a genetically-encoded Ca^{2+} sensor (**Fig. 1c**, AAV2/5.CaMKII.GCaMP6f) was injected in MGB before a GRIN lens was implanted above relaying the fluorescence of the infected cells⁷⁵. A miniature microscope was placed above the GRIN lens allowing to record these changes in fluorescence which act as a proxy for neuronal activity. Using this method, we tracked large populations of individual MGB neurons across a four-day auditory fear conditioning paradigm in freely moving mice.

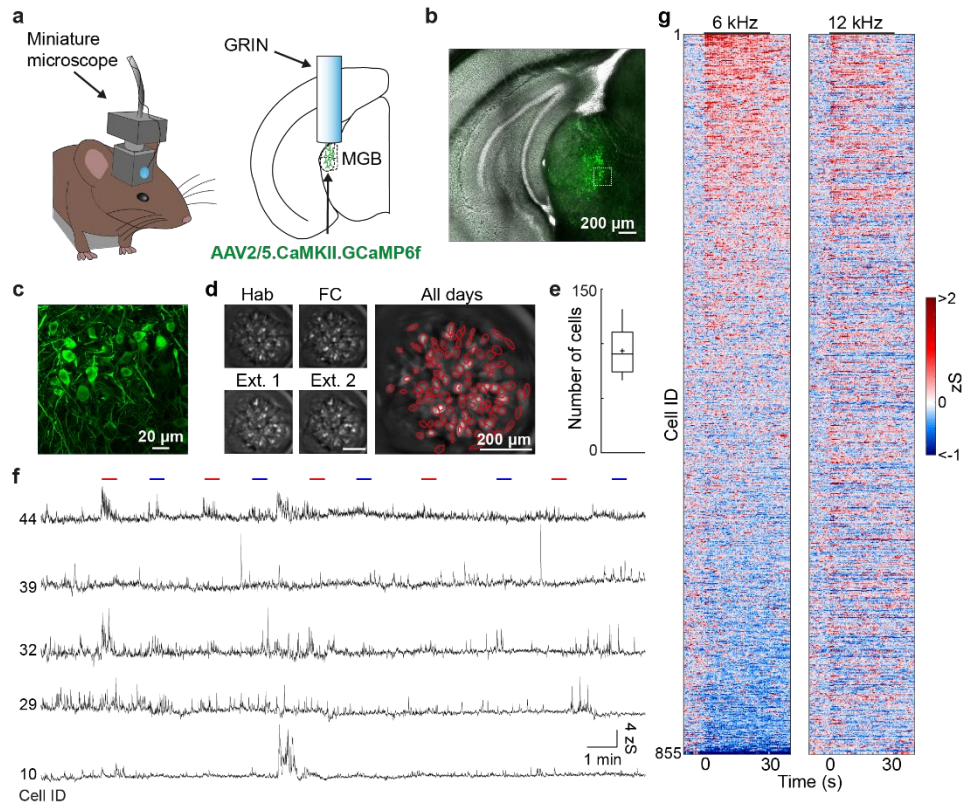


Fig. 1: Imaging neuronal activity of auditory thalamus in freely moving mice.

a. Mouse with a head-mounted miniaturized microscope (left). Location of gradient refractive index (GRIN) lens in the medial geniculate body (MGB, right). **b.** Example GCaMP6f expression in MGB. Similarly replicated expression patterns for all animals where GCaMP6f was injected in MGB ($N = 24$ mice). **c.** High magnification of GCaMP6f-expressing MGB neurons from B. **d.** Individual motion corrected fields of view (maximum intensity projection) of one example animal across a four-day fear conditioning paradigm (Hab, FC, Ext. 1, Ext. 2) as well as the maximum intensity projection across all days. Red circles indicate selected individual components. Replicated for all mice ($N = 24$) that underwent calcium imaging. **e.** Average number of individual ICs/animal (93 ± 4 neurons, $N = 24$ mice). Boxplots show median, 2nd, 3rd quartile, minimum and maximum. Cross indicates mean. **f.** Changes in Ca²⁺ fluorescence of five individual neurons during the habituation session. Lines indicate CS tone presentations (red: 12 kHz, blue: 6 kHz). **g.** Tone responses on habituation day 1 of all recorded MGB neurons in fear conditioning experiments ($N = 855$ neurons, $N = 9$ mice).

Similar to previous reports⁷⁶, we found GABAergic fibers, typically originating in IC and the TRN, but virtually no GABAergic somata in MGB (**Fig. 2**), indicating that we mainly imaged Ca²⁺ activity of thalamic relay neurons. We were able to follow 93 ± 4 GCaMP6f-expressing neurons per mouse (**Fig. 1d, e**, $N = 24$ mice) stably within and across sessions. MGB neurons exhibited diverse, spontaneous activity patterns in freely moving animals (**Fig. 1f**) as well as cell-specific responses to pure tone auditory stimuli (**Fig. 1g**).

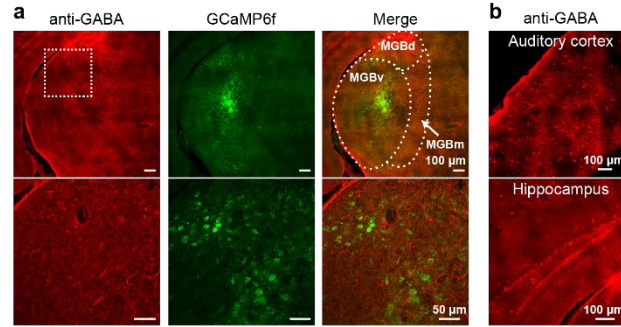


Fig. 2: Imaging of excitatory cells in MGB.

a. Immunohistochemistry for GABA in MGB (left), GCaMP6f-expressing cells (middle) and merge (right). Bottom row: higher magnification of square indicated in top left image. GABAergic fibers are distributed widely in MGB while GABAergic somata are mainly absent (N = 2 mice). **b.** GABA-positive somata in auditory cortex and hippocampus using the same antibody as in **a** (N = 2 mice).

Using this approach it was possible to image large populations of MGB neurons across several days and to observe the responses to different stimuli.

2.3. Individual cells respond to tones and footshocks

2.3.1. Response to CS and US

Using a classical fear conditioning paradigm where a CS+ tone was associated with a footshock (US) and a control tone, CS-, was also presented, it was possible to record the neuronal activity of MGB cells in response to the different stimuli (**Fig. 3a**). The total neuronal population (**Fig. 3b**) as well as individual MGB neurons (**Fig. 3c, d**) were strongly responsive to both the CS tones and to the US. The proportion of US responsive neurons ($75 \pm 5\%$) was significantly higher than the proportion of CS+ ($27 \pm 3\%$) and CS- neurons ($20 \pm 2\%$, N = 9 mice, see methods for classification of responsive neurons), while similar proportions of neurons were responsive to the CS+ and the CS- (**Fig. 3e**; Friedman test, $p < 0.001$ followed by Dunn's multiple comparisons test CS+ vs. CS- $p > 0.05$, CS+ vs. US $p < 0.05$, CS- vs. US $p < 0.001$). Furthermore, we found mixed selectivity in subpopulations of neurons that were responsive to combinations of tones and foot shocks, yet they were not enriched beyond chance level in the total population (**Fig. 3f**).

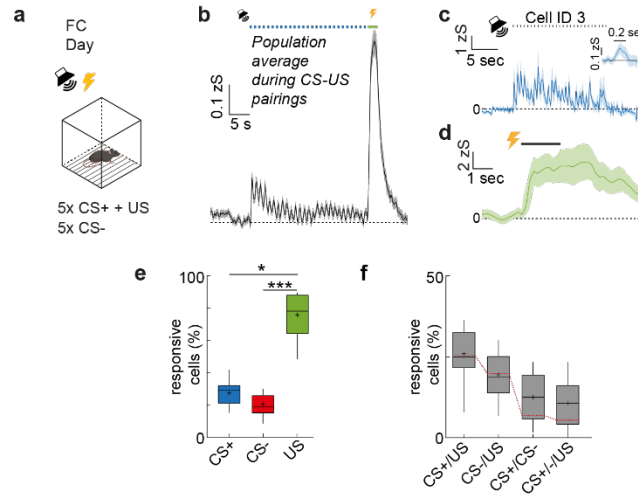


Fig. 3: Mixed selectivity tone CS+ and shock US coding of MGB neurons upon fear conditioning. **a.** Details of the fear conditioning paradigm. **b.** Population response of one example animal to the CS+ and US (mean \pm s.e.m.). Blue dots indicate CS+ tone pips. Green bar indicates shock US. Example cell response to the CS+ (**c**) and US (**d**). Mean \pm s.e.m. of five trials. Dots indicate CS+ tone pips. Inset represents average response to single pips. **e** Proportion of CS+, CS- and US responsive neurons. Friedman test, $p < 0.001$, followed by Dunn's multiple comparisons test: CS+ vs. US, $p = 0.029$; CS- vs. US, $p = 0.0005$ ($N = 9$ mice). Boxplots represent median, 2nd, 3rd quartile, minimum and maximum. Cross indicates mean. **f.** Proportion of mixed selectivity CS \pm and US coding neurons. Red line indicates chance overlap level ($N = 9$ mice). Boxplots represent median, 2nd, 3rd quartile, minimum and maximum. Cross indicates mean.

These results suggest that cells in MGB do not only respond to tone stimuli but also to the somatosensory/nociceptive footshock. Single cells were found to be unisensory and also multisensory. Perhaps surprisingly for the auditory thalamus, there were significantly more US responsive cells than CS responsive cells. To test if these US responses are in fact due to other factors than the somatosensory stimuli, we further analyzed these responses.

2.3.2. US response not solely due to movement

To test if US responses are solely driven by movement of the animal, e.g., escape runs during the aversive foot shock, we correlated the activity of individual MGB neurons with movement. It was first noted that the animals exhibit similar escape responses during the footshock across the five US presentations (**Fig. 4a, b**). Looking at the neuronal activity it first seemed that a large proportion of MGB neurons exhibited an apparent correlation between movement speed and Ca²⁺ activity during the US (**Fig. 4c**). However, this is most likely due to the simultaneous occurrence and conflation of the 2 s aversive foot shock and the behavioral output (escape), given that the activity in the large majority of MGB neurons was not motion or speed correlated during the habituation period (**Fig. 4d**).

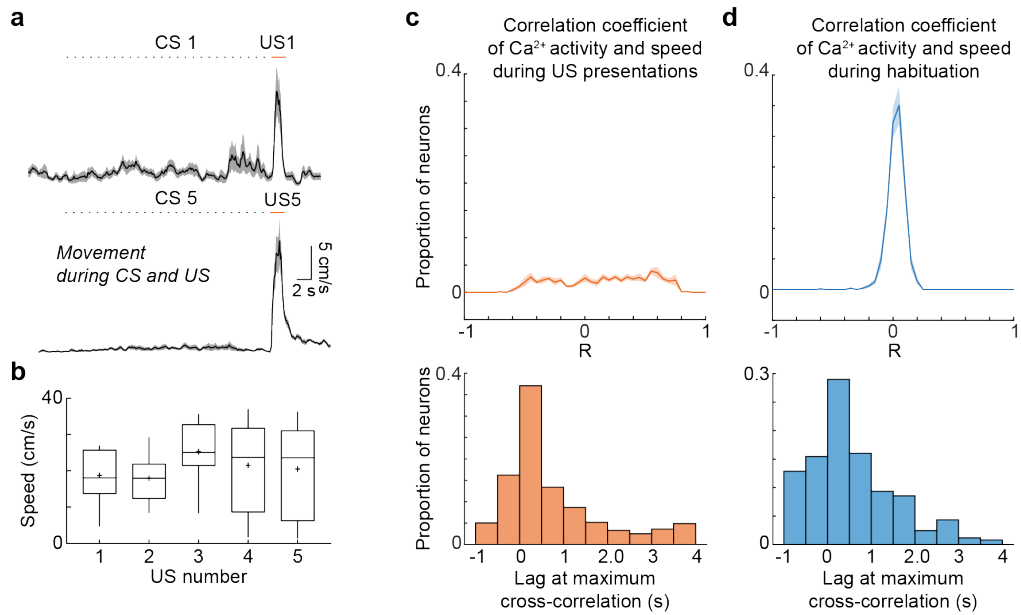


Fig. 4: Correlation of neuronal activity and mouse movement.

a. Average speed \pm s.e.m. of mouse during first CS+US presentation (top) and last CS+US presentation (bottom). **b.** Average speed across the 5 US presentations (Kruskal-Wallis test, $p > 0.05$, $N = 9$ mice). Boxplots represent median, 2nd, 3rd quartile, minimum and maximum. Cross indicates mean. **c.** Distribution of the maximum cross-correlation coefficients between Ca²⁺ activity of individual neurons and the mouse's speed during the footshock US ($n = 855$ neurons from $N = 9$ mice, top, data presented as mean \pm s.e.m.). Lag of maximum cross-correlation coefficient (bottom). **d.** Distribution of the maximum cross-correlation coefficients between Ca²⁺ activity of individual neurons and the mouse's speed during the habituation session outside of CS periods ($n = 855$ neurons from $N = 9$ mice, top, data presented as mean \pm s.e.m.). Lag of maximum cross-correlation coefficient (bottom).

These results would suggest that the neuronal activity seen during the US presentation cannot be solely explained by animal movement.

2.3.3. US response not solely due to self-generated sounds

In addition to animal movement, we also explored sounds present in the context during the US stimulation such as movement sounds or low frequency harmonic vocalization^{77,78}. Using an ultrasound microphone, it was possible to record the sounds in the context upon US stimulation and found that the mice emitted vocalizations during the footshock (**Fig. 5a-e**). However, given that US and CS+ responses were typically substantially larger in sound correlated neurons than responses to self-evoked sounds of the animal, it would indicate that it is not the auditory environment that is driving the neuronal response during the US stimulation (**Fig. 5g, h**). This indicates that MGB US responses are most likely driven by direct somatosensory input, pain signals or aversive state switches.

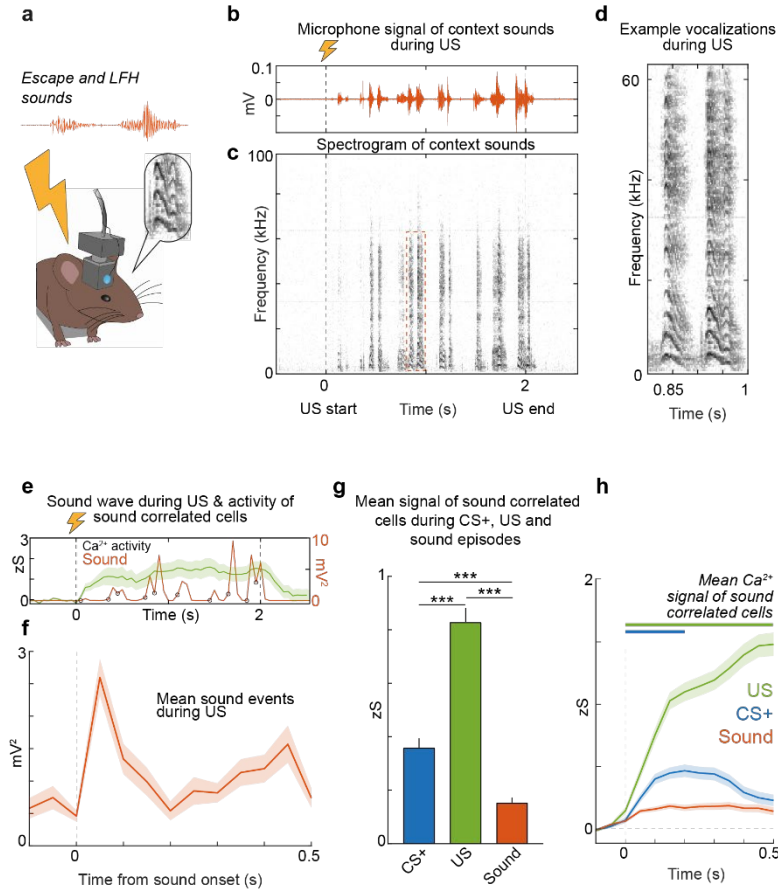


Fig. 5: Ca^{2+} activity of MGB neurons is weakly correlated with self-evoked sounds during the US.

a. Recordings of sounds in the conditioning context during US presentation. **b.** Recorded sounds in the conditioning context during the two second US shock. **c.** Frequency spectrogram of the sound wave in **b.** **d.** Example low-frequency vocalizations during the US from the outlined box in **c.** **e.** Downsampled squared sound wave from **a** and the mean Ca^{2+} activity \pm s.e.m. of cells which exhibited a cross-correlated Ca^{2+} response. Circles indicate the onset of sound events. **f.** Mean (\pm s.e.m.) of onset-aligned detected sound events during all US presentations ($n = 15$ US presentations and 135 sound events from $N = 3$ mice, downsampled to match 20 Hz imaging frequency). **g.** Summary statistics of the mean Ca^{2+} response in Fig. 2k (0-300 ms) indicate that US and CS responses are stronger than self-evoked sound responses (Kruskal-Wallis test with Dunn's multiple comparisons test, all $p < 0.001$, $N = 3$ mice, data presented as mean values \pm s.e.m.). **h.** Mean Ca^{2+} activity (\pm s.e.m.) of sound-correlated neurons during shock evoked sound events e.g., mouse escape sounds and low frequency harmonic vocalizations (LFH, orange), the first CS+ pip (blue) and the US (green) from $N = 550$ CS+/US or $N = 4956$ sound event trials from 110 cells out of $N = 3$ mice. *, **, *** indicate p values smaller than 0.05, 0.01 and 0.001, respectively.

2.4. Spatially intermingled unisensory and multisensory cells.

Using a GRIN lens approach allows us to observe the spatial distribution of cells within MGB (**Fig. 6a**). With these spatial maps, it was possible to calculate the across-group distance and within group distance of the different responses (**Fig. 6b, c**). These results show that, within MGB, cells responsive to the different stimuli are spatially intermingled and do not form spatial clusters.

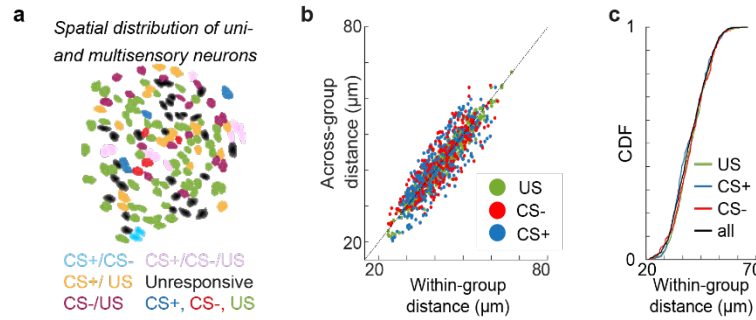


Fig. 6: Spatial distribution of unisensory and multisensory MGB neurons.

a. Example spatial map of unisensory and multisensory mixed selectivity CS and US coding neurons in MGB. **b.** Relationship between within response group and across response group pairwise spatial distance between neurons ($N = 855$ cells, $N = 9$ mice). **c.** Cumulative distribution function of pairwise distances between all, US-responsive, CS+ and CS- responsive neurons ($N = 855$ cells, $N = 9$ mice).

2.5. Discussion

The aim of this chapter was to observe neuronal responses to auditory and somatosensory stimuli in MGB.

We recorded large populations of excitatory MGB neurons in freely moving mice. Using deep brain calcium imaging across a 20-minute session, we could see that there were strong fluctuations in neuronal activity across the whole session. These fluctuations could be further explored to understand if they encode for something such as an external stimuli, state changes, specific behaviors (i.e. grooming) or if they are just spontaneous neuronal activity. Besides these strong fluctuations, looking specifically during the tone presentations we find that individual MGB neurons exhibit a neuronal response to the individual CS presentations.

On the population level we can see that there is a slightly stronger response at the onset of the tone presentation but there is still a sustained response across the whole 30 seconds. This follows on from the literature where it has been shown that MGB has stronger onset responses^{64,66,67}. Here we used individual pips of 200 ms every 1.1 Hz which reduces the adaptation seen in MGB and allows for a sustained response across the whole 30 seconds, however there still is a stronger onset response.

We found that MGB neurons exhibited a neural response to the footshock stimuli. In fact, a larger proportion of neurons responded to the US than to the different CSs. This could be due to the frequencies presented. Here the different CSs are either 6 or 12 kHz, by looking at a wider range of frequencies it is likely that there would be more tone responsive cells⁴¹.

Whilst it was unsurprising to find MGB neurons responsive to the US⁵², the fact that such a large proportion were responsive led to several controls being performed. The innate response to a mild footshock is a strong escape response. This was observed across all animals and across all US presentations, however MGB neuronal activity did not seem to be correlated with the mice's movement outside of these escape responses therefore suggesting that the neuronal response seen during the US presentation is not due to this escape response. It has also previously been shown that in response to pain mice emit low frequency vocalizations^{77,78}. With other studies showing that MGB is responsive to vocalizations^{79,80}, it was hypothesized that these self-generated sounds could be driving the neuronal response observed during the US presentation. Whilst there are some neurons which are responsive to vocalizations, US and CS+ responses were typically substantially larger in sound correlated neurons than responses to self-evoked sounds of the animal. This meant that the neuronal activity seen during the US presentations cannot be solely explained by movement or self-generated sounds. The MGB US responses are therefore most likely driven by direct somatosensory input, pain signals or aversive state switches.

This would suggest that a large number of individual neurons do not only respond to the auditory tone CSs but also to the somatosensory/nociceptive footshock US or a combination of the different stimuli. We looked at the spatial organization within MGB, we found that the unisensory cells are spatially intermingled within MGB. These results show that individual cells within MGB integrate both the CS and the US placing them in an ideal position for Hebbian plasticity.

We will further explore this hypothesis in the next chapter by looking at the plasticity of individual MGB neurons across a fear conditioning and extinction paradigm.

Chapter 3. The medial geniculate body: a center for associative learning

3.1. Introduction

This integration of CS and US inputs underlines that MGB neurons are ideal candidates for sensory plasticity upon associative learning. MGB neurons, particularly in the medial subdivision, have been shown to potentiate auditory CS responses upon fear learning³⁶. These previous studies were limited by the techniques available at the time and only a small number of cells were monitored across a short time period. The response diversity of these cells remains unknown. To understand the learning-related dynamics of MGB neurons, we followed the activity of large populations of individual MGB neurons across a 4-day fear conditioning paradigm.

3.2. Fear conditioning paradigm

We used a classical four-day fear conditioning and fear extinction paradigm¹⁹ (**Fig. 7**), in which mice learn to associate a mild foot-shock, US, with a predictive conditioned stimulus. This consisted of a first habituation (Hab) day, where the animal was presented with two tones of different frequencies (6 or 12 kHz pure tones, 200 ms pips, 27 pips per CS). The second day was the fear conditioning (FC) day, where the CS+ was associated with the mild footshock US (0.65 mA for 2 seconds). The mice were also presented with a control tone, CS-, not associated with the US. The next two days were the extinction days (Ext.1 and Ext. 2) where the mice were first presented with the CS- four times and then twelve times the CS+. The animals showed little to no freezing during the Hab day. During the FC day they learnt to associate the CS+ with the US as they froze more to the CS+ with increasing numbers of CS+-US pairings. After fear conditioning, mice exhibited enhanced freezing to the CS+ ($61 \pm 6\%$) when compared to a neutral CS- ($42 \pm 8\%$, $N = 15$, $p < 0.01$, Mann–Whitney test, **Fig. 7b, c**), which extinguished upon repetitive CS+ presentation (Friedman test, $p < 0.001$, followed by Dunn's multiple comparisons test, Extinction 1 early vs. Extinction 1 late $p < 0.01$, Extinction 1 early vs. Extinction 2 late $p < 0.001$, Extinction 2 early vs. Extinction 2 late $p < 0.05$).

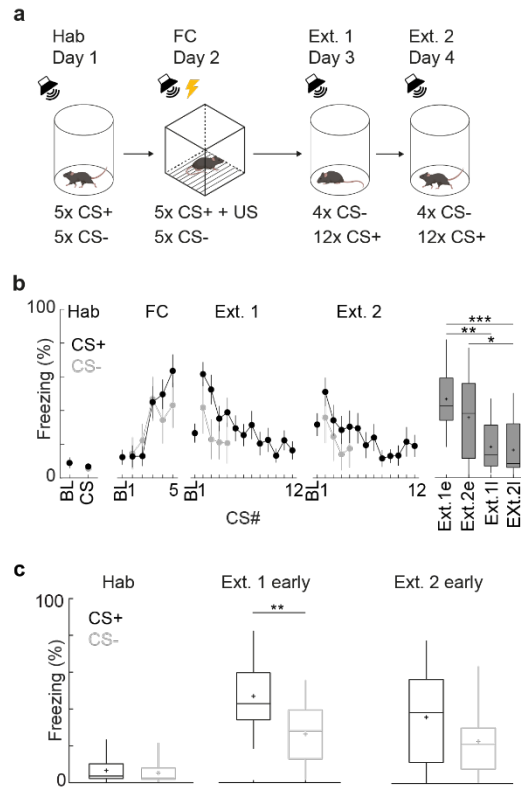


Fig. 7: Fear conditioning paradigm and behavioral response.

a. Details of the 4-day fear conditioning paradigm. **b.** Conditioned stimulus (CS) CS+ and CS- freezing (mean \pm s.e.m.) during the habituation, fear conditioning as well as extinction days (Ext. 1, Ext. 2. e and l indicate early and late phases of extinction, i.e., the first four or last four CS+ of the session. Friedman test, $p < 0.001$, followed by Dunn's multiple comparisons test, Ext.1e vs Ext.1l $p = 0.0069$, Ext.1e vs Ext.2l $p = 0.0002$, Ext.2e vs Ext.2l $p = 0.0281$, $N = 15$ mice). Boxplots represent median, 2nd, 3rd quartile, minimum and maximum. Cross indicates mean. **c.** Freezing to the CS+ and CS- during auditory fear conditioning. Ext. 1 early: CS+ $61 \pm 6\%$, CS- $42 \pm 8\%$, $p = 0.0075$, two-tailed Mann-Whitney test, $N = 15$ mice. Boxplots represent median, 2nd, 3rd quartile, minimum and maximum. Cross indicates mean.

These results suggest that using this paradigm the animals learn to associate a tone with the upcoming aversive stimuli US. This association is enhanced in response to the CS+ however there is some generalization as there is some freezing to the CS-. The animals learn to dissociate the CS+ from the US as shown by the reduced freezing to the CS+ in late extinction. Using this paradigm, it is possible to explore the role of MGB neurons in associative learning.

3.3. MGB is necessary for fear learning

To understand the role of MGB upon learning, we used an optogenetic approach to inhibit MGB during fear conditioning (**Fig. 8 a, b**). For this, an inhibitory opsin (ArchT.GFP) or a control fluorophore (GFP) was injected bilaterally in MGB before implantation of optic fibers above MGB. The same fear conditioning paradigm described previously was used. Upon FC, all CS+/US pairings received optogenetic stimulation starting 2s prior to CS+ onset until 2s after

the end of US, for a total of 36s. Inhibition of MGB did not have a significant effect on acquisition of the learnt behavior (**Fig. 8e**). However, there seems to be a faster acquisition of the learnt behavior upon inhibition of MGB (3rd CS+ freezing, Control: $41 \pm 7\%$, ArchT: $75 \pm 9\%$). Strikingly, the next day upon fear recall there was a significant reduction in freezing in the ArchT group compared to the control group (Control: $48 \pm 6\%$, ArchT: $13 \pm 4\%$, **Fig. 8f**).

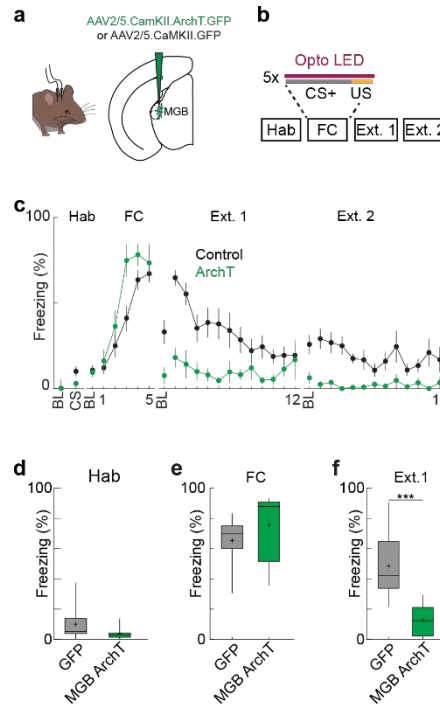


Fig. 8: Optogenetic inhibition of MGB neurons suppresses consolidation of fear learning.

a. Viral expression strategy for optogenetic manipulation of MGB neurons **b.** Schematic of optogenetic manipulation on the fear conditioning day. **c.** Mean \pm s.e.m. freezing across the 4-day fear conditioning paradigm for GFP (black, N = 13 mice) and MGB ArchT mice (green, N = 8). **d.** Quantification of freezing on the habituation day (Mann-Whitney test, $p = 0.0609$), GFP (black, N = 13 mice) and MGB ArchT mice (green, N = 8). Boxplots represent median, 2nd, 3rd quartile, minimum and maximum. Cross indicates mean. **e.** Average freezing of GFP (N = 13 mice) and ArchT-expressing animals at the end of the fear conditioning paradigm (freezing to last two CS, control: $65 \pm 4\%$ freezing, total MGB ArchT (N = 8 mice): $75 \pm 8\%$ freezing; Mann-Whitney test $p = 0.0511$). Boxplots represent median, 2nd, 3rd quartile, minimum and maximum. Cross indicates mean. **f.** Average freezing of control and ArchT-expressing animals upon fear recall during early extinction 1 (Ext. 1, freezing during first four CS+, control: $48 \pm 6\%$, N = 13 mice, MGB ArchT: $13 \pm 4\%$, N = 8 mice, Mann-Whitney test $p < 0.001$). Boxplots represent median, 2nd, 3rd quartile, minimum and maximum. Cross indicates mean. *** indicate p-values smaller than 0.001.

These results suggest that MGB neuronal activity upon CS+ and US presentations is necessary for overnight consolidation of the learnt behavior. To understand why this is, we next observed large populations of MGB neurons upon fear conditioning.

3.4. Intraday US plasticity

Given MGB's necessary role in fear learning and that individual cells integrate both the tone CS+ and the footshock US, we recorded large population of MGB neurons upon fear conditioning and tracked their responses. We find that on the fear conditioning day US responsive neurons can be subdivided into stable ($8 \pm 1\%$) and plastic cells ($92 \pm 1\%$). Using a cluster analysis approach, we identified neurons that demonstrated intra-session potentiation or depression and subtypes of inhibited as well as off-responsive neurons that potentially signal relief from the shock. Interestingly the most prominent group was the down group (**Fig. 9**), potentially suggesting that the US acts as a teaching signal. To test this hypothesis, it is important to look at CS+ responses.

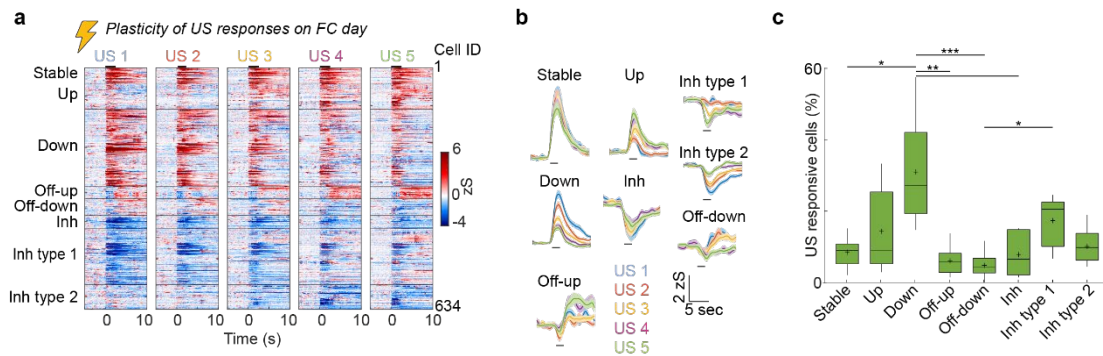


Fig. 9: Single cell US plasticity.

a. Heat maps of single cell US responses to the five US stimulations during the fear conditioning day ($N=634$ cells, $N=9$ mice). **b.** Average response \pm s.e.m of plasticity subtypes of US-responsive MGB neurons ($N=634$ cells, $N=9$ mice). **c.** Proportion of individual plasticity groups within US responsive cells/animal (Kruskal-Wallis test, $p < 0.01$ followed by Dunn's multiple comparisons test; Stable vs down, $p = 0.043$; down vs off-up, $p = 0.0006$; down vs. off-down, $p < 0.001$; down vs. inh, $p = 0.0055$; off-down vs inh type 1, $p = 0.018$; $N=9$ mice). Boxplots represent median, 2nd, 3rd quartile, minimum and maximum. Cross indicates mean. *, **, *** indicate P values smaller than 0.05, 0.01 and 0.001, respectively.

3.5. Interday CS plasticity

To understand the learning-related dynamics of MGB neurons, we followed the activity of large populations of individual MGB neurons across the 4-day fear conditioning paradigm. Using a cluster analysis approach, we classified CS+ responsive neurons according to their response dynamics before and after fear conditioning and fear extinction (**Fig. 10a-c**). On the habituation day and on the two extinction days, we identified eight subgroups of CS+ responsive neurons. $7 \pm 1\%$ of cells show stable CS+ responses across days. The remainder could be separated in the following subgroups of plastic neurons: neurons that abolish their complete ($21 \pm 3\%$, CS down cells) or onset ($9 \pm 2\%$, on-down cells) CS+ response after fear conditioning, neurons

with enhanced CS+ responses when the animal is in a high fear state ($23 \pm 5\%$, fear cells), neurons that are inhibited when the animal is in a high fear state ($4 \pm 1\%$, fear-down cells) as well as neurons that enhance or decrease their response when the animal extinguished the fear behavior ($14 \pm 3\%$, extinction-up cells; $8 \pm 2\%$, extinction-down cells). In addition, we identified cells that had stable, enhanced CS+ responses after fear learning ($14 \pm 4\%$, persistent cells, **Fig. 10c**). These results suggest that MGB neurons show a wide-range of plasticity profiles upon fear conditioning. We next looked to see if this plasticity was specific to the CS+ or if it was also present in response to the CS-.

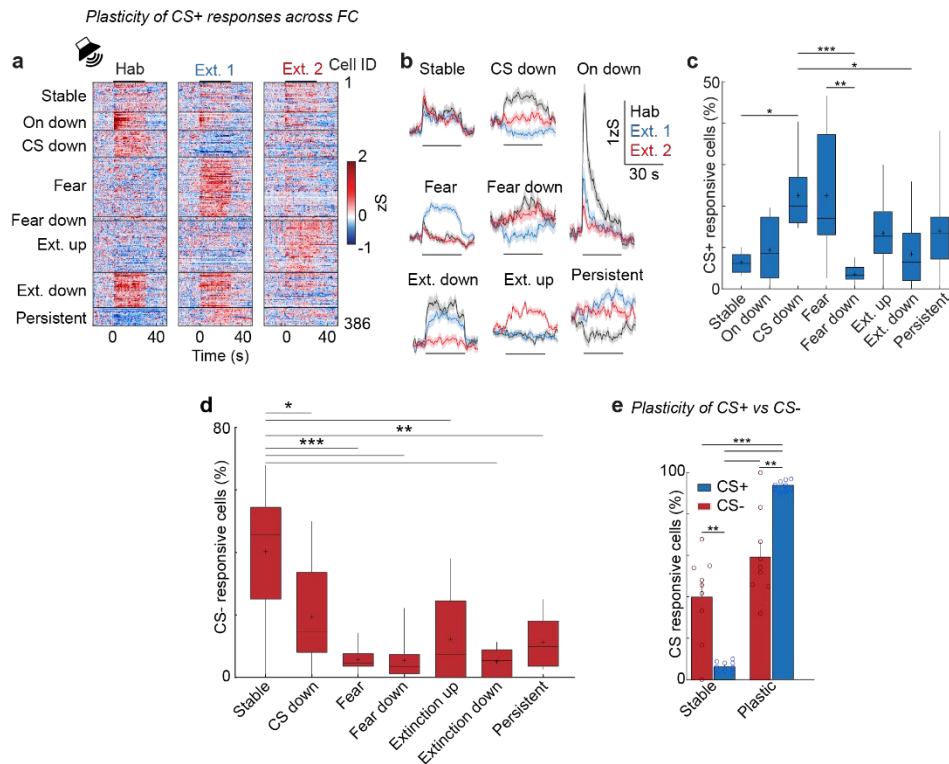


Fig. 10: Single cell CS plasticity.

a. Heat map of single cell CS+ responses on the habituation, extinction 1 and extinction 2 days. Cells were clustered into groups depending on their CS+ response pattern ($N=386$ cells, $N=9$ mice). **b.** Average traces \pm s.e.m of neuronal clusters in (a). **c.** Proportion of individual plasticity groups within CS+ responsive cells/animal (Kruskal-Wallis test, $p < 0.05$, followed by Dunn's multiple comparisons test; Stable vs cs down, $p = 0.013$, cs down vs fear down, $p = 0.0003$, cs down vs extinction down, $p = 0.035$, fear vs fear down $p = 0.0041$; $N = 9$ mice). Boxplots represent median, 2nd, 3rd quartile, minimum and maximum. Cross indicates mean. **d.** Quantification of CS- responses (Friedman test, $p < 0.001$, followed by Dunn's multiple comparisons test, stable vs CS down $p = 0.036$, stable vs fear $p < 0.0001$, stable vs fear down $p < 0.01$; stable vs persistent $p = 0.0009$, $N = 9$ mice). Boxplots represent median, 2nd, 3rd quartile, minimum and maximum. Cross indicates mean **e.** Proportion of CS+ and CS- stable and plastic neurons (2-way ANOVA followed by Sidak multiple comparisons test, $p < 0.001$; stable CS- vs. stable CS+, $p = 0.002$; stable CS- vs. plastic CS+, $p < 0.001$; stable CS+ vs. plastic CS-, $p < 0.001$; stable CS+ vs. plastic CS+, $p < 0.001$; plastic CS- vs. plastic CS+, $p = 0.002$, $N = 9$ mice, data presented as mean values \pm s.e.m.). Circles represent individual animals. *, **, *** indicate P values smaller than 0.05, 0.01 and 0.001, respectively.

Similar subgroups were found for CS- responsive neurons. However, in contrast to the US-paired CS+, the group of CS- stable cells was most prominent across days (**Fig. 10d**). In fact, the proportion of neurons that were plastic and changed their CS responses across days was significantly higher in the CS+ group ($93 \pm 1\%$) compared to the CS- group ($60 \pm 7\%$, 2-way ANOVA, $p < 0.0001$, followed by Tukey post hoc test, $p < 0.05$), while the proportion of stable neurons was higher in the CS- ($40 \pm 7\%$) compared to the CS+ group ($7 \pm 1\%$, 2-way ANOVA, $p < 0.0001$, followed by Tukey post hoc test, $p < 0.05$, **Fig. 10e**), indicating that neural response plasticity is learning-specific and more prominent for the paired conditioned stimulus than the control stimulus.

All-in-all, this data reveals a broad response diversity of MGB neurons upon fear learning that extends previous observations of fear conditioning potentiated neurons^{53,81}. Interestingly, the plastic CS+ subgroups are similar to previously described functional groups in the amygdala^{19,22,82}. There is a wide-array of plasticity subgroups, indicating that diverse CS+ response plasticity occurs not only in the amygdala, but also upstream in auditory thalamus.

3.6. Intraday plasticity not predictive of interday plasticity

To further explore the hypothesis that the intraday US plasticity was acting as a teaching signal, we explored whether the US response type was predictive of CS plasticity in MGB neurons. However, despite its prominent diversity, the US response type was not predictive of CS plasticity in MGB neurons. US response and plasticity type did not overlap with CS response and plasticity type above chance levels (**Fig. 11**), indicating that US inputs per se do not drive plasticity in MGB neurons. Nevertheless, adaptive US responses in MGB could act as an upstream teaching signal in addition to local circuit mechanisms²¹, which direct plasticity in downstream areas like the amygdala.

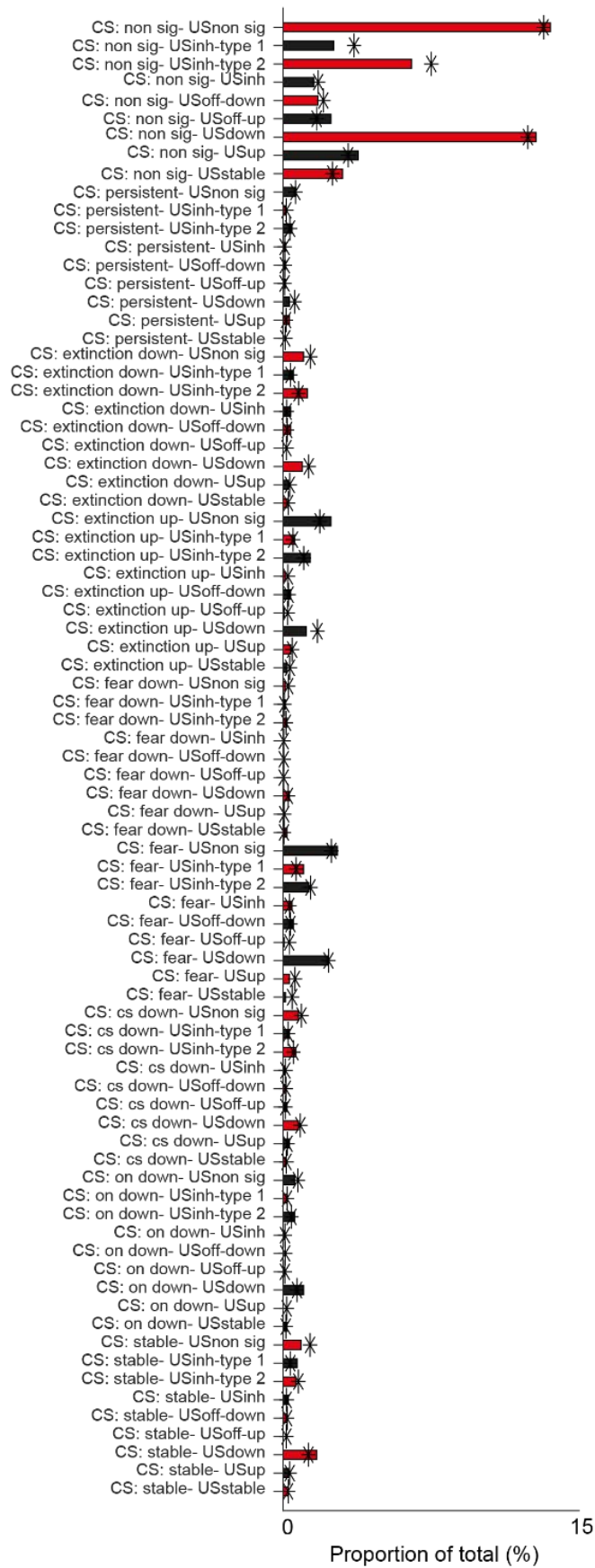


Fig. 11: US response type is not predictive of CS plasticity.

Proportion of overlapping subgroups of CS+ and US responsive cells (N = 9 mice). * indicates chance levels of finding overlapping groups based on the product of the proportions of individual subgroups.

3.7. Plasticity in MGB's different subdivisions

As previously described, MGB is subdivided into a first order, auditory cortex-projecting nucleus (MGBv) as well as higher order nuclei (MGBd, MGBm), which send axons to cortical and limbic brain areas, e.g., the amygdala. To test if MGB CS and US plasticity types are different between first order and higher order nuclei, we subdivided the cells depending on their location in the GRIN lens field of view between MGBv and MGBm after anatomical verification of the lens front location for all mice where MGBv and MGBm were simultaneously imaged ($N = 5$ mice, **Fig. 12a, b**). Similar to the total population of MGB neurons, large fractions of MGBv and MGBm neurons exhibited plasticity to the US or CS+ (**Fig. 12c**). Nevertheless, plastic cells were not significantly different between either subdivision (**Fig. 12c**) and the diversity of plasticity subtypes was similar in the first order (MGBv) vs. higher order (MGBm) area of auditory thalamus (**Fig. 12d-f**).

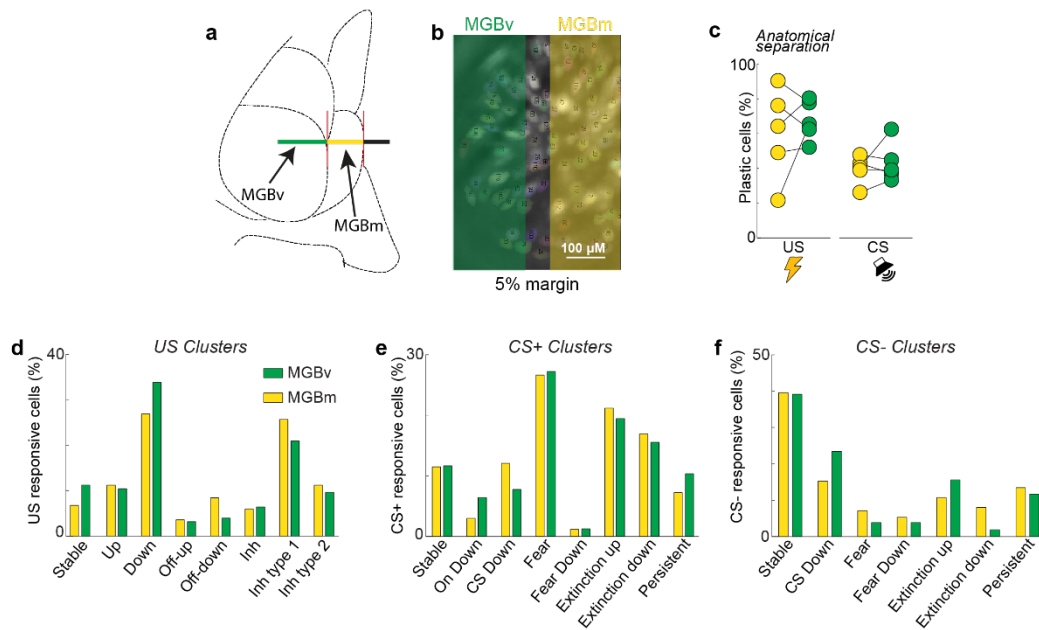


Fig. 12: Similar CS and US plasticity types between MGB subdivisions.

a. Schematic of GRIN lens location above different MGB subdivisions. **b.** Field of view divided into subregions. Done for all mice with a GRIN lens above both MGBv and MGBm ($N = 5$ mice). **c.** Proportion of US ($N = 5$ mice, $p > 0.05$, Wilcoxon signed-rank test) and CS plastic cells ($N = 5$ mice, $p > 0.05$, two-tailed Wilcoxon signed-rank test) in the ventral (MGBv) and medial (MGBm) subdivisions of MGB. **d-f** Proportion of cells belonging to the different US plasticity types (**d**), CS+ plasticity types (**e**) and CS- plasticity types (**f**) for each subdivision.

These results suggest that the different subdivisions of MGB exhibit similar plasticity levels and that MGB distributes these experience dependent changes to a wider network than just the amygdala. This idea will be further explored when analyzing specifically the amygdala projectors (MGB→BLA) neurons.

3.8. Association of CS-US is necessary for MGB plasticity

To rule out that the CS+ plasticity observed in MGB is not just a result of a general drift in tone responsiveness across days or due to attentional effects, we performed an unpaired conditioning paradigm where the footshock was not temporally contingent with the tone CS+ (**Fig. 13a**). This allowed the mice to experience similar sensory stimuli to the fear conditioned animals but they do not associate the CS+ with the US and fail to learn to freeze to the CS+ (**Fig. 13b**).

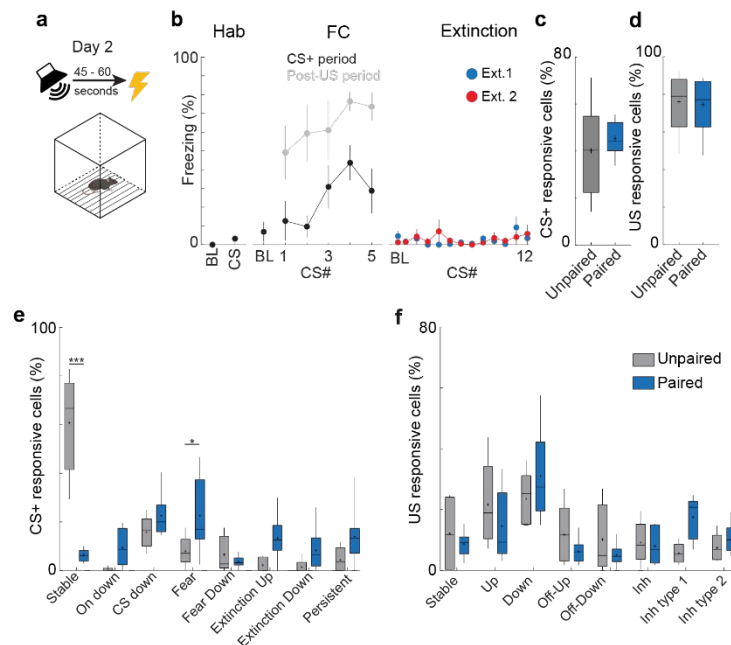


Fig. 13: CS+ responses are mostly stable across days upon unpaired conditioning.

a. Schematic of unpaired conditioning paradigm. The CS+ and US are separated by random intervals between 45 to 60 s. **b.** Mean \pm s.e.m. trial-by-trial freezing to CS+ or the post-US period (grey) on the habituation, fear conditioning and extinction days (N = 5 mice). **c.** Proportion of CS+ responsive neurons in fear conditioned (paired, $45 \pm 2\%$, N = 9 mice, see **Fig. 9**) and unpaired conditioned animals (unpaired, $40 \pm 8\%$, N = 5 mice, two-tailed Mann-Whitney test, $p = 0.529$). Boxplots represent median, 2nd, 3rd quartile, minimum and maximum. Cross indicates mean. **d.** Percentage of US responsive cells in the paired ($74 \pm 5\%$, N = 9) and unpaired ($76 \pm 7\%$, N = 5) group (two-tailed Mann-Whitney test, $p = 0.898$). Boxplots represent median, 2nd, 3rd quartile, minimum and maximum. Cross indicates mean. **e.** Quantification of the proportion of neurons within each CS+ plasticity clusters for fear conditioned and unpaired animals (2-way ANOVA, $p < 0.05$ followed by Sidak's multiple comparisons test; stable: paired vs unpaired, $p < 0.001$, Fear neurons: paired vs unpaired, $p = 0.0303$; N = 9 mice for fear conditioning (see **Fig. 2**) and N = 5 mice for unpaired conditioning). Boxplots represent median, 2nd, 3rd quartile, minimum and maximum. Cross indicates mean. **f.** Quantification of the proportion of US clusters for fear conditioned and unpaired animals (2-way ANOVA, $p < 0.05$, followed by Sidak's multiple comparisons test $p > 0.05$, N = 5 mice for unpaired conditioning and N = 9 for paired conditioning). Boxplots represent median, 2nd, 3rd quartile, minimum and maximum. Cross indicates mean. * indicate p-values smaller than 0.05.

Unpaired conditioning did not affect the proportions of tone and foot shock responsive neurons in MGB (**Fig 13c, d**). It was also shown that the proportion of US plasticity subtypes was similar between the two groups therefore suggesting that the innate response and adaptation to the US was unaffected by dissociating the CS from the US (**Fig. 13f**). However, compared to fear conditioned animals, the majority of the unpaired group of neurons exhibited stable across-day CS+ tone responses in the unpaired condition ($61 \pm 9\%$), while the proportion of plastic neurons was significantly decreased ($39 \pm 9\%$, $N = 5$ mice, **Fig. 13e**). This data indicates that MGB single cell tone responses are by-and-large stable across days, while CS+ response dynamics of individual neurons after fear conditioning are due to associative learning-induced plasticity and not just a general drift of tone-responsiveness in MGB across days. Notably, for the minority of MGB neurons that exhibited CS+ plasticity, the relative proportion of fear cells is significantly decreased (**Fig. 13e**) when compared to fear conditioned animals, indicating that the emergence of this population of neurons with potentiated CS+ responses is specific to auditory fear learning.

This data confirms the hypothesis that the plasticity observed in MGB is not due to a general drift in tone responses but is in fact due to the mice learning to associate and then disassociate the CS+ from the US. How exactly these tone responses change across learning will be further explored in a later chapter.

3.9. Discussion

The aim of this chapter was to observe changes in neuronal activity in MGB across an auditory fear learning and extinction paradigm.

Using a classical fear conditioning and extinction paradigm where the animals learnt to associate and then to dissociate the tone from a mild footshock, it was possible to explore the role of MGB neurons upon associative learning. This classical fear paradigm led to enhanced freezing with increased numbers of CS-US presentations. This learning was shown on the next day with high freezing levels in early extinction 1. This freezing behavior was extinguished as the animals learnt to disassociate the CS from the US across the session. Interestingly, in this group of animals, there was little to no intraday extinction with only a small, non-significant, reduction in freezing between early extinction 1 and early extinction 2. The animals did however show strong intraday extinction with very little freezing at the end of extinction 2.

By inhibiting MGB neurons, it was found that their activity during the CS+-US pairing is necessary for the consolidation of the memory but does not affect acquisition. Interestingly, it was also found that the animals had reduced freezing to the tone but also during the baseline

suggesting that the animals were generally in a lower fear state or that they had learnt to associate the fear conditioning context with the footshock. This could be further explored by repeating these experiments whilst adding a 5th day where the animals would be placed in the fear conditioning context without any stimulus.

Recording large populations of MGB neurons we found that responses of individual MGB neurons to the CS and US are plastic upon fear conditioning. In addition to previously reported potentiated auditory neurons, we find highly diverse subtypes of CS or US plastic neurons that go beyond FC-driven response potentiation. These plasticity profiles have previously been described in the amygdala¹⁹, therefore showing that the plasticity observed in BLA is occurring one synapse up in MGB. Interestingly, the proportion of plastic cells was distributed similarly across both first order and higher order MGB subdivisions. This was observed by dividing the field of view under the GRIN lens based on anatomical location. To counter imprecisions in the methodology many cells were excluded from the analysis. To circumvent this issue, it would have been better to use a virus which labels specifically the ventral part of MGB however this was not feasible. With the advent of the two channel miniature microscope it would be possible to use a calretinin-cre mouse (calretinin being only present in higher order MGB areas) and inject a cre-dependent fluorophore in MGB as well as the GCaMP. This would allow to image total MGB population and to know that cells that are also expressing the fluorophore are in the higher-order MGB whilst the others are most likely in the ventral MGB.

The US response subtypes observed were not predictive of CS plasticity indicating that MGB neurons do not necessarily require converging CS and US input to drive functional plasticity upon associative learning, arguing for plasticity mechanisms that go beyond classical Hebbian plasticity. However, one caveat of calcium imaging is that it is not possible to detect subthreshold depolarizations and the detected changes in calcium are limited to the soma. Therefore, changes in the spines go undetected. Both of these cellular events could be important for Hebbian plasticity and could be induced by US.

This CS plasticity was shown to be due to the pairing of the CS+-US neurons. Firstly, there was significantly less plasticity in response to the control tone CS-. Secondly, when the US was not temporally contingent with the tone CS+, the animals did not learn to associate the tone with the US and there was significantly less plasticity in response to the CS+ compared to the paired group. It is important to note that the animals did show an innate fear response with post-US freezing being high and this was reflected in the neuronal activity where the US intraday plasticity was similar between the paired and unpaired groups.

This shows that MGB is a center for associative learning, occurring upstream of the amygdala. We will next explore in more detail what is encoded in MGB and the place of MGB in the fear circuit.

Chapter 4. Medial geniculate body neurons encode fear learning

4.1. Introduction

MGB neurons show different responses across the fear conditioning paradigm with some cells, such as the fear cells, being only responsive when the animal is in a high fear state and others, such as extinction up cells, showing a response only when the animal is in a low fear state. This leads to the question of what is encoded in these neuronal responses. To answer this question, we looked at the different responses to the CS+ and their links with the animal's state and behavior.

4.2. Neuronal responses in a high fear state

During early extinction day 1, the animal is in a high fear state. This is shown through high freezing levels in response to the CS+ (**Fig. 7b, c**). During this period there are approximately $25 \pm 2\%$ of cells which are responsive to the CS+ (**Fig. 14a**). These cells consist of stable cells which are activated throughout the fear conditioning paradigm, fear cells which are activated only during this high fear state and persistent cells which are not active pre fear conditioning but are responsive post fear conditioning and extinction. These responsive cells were further explored to study their dynamics across the CS+ presentations. It was found that there were a multitude of response dynamics to the CS+ (**Fig 14b**). Non-adapting cells showed a response throughout the 30 seconds of CS+ presentation whereas slow and fast adapting neurons exhibited an initial strong response which decayed at different speeds during the CS+ presentation. The delayed cells exhibited a response during the CS+ presentation which was not time-locked to any specific event. The late cells were responsive during the end of the 30 seconds perhaps signaling the expected upcoming shock. Finally, the ramp-up cells showed an increase in response throughout the 30 seconds, once again perhaps signaling for an expected upcoming shock. The non-adapting and ramp-up cells were the most prominent groups during early extinction 1 ($33 \pm 4\%$ and $36 \pm 4\%$ respectively, **Fig. 14c**).

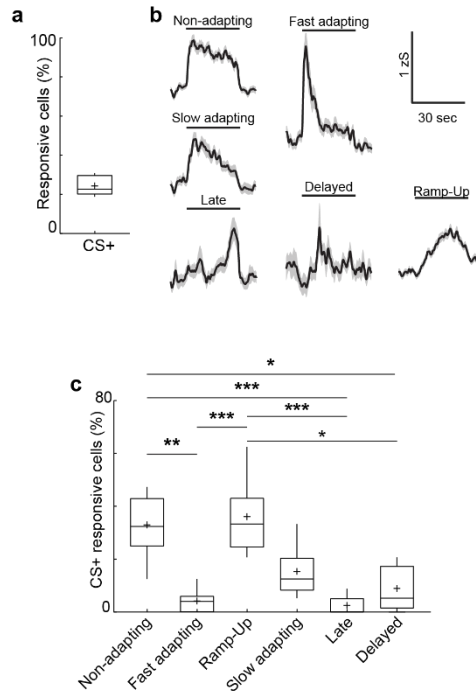


Fig. 14: Multitude of neuronal responses to the CS+ when in a high fear state.

a. Percentage of cells that are responsive to the CS+ during early extinction 1 (N = 9 mice). Boxplots represent median, 2nd, 3rd quartile, minimum and maximum. Cross indicates mean. **b.** Average traces of the different responses to the CS+. **c.** Quantification of the different responses to the CS+ (N = 9 mice). Boxplots represent median, 2nd, 3rd quartile, minimum and maximum. Cross indicates mean. Kruskal-Wallis test $p < 0.001$ followed by Dunn's multiple comparisons test. *, **, *** indicate $p < 0.05$, 0.01 and 0.001 respectively.

4.3. Neuronal responses across the fear conditioning paradigm

To further understand what these different responses encode for, we next looked at their responses to the CS+ pre-fear conditioning (habituation day) and post-extinction (late extinction 2) (**Fig 15**). As expected, many of these cells were unresponsive when the animals were not in a high fear state. It was however worth noting that most cells showed dynamic response types as a non-adapting cell on one day may be adapting or unresponsive on another. Interestingly though, despite being one of the larger groups when the animal was in a high fear state, the ramp-up cells were not present pre-fear conditioning and a small proportion of them post-extinction.

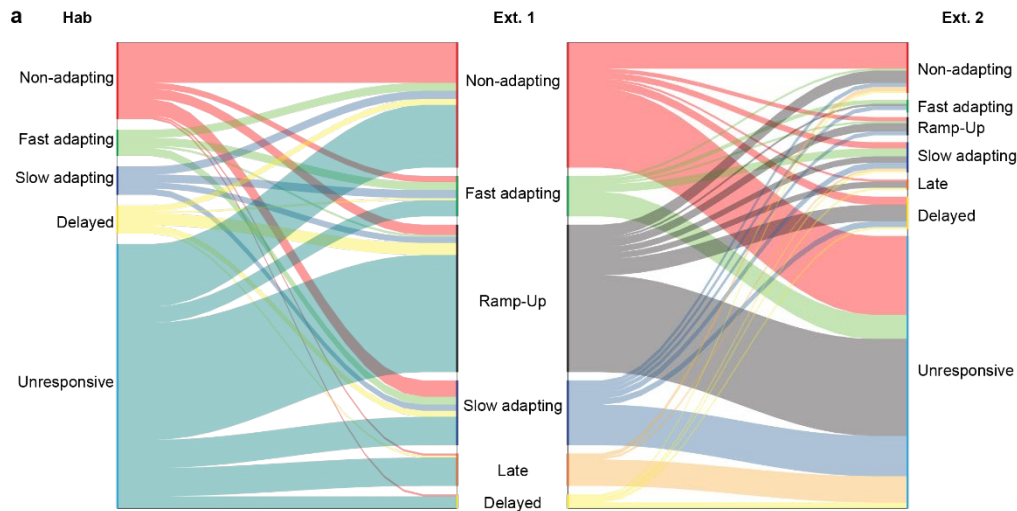


Fig. 15: CS+ responses are dynamic across the fear conditioning paradigm.

Alluvial plot of CS+ responses of all Ext. 1 CS+ responsive cells (N = 9 mice) from habituation, early extinction 1 and late extinction 2.

This led us to explore these ramp-up cells across the whole paradigm to understand when they first appear and disappear (**Fig 16**).

We first found ramp-up cells during the 2nd CS+/US pairing on the FC day and the proportion increased with further CS+/US pairings. There also seemed to be overnight consolidation with a further increase in ramp-up cells during early extinction 1 ($36 \pm 4\%$) but as the animal learnt to dissociate the tone from the footshock during extinction the percentage of ramp-up cells decreased (late extinction 2: $11 \pm 1\%$, **Fig. 16a**).

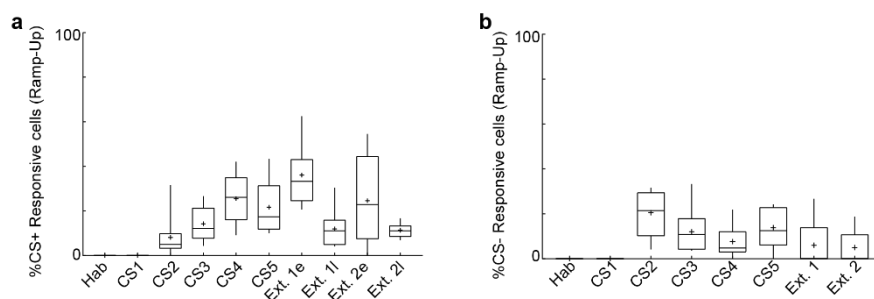


Fig 16: Proportion of Ramp-up cells changes throughout the fear conditioning paradigm.

a. Percentage of CS+ responsive exhibiting ramp-up activity during habituation, fear conditioning (CS1, CS2, CS3, CS4 and CS5), extinction 1 (X1e, X1l) and extinction 2 (X2e, X2l) days. Boxplots represent median, 2nd, 3rd quartile, minimum and maximum. Cross indicates mean. **b.** Percentage of CS- responsive exhibiting ramp-up activity during habituation, fear conditioning (CS1, CS2, CS3, CS4 and CS5), extinction 1 and extinction 2 days. Boxplots represent median, 2nd, 3rd quartile, minimum and maximum. Cross indicates mean.

The responses to the CS- were also studied and it was found that there was also ramp-up activity in response to the control tone (**Fig. 16 b**). It was not present pre-fear conditioning and appeared during the 2nd CS- presentation. However, in contrast to the CS+, the percentage of ramp-up cells remained relatively stable across the paradigm and at a low value ($6 \pm 3\%$ during X1). These results suggest that the ramp-up cells encode for something relating to the state or the behavior of the animal as the activity is specific to when the animal exhibit freezing response.

4.4. Ramp-Up cells are correlated with freezing

To further explore the idea that the ramp-up cells neuronal activity is linked to the animal freezing, we looked at the correlation between the neuronal activity and the probability of an animal freezing during the 30 seconds of CS+ presentation in early extinction 1. We found a strong correlation of 87% between the average neuronal activity of ramp-up cells and of the probability of an animal freezing throughout the 30 seconds (**Fig 17a**).

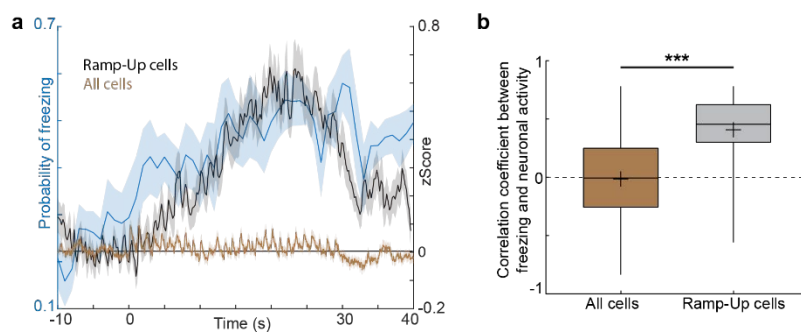


Fig. 17: Ramp-up cells are correlated with freezing behavior.

a. Probability of an animal freezing during the 30 seconds CS+ presentation (blue), average neuronal activity of ramp-up cells (black) and of all cells (brown). **b.** Correlation coefficient of neuronal activity and freezing for all cells (-0.014 ± 0.012 , $n = 855$ cells from 9 mice) and for ramp-up cells (0.41 ± 0.03 , $n = 73$ cells from $N = 9$ mice). Boxplots represent median, 2nd, 3rd quartile, minimum and maximum. Cross indicates mean. Mann-Whitney test, *** indicates $p < 0.001$

This is in contrast to the average neuronal activity of all cells which does not exhibit any correlation with the probability of freezing. The ramp-up cells are significantly more correlated with freezing than all MGB neurons (**Fig 17b**). This leads to the question whether these ramp-up cells encode for the animals' state or if these are cells which are anti-correlated with an animals movement. To test this, we looked at the correlation of these cells with the animals' speed during the baseline of habituation (before any stimulus presentation, **Fig. 18a**).

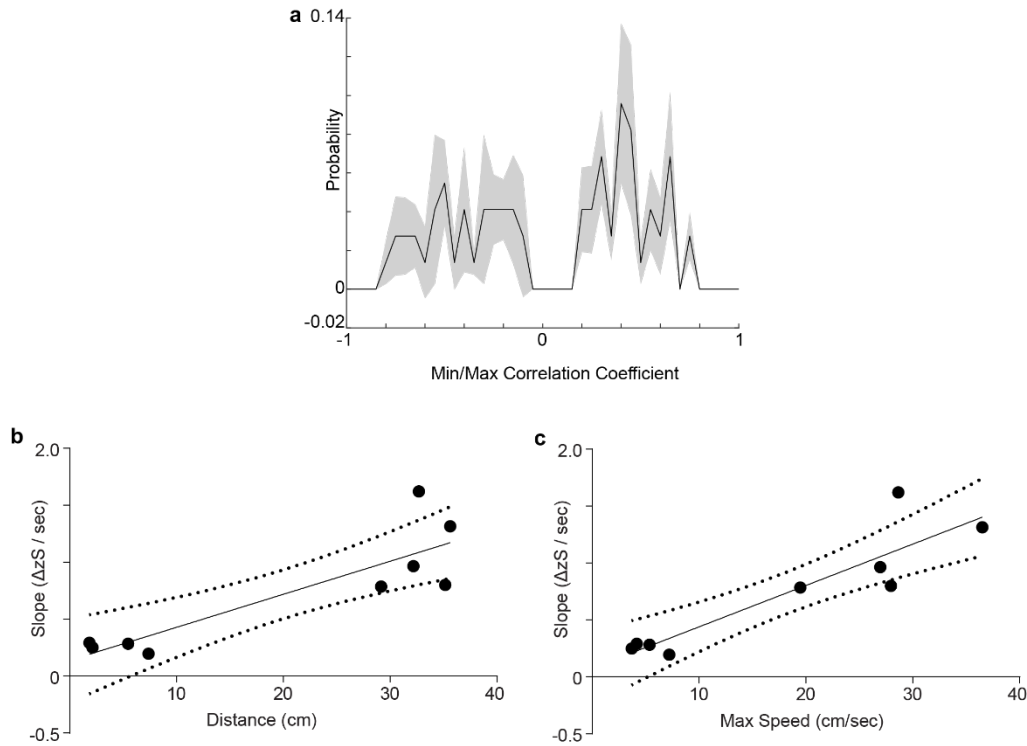


Fig. 18: Ramp-up cells are correlated with US response.

a. Distribution of the maximum or minimum (whichever was the largest absolute value) cross-correlation coefficients between Ca^{2+} activity of individual neurons and the mouse's speed during the habituation baseline period. **b.** Linear regression between the slope of ramp-up cells during the final CS+ presentation on FC day and the distance travelled during the 2 seconds US presentation ($R^2 = 0.75$, $p < 0.01$). **c.** Linear regression between the slope of ramp-up cells during the final CS+ presentation on FC day and the maximum speed during the 2 seconds US presentation ($R^2 = 0.82$, $p < 0.001$).

We found that some cells exhibited a strong anti-correlation with speed however, many cells exhibited little or strong correlation with speed therefore that the neurons in MGB that exhibit ramp-up activity are not encoding the freezing behavior.

Looking at final CS-US pairing on the FC day, we found that the slope of the ramp-up cells during the CS+ was correlated with the distance travelled during the US presentation as well as the maximum speed (**Fig. 18 b, c**). This would suggest that the activity of the ramp-up cells during the CS+ was predictive of the mice's action during the US presentation.

4.5. Discussion

The aim of this chapter was to further understand what MGB is encoding during auditory fear conditioning. We found that the responses to the CS+ vary with some cells responsive throughout the 30 seconds of tone presentation whilst others showed more dynamic responses.

In this analysis we concentrated on the ramp-up cells which were prominent when the animal was in a high fear state but not present pre-fear conditioning and only present in a few cells post-extinction. These ramp-up cells showed an increase in neuronal activity throughout the 30 seconds of CS+ presentation. The proportion of cells showing this response type increased as the animals learnt to associate the tone with the footshock and decreased in number as the animals learnt to dissociate the tone from the footshock and extinguished the learned behavior.

Whilst they are also present in response to the CS-, their numbers stay low and are perhaps a sign of some generalization. The neuronal activity of these cells mirrors the probability of an animal freezing during the 30 seconds but these cells are not clearly correlated or anti-correlated with an animal's speed. This would suggest that these cells are not encoding (lack of) movement but another aspect of the animals' behavior or state. It was found that the slope of these ramp-up cells was correlated with the animal's response to the US suggesting that they are predictive of the upcoming action. Cells with ramping activity have been previously described in several brain areas such as the striatum⁸³, the prefrontal cortex⁸⁴ and the motor thalamus⁸⁵. In these studies, the ramping activity is believed to encode for temporal control of action⁸⁶. The cells exhibiting ramp-up activity in these experiments could also be encoding for this temporal control of action. The animals are preparing for the upcoming shock and the escape behavior associated with it (see also **Fig. 4**). Similarly to a sprinter waiting for the start gun, the mice are waiting for the shock. This waiting is encoded by the ramp-up cells and is only present when the animals are in a high fear state as this is when the animals expect the upcoming footshock.

One limitation of imaging is that the changes in fluorescence are a proxy for neuronal activity and the ramp-up activity could be due to the time course of calcium indicators and not actually a change in neuronal activity. To test if these ramp-up cells are truly showing increased activity throughout the 30 seconds of CS+ presentation electrophysiological recordings could be performed and an increase in firing rate would be expected throughout the 30 seconds tone presentation. However, as these ramp-up cells are not present throughout the paradigm and their numbers increase and decrease throughout the course of the learning and extinction, it is very unlikely to be due to the time course of the calcium indicators and more likely to be reflective of neuronal activity.

Other response types were also observed when the CS+ was presented. They also changed in proportion along the course of the auditory fear conditioning paradigm.

The late cells, similarly to the ramp-up cells, could also be encoding for an expected upcoming shock and be reflective of the temporal control of action as they are also not present pre-learning but are present when the animal is in a high fear state. However, there were only a small proportion of cells that showed late activity making them hard to study and difficult to infer many conclusions. Indeed, it is possible that these cells are also present pre-learning but there are too few that they were missed in this analysis despite the recording of a large population of neurons.

The fast and slow adapting cells are present throughout the paradigm and are to be expected as it is well known that there is a strong onset response in MGB^{64,66,73}. These cells are probably encoding for the sound itself with no emotional valence encoded. The non-adapting cells could also be encoding the sound itself.

The delayed cells are of interest, they are present throughout the paradigm and their activity is not linked to any event. This could be spontaneous activity or it could be that individual neurons are firing throughout the 30 seconds which allows to retain the information without having all of the neurons consistently firing. This would be similar to the idea elicited by the Halassa lab whereby the thalamus, linking with the cortex, retains an information not on the single cell level but on the population level by having neurons fire throughout a delay period⁸⁷. This allows neurons to be ready to signal new information whilst retaining the current information.

Overall, this chapter has shown that there is information related to the behavior that is encoded in MGB. The role of MGB goes beyond that of sensory processing. We will next look at the role of MGB within the fear circuit. For this we will look at some of the inputs MGB receives and then what information is passed on by the MGB to different brain areas.

Chapter 5. The medial geniculate body's inputs and their role in auditory fear conditioning

5.1. Introduction

Being a part of the auditory pathway, MGB receives feedforward inputs from the inferior colliculus but also feedback from the auditory cortex^{42,43}. It has also been shown that MGB receives inputs from the TRN, an inhibitory thalamic nucleus^{50,51}. MGB also receives neuromodulatory inputs, with acetylcholine being of particular interest. Indeed, the role of the cholinergic pathways in auditory fear conditioning has been well-studied as inhibition of the basal forebrain cholinergic inputs to the amygdala led to decreased levels of freezing whereas activation of those same inputs led to increased levels of freezing⁸⁸. The main cholinergic input to MGB comes from the pedunculo pontine tegmental nucleus (PPT)^{89,90}. Understanding what information MGB receives from its different inputs would help understand the role of MGB in the fear circuit.

The aim of this chapter is to study the role of some of these inputs on MGB neuronal activity and on behavior.

5.2. Cholinergic inputs to MGB modulate behavior

The cholinergic inputs from basal forebrain to the amygdala have been studied in fear conditioning however, the inputs from PPT to MGB have not been well-studied. Here these inputs were optogenetically manipulated during the CS-US pairings. This was done by bilaterally injecting cre-dependent opsins in PPT of ChAT-Cre (choline acetyltransferase-Cre) mice and by implanting optic fibers above MGB (**Fig. 19a, b**).

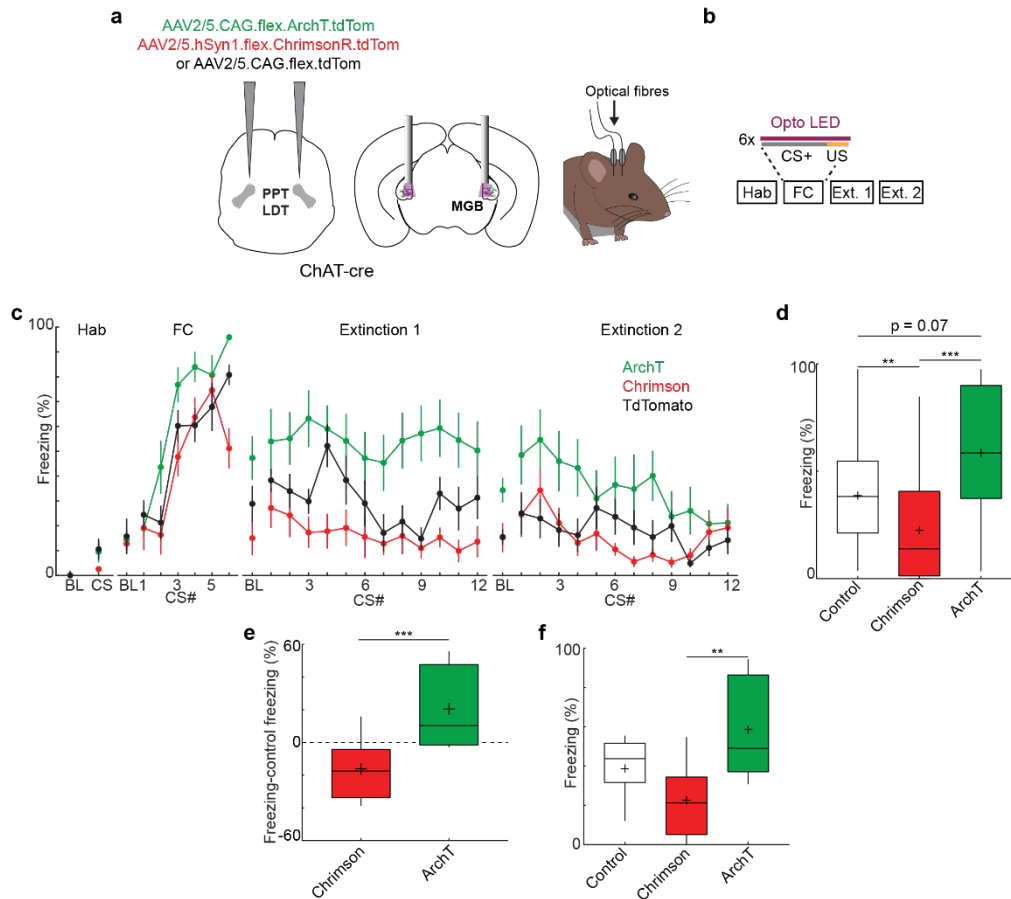


Fig. 19: Optogenetic manipulation of cholinergic PPT fibers in MGB during fear conditioning.

a. Schematic of experimental approach, cre-dependent of opsins or control were injected in PPT of ChAT-cre mice and optic fibers were implanted above PPT fibers in MGB. **b.** Schematic of fear conditioning protocol, optogenetic manipulation was performed on the fear conditioning day starting 2 seconds before the CS+ start and finishing 2 seconds after the end of the US presentation for a total of 36 seconds. **c.** Percentage of time spent freezing during 2 minutes baseline (BL) or during CS+ presentations. TdTomato control (N = 11, black), Chrimson (N = 10, red) and ArchT (N = 9, green). **d.** Freezing during early X1. Control (n = 44 from 11 mice and 4 CS+), Chrimson (n = 40 from 10 mice and 4 CS+), ArchT (n = 36 from 9 mice and 4 CS+). Boxplots represent median, 2nd, 3rd quartile, minimum and maximum. Cross indicates mean. Kruskal-Wallis test $p < 0.05$ followed by Dunn's multiple comparisons test. **e.** Freezing in early X1 minus the average freezing of controls. Chrimson (N = 10), ArchT (N = 9). Mann-Whitney test. Boxplots represent median, 2nd, 3rd quartile, minimum and maximum. Cross indicates mean. **f.** Average freezing during first 4 CS+ presentations on X1. Control (N = 11), Chrimson (N = 10), ArchT (N = 9). Boxplots represent median, 2nd, 3rd quartile, minimum and maximum. Cross indicates mean. Kruskal-Wallis test $p < 0.05$ followed by Dunn's multiple comparisons test. ** and *** indicate $p < 0.01$ and $p < 0.001$ respectively.

Inhibition of cholinergic PPT fibers in MGB led to an increase in freezing levels during the fear conditioning day (**Fig. 19c**). This increase in freezing was also observed during fear recall with higher freezing levels observed during early extinction 1 (**Fig. 19d, f**), these mice also showed less extinction as the freezing levels stayed high throughout the extinction 1 day. This was also the case the next day, on extinction 2, where the animals still had high freezing levels in response to the CS+. At the end of the session, the animals did however exhibit some extinction. It is worth noting that this increase in freezing was not specific to the CS+ as these

mice also exhibited high freezing levels throughout the paradigm, during the baseline periods and in response to the control tone CS- (**Fig. 20**).

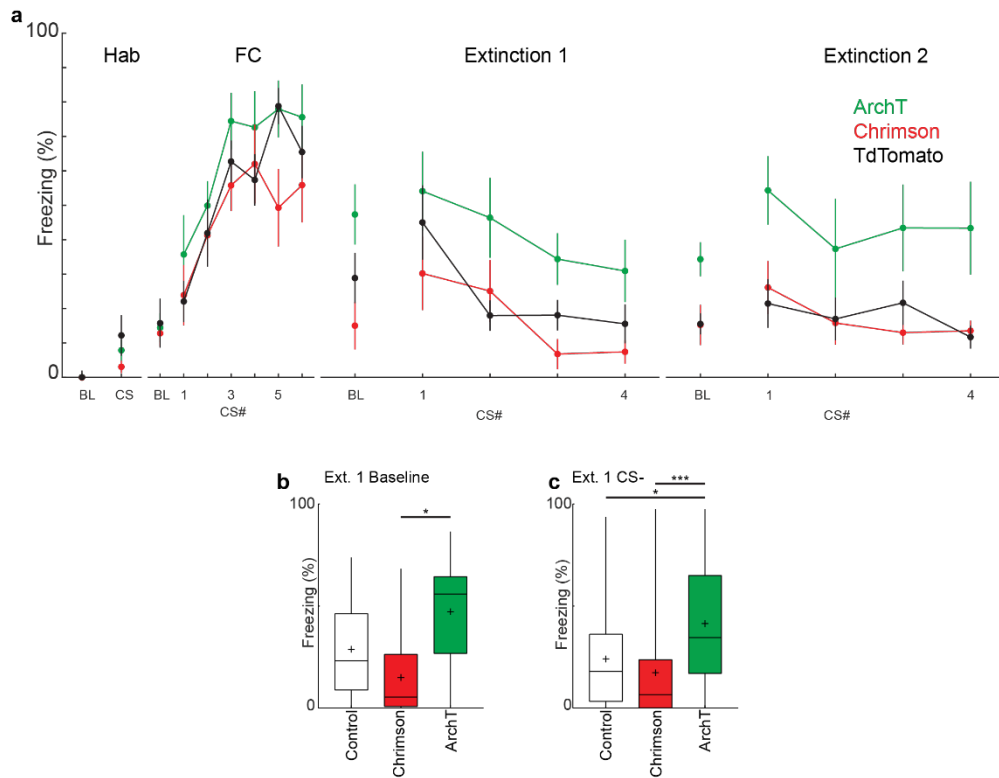


Fig. 20: Inhibition of cholinergic PPT fibers in MGB during fear conditioning leads to a high fear state.

a. Percentage of time spent freezing during 2 minutes baseline (BL) or during CS- presentations. TdTomato control (N = 11, black), Chrimson (N = 10, red) and ArchT (N = 9, green). **b.** Percentage of time spent freezing during the baseline of fear recall (Ext. 1). Control (N = 11), Chrimson (N = 10), ArchT (N = 9). Boxplots represent median, 2nd, 3rd quartile, minimum and maximum. Cross indicates mean. Kruskal-Wallis test $p < 0.05$ followed by Dunn's multiple comparisons test. **c.** Average freezing during the 4 CS- presentations on Ext. 1. Control (N = 11), Chrimson (N = 10), ArchT (N = 9). Boxplots represent median, 2nd, 3rd quartile, minimum and maximum. Cross indicates mean. Kruskal-Wallis test $p < 0.05$ followed by Dunn's multiple comparisons test. * and *** indicate $p < 0.05$ and $p < 0.001$ respectively.

Contrary to the inhibition, the activation of these cholinergic fibers led to slightly reduced freezing levels during extinction 1 suggesting an impairment in learning (**Fig. 19c, d, f**). This small decrease in freezing can also be observed in the baseline period and in response to the CS-, albeit not significantly (**Fig. 20b, c**). The decrease in freezing levels when PPT cholinergic fibers are activated and increase in freezing when these same fibers are inhibited suggests a bidirectional effect for cholinergic modulation of fear learning (**Fig. 19e**). These results show that the cholinergic inputs from PPT to MGB modulate the animals' state with a decrease in cholinergic activity leading to a higher fear state whereas an increase in cholinergic activity leads to a lower fear state.

5.3. Cortical feedback is not driving the plasticity in MGB

MGB sends projections to the auditory cortex however, layer 6 of the auditory cortex sends feedback to MGB. What role does this feedback play in auditory fear conditioning and how does it influence neuronal activity in MGB?

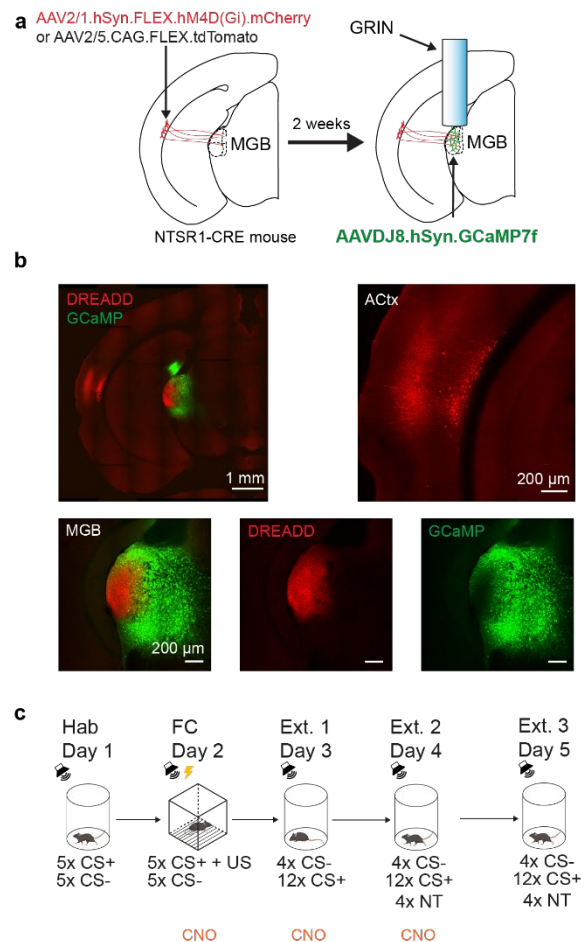


Fig. 21: Inhibition of cortical feedback during auditory fear conditioning.

a. Schematic of experimental procedure. A cre-dependent inhibitory DREADD or control fluorophore was injected in auditory cortex of NTSR1-Cre mice. Two weeks later a GCaMP7f was injected in MGB immediately followed by the GRIN lens implantation. **b.** Confocal images of virus expression. Top left overview of left hemisphere with DREADD expressed in layer 6 of auditory cortex and fibers found in MGB along with GCaMP. Top right, DREADD expression in auditory cortex. Bottom left, GCaMP and fibers from ACTx in MGB. Bottom center, fibers from ACTx. Bottom right GCaMP in MGB. **c.** Schematic of experimental paradigm. CNO was injected 45-60 minutes before the session on FC, Ext. 1 and Ext. 2 days. At the end of the Ext. 2 and a third extinction day (Ext. 3) without CNO, a neutral tone (NT) was presented 4 times to compare the effects of CNO on tone responses.

To answer these questions, we used NTSR1-Cre mice that have CRE expressed specifically in layer 6 of the cortex, therefore in the cells which project back to the MGB. By expressing an inhibitory DREADD in these cells, it was possible to inhibit the cortical feedback whilst recording neuronal activity in MGB (**Fig. 21a, b**). To see whether these cells had an effect during the paradigm we inhibited them during the acquisition (fear conditioning), recall (Ext.1) and extinction (Ext. 2) (**Fig. 21c**). To also check for any intrinsic effects of the CNO itself we presented the mice with neutral tones (NT) at the end of Ext. 2 with CNO and at the end of a third extinction day (Ext. 3) without CNO (**Fig. 21c**).

We found that inhibition of cortical feedback did not have an effect on the freezing levels of mice during the auditory fear conditioning and extinction paradigm (**Fig. 22a**). This inhibition did not have an effect on the percentage of cells that were responsive to the CS+ (**Fig. 22b**).

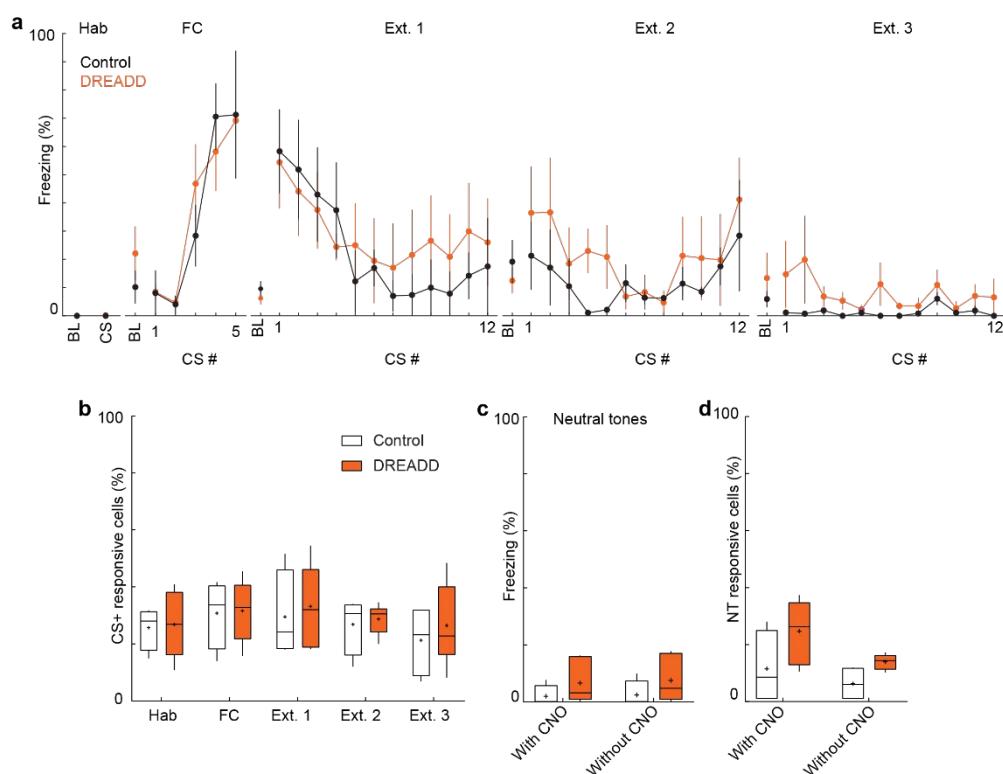


Fig. 22: Inhibition of cortical feedback does not alter behavior nor tone responses.

a. Percentage of time spent freezing during 2 minutes baseline (BL) or during CS+ presentations. TdTomato control (N = 4, black), Inhibitory DREADD (N = 6, orange). **b.** Percentage of cells responsive to the CS+ on individual days. There was no significant difference between control (N = 4, white) and DREADD group (N = 6, orange) Boxplots represent median, 2nd, 3rd quartile, minimum and maximum. Cross indicates mean. 2-way ANOVA $p > 0.05$. **c.** Percentage of time spent freezing to the neutral tone in the presence or absence of CNO. Boxplots represent median, 2nd, 3rd quartile, minimum and maximum. Cross indicates mean. 2-way ANOVA $p > 0.05$. **d.** Percentage of cells responsive to the neutral tone in the presence or absence of CNO. Boxplots represent median, 2nd, 3rd quartile, minimum and maximum. Cross indicates mean. 2-way ANOVA $p > 0.05$.

We also found that the CNO itself did not have an effect on neuronal responses, as there was no difference in freezing nor any difference in proportion of responsive cells (**Fig. 22c, d**).

On the fear conditioning day, we found that the average response was not altered by inhibition of cortical feedback (**Fig. 23a**) and the proportion of cells responsive to the different stimuli or combination of stimuli were also similar between animals with and without inhibition of cortical feedback (**Fig. 23b**, 2-way ANOVA $p > 0.05$).

Using the same clustering approach as previously described, we found that the wide range of plasticity profiles in response to the CS+ was conserved when cortical feedback was inhibited (**Fig. 23c**, 2-way ANOVA $P > 0.05$). Similarly, there were no differences observed for the intraday US plasticity (**Fig. 23d**). This suggests that cortical feedback to MGB is not necessary for associative auditory fear learning nor is it the driver for the plasticity previously observed in MGB.

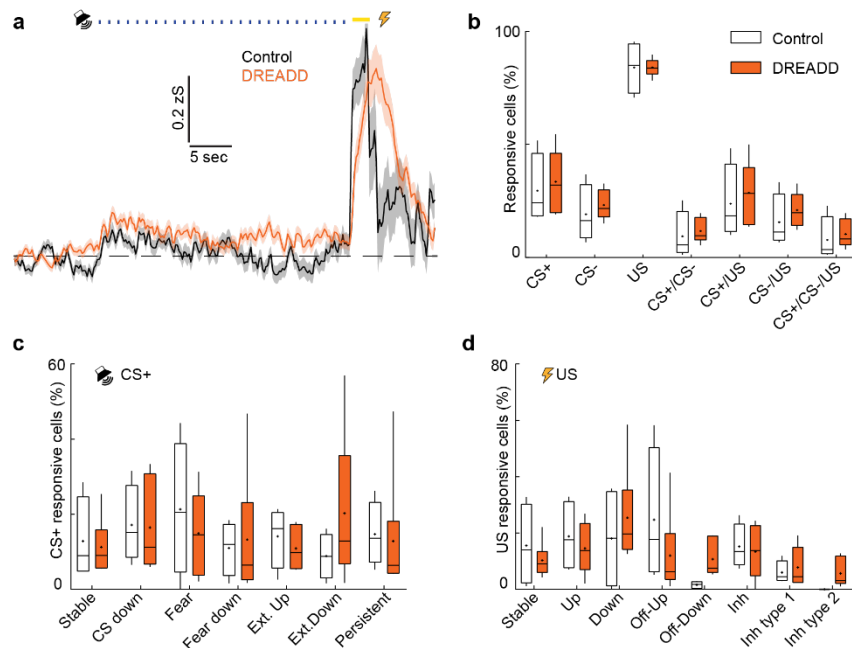


Fig. 23: Inhibition of cortical feedback does not influence plasticity in MGB.

a. Mean MGB population activity \pm s.e.m in response to CS+ and US stimuli of control (black, N = 4 mice) and DREADD animals (orange, N = 6 mice). **b.** Proportion of CS +, CS-, US and mixed selectivity CS \pm /US responsive neurons for control animals and DREADD animals. Boxplots represent median, 2nd, 3rd quartile, minimum and maximum. Cross indicates mean. 2-way ANOVA $p > 0.05$. **c.** Proportion of individual plasticity groups within CS + responsive cells / animal. Boxplots represent median, 2nd, 3rd quartile, minimum and maximum. Cross indicates mean. (2-way ANOVA, $p > 0.05$, N = 4 mice for control mice and N = 6 for DREADD mice). **d.** Proportion of individual plasticity groups within US responsive cells / animal. Boxplots represent median, 2nd, 3rd quartile, minimum and maximum. Cross indicates mean. (2-way ANOVA, $p > 0.05$, N = 4 mice for control mice and N = 6 for DREADD mice).

We also tested whether inhibition of cortical feedback had an effect on the encoding of the CS+. For this, the analysis previously performed was used during early extinction 1. We found that when the animal was in a high fear state, there were similar levels of non-adapting and adapting cells with the ramp-up cells being the most prevalent (**Fig. 24a**, 2-way ANOVA $p > 0.05$).

The analysis of the ramp-up cells across days showed that inhibiting cortical feedback did not change their proportions and that their numbers mirrored freezing behavior (**Fig 24b**). Overall, this suggests that the feedback MGB receives from auditory cortex does not influence the encoding of the CS+.

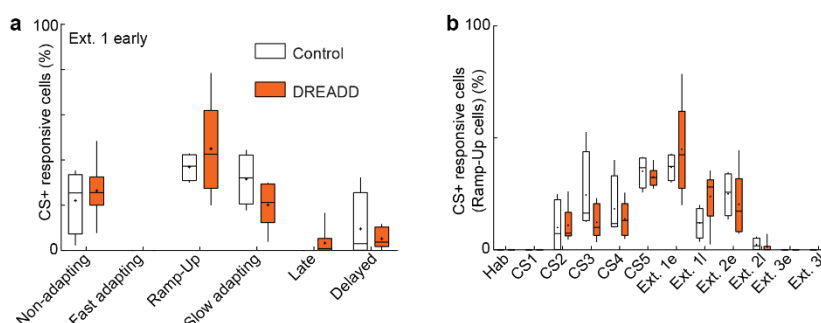


Fig. 24: Inhibition of cortical feedback does not alter the CS+ encoding.

a. Proportion of individual response type groups within CS+ responsive cells/animal on early extinction 1. Boxplots represent median, 2nd, 3rd quartile, minimum and maximum. Cross indicates mean (2-way ANOVA, $p > 0.05$, $N = 4$ mice for control mice and $N = 6$ for DREADD mice). **b.** Proportion of ramp-up cells within CS+ responsive cells/animal. Boxplots represent median, 2nd, 3rd quartile, minimum and maximum. Cross indicates mean (2-way ANOVA, $p > 0.05$, $N = 4$ mice for control mice and $N = 6$ for DREADD mice).

5.4. Discussion

The aim of this chapter was to explore the role of some of the inputs into MGB. Acetylcholine has previously been shown to play a key role in modulating associative fear learning but through the basal forebrain-amygdala pathway. With MGB receiving strong cholinergic input from PPT, we looked at the role of this pathway by optogenetically modulating PPT→MGB fibers during fear conditioning. There was a bidirectional effect with the inhibition of this pathway leading to increased freezing and activation of this pathway leading to decreased freezing. These changes in freezing were not specific to the CS+ as the inhibition led to increased freezing during the CS- and baseline periods indicating that the animal is in a higher fear state in general and not specifically to the associated tone. This suggests that cholinergic drive to MGB is essential for modulating the anxiety levels of mice. High acetylcholine levels

lead to a low fear state whereas low acetylcholine levels lead to a high fear state. This is the role of just one of the inputs to MGB. We also looked at the role of cortical feedback to MGB.

The corticocentric view would suggest that the plasticity observed in MGB is due to the feedback it receives from layer 6 of auditory cortex. Using NTSR1-CRE mice and chemogenetics it was possible to inhibit these cells specifically during auditory fear conditioning and recall. We found that the feedback from auditory cortex was not the driver of the plasticity observed in MGB. The paradigm used here is with pure tones and it would be expected that with more complex sounds the role of the auditory cortex, and the feedback to MGB, would be more pivotal than with pure tones^{80,91}.

The fact that inhibition of auditory cortex does not seem to have an effect on MGB coding and plasticity leads to the question of what role these cells play in auditory fear conditioning. To answer this question, it would be possible to inject a cre-dependent GCaMP in the auditory cortex of NTSR1-cre mice and either image directly the soma of these cells or, using a fiberscope, image the fibers in MGB.

Here we looked at two of the inputs that MGB receives but it would also be of interest to look at more of the inputs such as the inferior colliculus, which is one synapse down in the auditory pathway and is at the core of the input drive to MGB⁹². The IC has already been studied upon auditory fear conditioning and it was found that the CS+ encoding was changed between pre and post conditioning when the tone was paired with the US. These changes were not observed when the CS+ was unpaired from the US⁹³. The changes in CS+ encoding observed throughout the fear conditioning paradigm in MGB could be due to a change in the information received from IC. To test this, it would be possible to perform an all-optical approach which would allow us to record MGB neurons whilst inhibiting the incoming IC fibers.

Another thalamic nucleus of interest is the TRN which send inhibitory inputs to MGB which itself receives inputs from the amygdala thus creating an indirect feedback loop between the amygdala and MGB. Activation of this pathway leads to an increase in sound response in MGB⁹⁴. This would therefore suggest that TRN could play a key role in auditory fear conditioning in providing feedback to MGB.

Overall, we have shown that MGB receives diverse information from various inputs. MGB integrates this information and sends it towards its output pathways. One of the most important output pathways for auditory fear conditioning is the amygdala. In the next chapters, we will explore the role of these MGB→Amygdala projectors (MGB→BLA) during auditory fear conditioning.

Chapter 6. Medial geniculate body projections to amygdala not an enriched line

6.1. Introduction

We have previously shown that on the single cell level there is no difference in plasticity between the different subdivisions of MGB. Higher order MGBm neurons project to different output targets including primary and secondary auditory cortex, striatum and the basolateral amygdala^{95–98}. Enrichment of plastic neurons in the MGB→BLA pathway might be crucial for fear learning, given BLA's key role in aversive memory formation⁹⁹.

6.2. Anatomical distribution of MGB→BLA neurons

To start understanding the role of MGB→BLA neurons, we looked at the anatomical distribution of these cells using a retrograde approach. Similar to previous reports¹⁰⁰, we found BLA-projecting MGB neurons to be typically located in higher order MGB areas and particularly enriched in the medial subdivision of MGB (**Fig. 25a, b**, MGBm, 70 ± 7 vs. $23 \pm 6\%$ dorsal, MGBd or $7 \pm 3\%$ ventral, MGBv).

By-and-large, 30% of MGBm and 10% of MGBd neurons were amygdala-projecting (**Fig. 25c**). In contrast, only a small fraction of MGBv neurons (2%) were retrogradely traced from the amygdala. Furthermore, $85 \pm 2\%$ of amygdala-projecting MGB neurons (**Fig. 25d**, $N = 6$ mice) were positive for the higher-order MGB area marker calretinin⁴⁹, suggesting that calretinin is a highly prevalent but not exclusive marker of BLA-projecting MGB neurons.

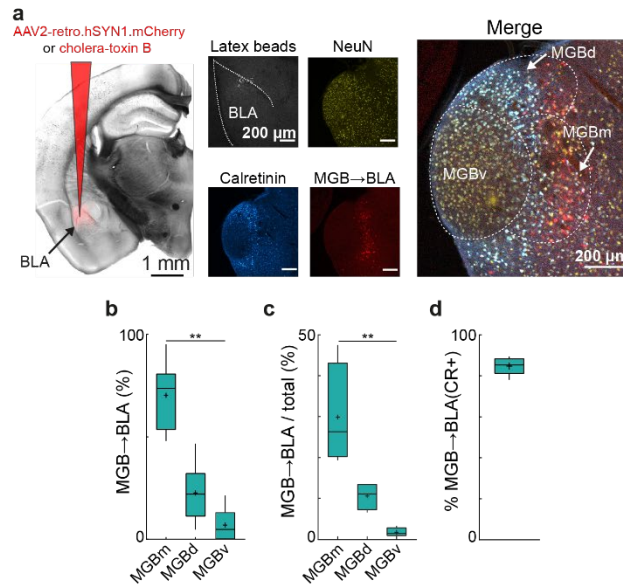


Fig. 25: Anatomical distribution of amygdala projecting neurons in MGB.

a. Injection of AAV2-retro.hSyn1.mCherry.WPRE.hGHp(A) and latex beads in the basolateral amygdala (BLA). MGB was counterstained for calretinin (cyan) and NeuN (yellow) to quantify the BLA projectors (red). **b.** Distribution of BLA-projecting neurons within MGB ($N=6$ mice, Friedman test $p < 0.001$, followed by Dunn's multiple comparisons test %MGBm vs. %MGBv, $p = 0.0016$). Boxplots represent median, 2nd, 3rd quartile, minimum and maximum. Cross indicates mean. **c.** Region-specific proportion of BLA-projecting neurons within MGB subdivisions ($N=4$ mice, Friedman test, $p < 0.01$, followed by Dunn's multiple comparisons test, %MGBm vs. %MGBv, $p = 0.014$). Boxplots represent median, 2nd, 3rd quartile, minimum and maximum. Cross indicates mean. **d.** Proportion of calretinin-positive BLA-projecting neurons ($N=4$ mice). Boxplots represent median, 2nd, 3rd quartile, minimum and maximum. Cross indicates mean.

Using a double viral approach including axon.GCaMP6f allowing us to fully label the axons of the MGB→BLA neurons, it was found that these neurons send collaterals to the auditory cortex and in particular layer 1 (**Fig. 26**).

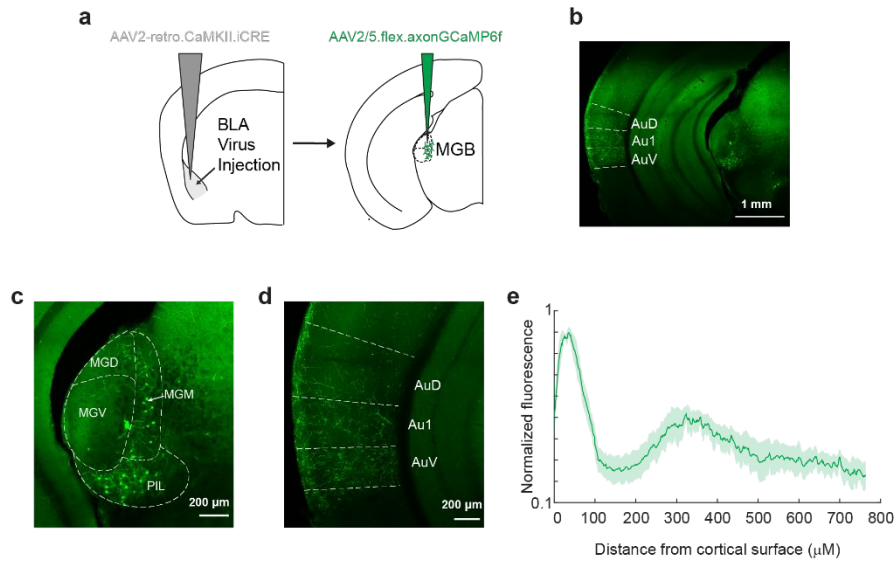


Fig. 26: MGB→BLA neurons send collaterals to auditory cortex.

a. Schematic of tracing approach. b. Overview confocal microscopy image of stained neurons and axons. c. Magnification of MGB from b. d. Magnification of auditory cortex from b. e Average fluorescence \pm s.e.m. across auditory cortex ($n = 3$ slices / mouse, $N = 3$ mice).

6.3. MGB→BLA plastic but not enriched.

To test the physiological function and neuronal activity of amygdala-projecting MGB neurons in fear learning, we used a retrograde virus approach to specifically express GCaMP6f in MGB→BLA-projectors (**Fig. 27a, b**).

On average, we could identify 69 ± 9 BLA-projecting GCaMP6f-positive MGB neurons per mouse (**Fig. 27c**, $N = 6$ mice). Similar to the total MGB population average response (**Fig. 3b**), MGB→BLA projectors were activated by the CS+ and the US (**Fig. 27d**). Across animals, $22 \pm 5\%$, $10 \pm 2\%$ or $68 \pm 7\%$ of neurons were responsive to the CS+, CS- or US, respectively. These proportions are comparable to the total MGB population (**Fig. 27e**, 2-way ANOVA, $p > 0.05$). Furthermore, we did not find that combinations of CS+, CS- and US coding neurons were enriched above chance levels (**Fig. 27f**).

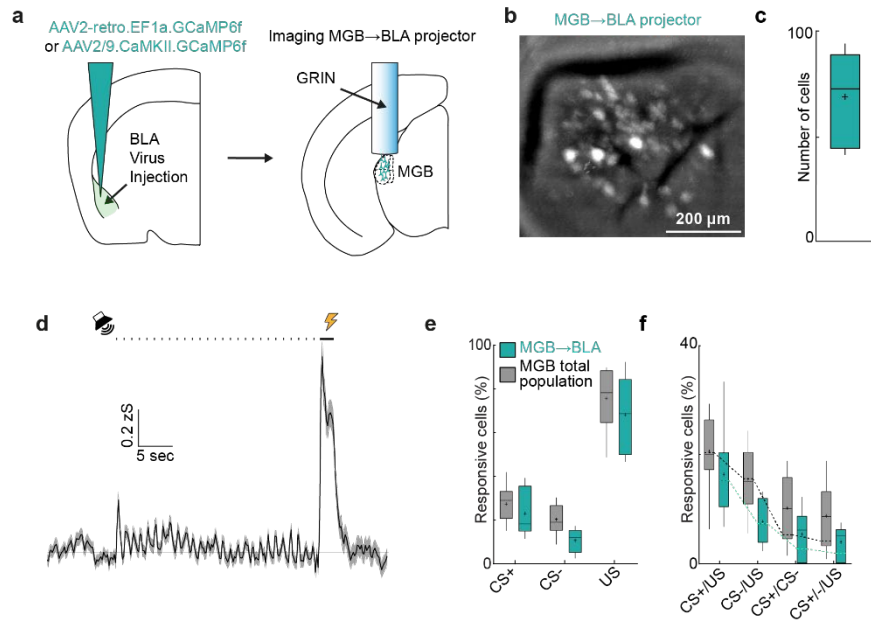


Fig. 27: MGB→BLA responses to CS and US stimuli.

a. Schematic of viral strategy and location of GRIN lens in MGB to image neuronal activity of MGB→BLA-projecting neurons. **b.** MGB field of view with MGB→BLA-projecting neurons. Replicated in all animals that underwent calcium imaging ($N = 6$ mice). **c.** Number of identified individual components per animal (69 ± 9 , $N = 6$ mice). **d.** Mean \pm s.e.m population response of one example animal to the CS+ and US. Black dots indicate CS+ tone pips. Bar indicates shock US. Boxplots represent median, 2nd, 3rd quartile, minimum and maximum. Cross indicates mean. **e.** Proportion of CS+, CS- and US responsive neurons for the total MGB population and amygdala-projecting neurons (2-way ANOVA, main effect group, $F_{(1,13)} = 3.3$, $p > 0.05$, $N = 9$ total MGB population mice and $N = 6$ MGB→BLA projection neurons mice). Boxplots represent median, 2nd, 3rd quartile, minimum and maximum. Cross indicates mean. **f.** Proportion of mixed selectivity CS± and US coding neurons for the total MGB population and amygdala projecting neurons 2-way ANOVA, $F_{(1,13)} = 3.9$, $p > 0.05$, $N = 9$ mice for the total MGB population and $N = 6$ mice for the population of MGB→BLA projection neurons. Boxplots represent median, 2nd, 3rd quartile, minimum and maximum. Cross indicates mean. Dotted lines indicate chance overlap level.

Using a cluster analysis approach, we found the same subgroups of CS+ plasticity types in the subpopulation of MGB→BLA projecting neurons (**Fig. 28a**) across the conditioning paradigm, including stable cells, onset-down cells, CS-down cells, fear cells, fear-inhibited cells, extinction up cells, extinction down cells as well as persistent cells. The proportions of the CS+ plasticity subgroups were similar to the total population in MGB (2-way ANOVA, $p > 0.05$). Analogous to the CS+ representation across days, we found comparable proportions of US plasticity types in MGB→BLA projectors when compared to the total population (**Fig. 28b**; 2-way ANOVA, $p > 0.05$).

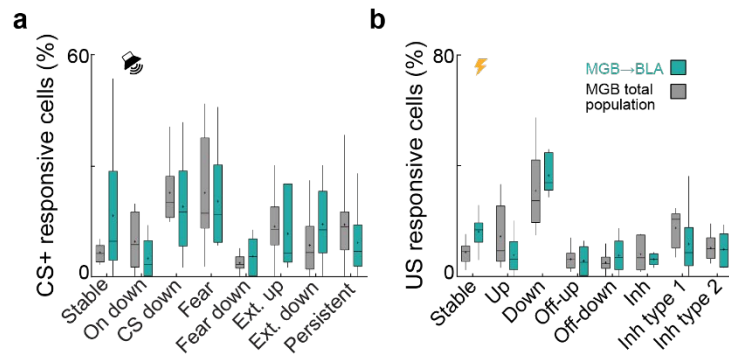


Fig. 28: Plasticity of MGB→BLA neurons.

a. Proportion of individual plasticity groups within CS+ responsive cells / animal (2-way ANOVA, $F_{(1,13)} = 1.2$, $p > 0.05$, $N = 9$ mice for the total MGB population and $N = 6$ mice for the population of MGB→BLA projection neurons). Boxplots represent median, 2nd, 3rd quartile, minimum and maximum. Cross indicates mean. **b.** Proportion of individual plasticity groups within US responsive cells / animal (2-way ANOVA, $F_{(1,13)} = 0.5$, $p > 0.05$, $N = 9$ mice for the total MGB population and $N = 6$ mice for the population of MGB→BLA projection neurons). Boxplots represent median, 2nd, 3rd quartile, minimum and maximum. Cross indicates mean.

This data demonstrates that CS as well as US information is encoded by BLA-projecting MGB neurons, identifying MGB→BLA projectors not only as a source of CS tone inputs but also as a strong source of aversive US signals. However, CS and US plasticity is functionally diverse beyond response potentiation and, compared to the total MGB population, CS and US signaling is not enriched in this specific subpopulation of amygdala-projecting MGB neurons.

6.4. Ramp-Up cells in MGB→BLA neurons

We next looked at the CS+ encoding when the animals were in a high fear state (early extinction 1). The proportions of CS+ responsive groups were similar between the MGB total population and the MGB→BLA neurons (**Fig. 29a**, 2-way ANOVA, $p > 0.05$). On average $36 \pm 5\%$ of MGB→BLA CS+ responsive neurons showed ramp-up activity on early extinction 1 making it the largest group. We therefore observed the proportion of these neurons across days and found a similar proportion of CS+ responsive cells showing ramp-up activity across days compared to the total MGB population (**Fig. 29b**, 2-way ANOVA $p > 0.05$).

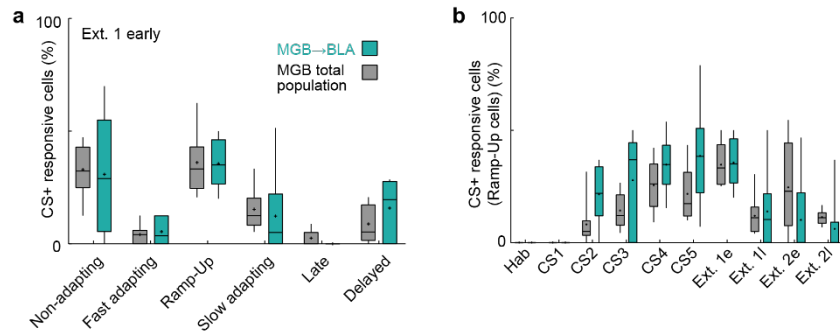


Fig. 29: MGB→BLA neurons show similar CS+ encoding to total MGB population.

a. Proportion of individual response type groups within CS+ responsive cells/animal on early extinction 1 (2-way ANOVA, $p > 0.05$, $N = 9$ mice the total MGB population and $N = 6$ mice for the population of MGB→BLA projection neurons). Boxplots represent median, 2nd, 3rd quartile, minimum and maximum. Cross indicates mean. **b.** Proportion of ramp-up cells within CS+ responsive cells/animal across days (2-way ANOVA, $p > 0.05$, $N = 9$ mice the total MGB population and $N = 6$ mice for the population of MGB→BLA projection neurons). Boxplots represent median, 2nd, 3rd quartile, minimum and maximum. Cross indicates mean.

This data demonstrates that the CS+ encoding is similar between the total MGB population and the subpopulation of amygdala-projecting neurons.

6.5. Discussion

Given the known prominent role of the amygdala in associative fear learning, the study of the MGB projections to amygdala is essential to better understand the fear circuitry. This cell specificity allows us to go beyond the subdivision of MGB studied previously (see **Fig. 11**) even though these cells are found in majority in higher order areas of MGB. The aim of this chapter was to look at the neuronal responses of MGB→BLA neurons upon auditory fear conditioning. We hypothesized that these amygdala-projectors would show enhanced plasticity compared to total MGB population as the amygdala is often regarded as the center for fear learning.

To test this hypothesis, we used a retrograde viral approach which allowed us to specifically image the MGB→BLA neurons, distinguishing them from the general population. Surprisingly, it was found that the proportion of plastic neurons was not enhanced in MGB→BLA neurons and was in fact similar to the proportion of plastic neurons in the total MGB population. This was the case for the intraday US plasticity as well as for the across day CS+ plasticity. It was also observed that the CS+ encoding was similar between the total MGB population and the subpopulation of amygdala-projection neurons. This lack of enrichment of neurons with dedicated functions in associative learning suggests that MGB→BLA neurons is most likely not a labelled line, but that MGB propagates experience-dependent changes of neuronal activity in associative fear learning to a wider brain network such as the auditory cortex and

striatum⁹⁵. This finding can be compared to recent studies involving the amygdala and the striatum^{101,102}. In both of the studies, it was found that heterogeneous behavior-related neural activity of projection neurons of amygdala or striatum is broadcast simultaneously and in parallel to different downstream targets irrespective of the output pathway. In this case, this broadcasting might be achieved by the same subsets of individual MGB neurons as we showed that MGB→BLA neurons also project to the auditory cortex confirming the results of previous studies^{92,103}.

Given that the microcircuitry of the amygdala has been well-studied within the context of auditory fear conditioning it would be of interest to study more specifically the MGB neurons that project to specific parts of the microcircuitry perhaps using a cre-dependent retrograde virus in Somatostatin-Cre, vasoactive intestinal peptide -Cre or Parvalbumin-Cre mice^{20,21}. This would enhance our understanding of both the role these inhibitory interneurons play in auditory fear conditioning but also the role of these amygdala projectors.

We have explored the role of individual MGB→BLA neurons upon associative fear learning and found that these cells were plastic. We will next explore what effect their manipulation has on the animals' behavior during auditory fear conditioning and the wider role they play in the fear circuit.

Chapter 7. Medial geniculate body projections to amygdala are necessary for learning and for neuronal stability

7.1. Introduction

The amygdala is regarded as the center for auditory fear conditioning⁵⁸, therefore the result showing that there was no enhanced plasticity in MGB→BLA neurons compared to total MGB population is somewhat surprising and argues for a more distributed coding of auditory fear conditioning. The aim of this chapter is to further understand the role of these amygdala-projecting neurons by optogenetically manipulating them.

7.2. MGB→BLA neurons are necessary for associative learning

To understand the role of MGB→BLA neurons, we bilaterally manipulated them by specifically expressing an inhibitory opsin ArchT, an excitatory opsin Chrimson or a control fluorophore in MGB→BLA projection neurons (**Fig. 30a, b**). Inhibition and activation of MGB→BLA projectors during CS-US pairing on the conditioning day (**Fig. 30c**) had no effect on fear acquisition (**Fig. 30d**). However, freezing levels were significantly reduced during the fear test 24 h later when these neurons were inhibited (**Fig. 30d**, mean freezing during the first four CS+, Control: $46 \pm 5\%$, N = 17 mice; MGB→BLA ArchT: $22 \pm 5\%$, N = 9 mice and Chrimson: $45 \pm 5\%$, N = 8 mice; $p < 0.05$, Kruskal-Wallis test followed by Dunn's multiple comparisons test.), indicating that activity in MGB→BLA projectors is necessary for the consolidation of fear memories.

The activation of these neurons did not lead to enhanced freezing nor a reduction in freezing (**Fig. 30d**). It is possible that there is a ceiling effect and that activation of these neurons could lead to an increase in freezing if a weaker footshock was presented as the freezing does increase faster during the FC day compared to control.

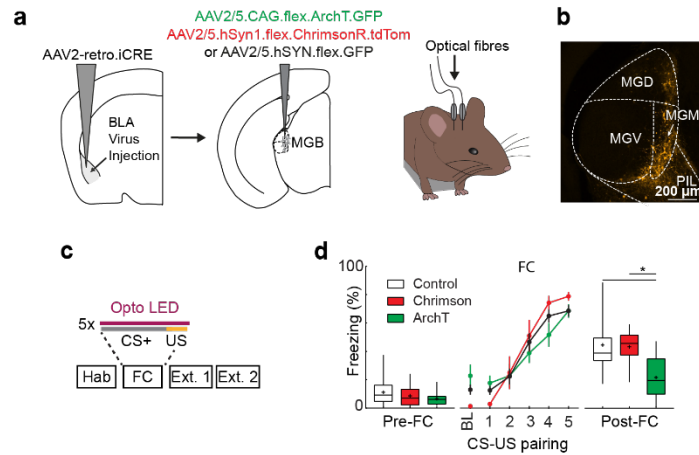


Fig. 30: Optogenetic manipulation of MGB→BLA neurons.

a. Schematic of experimental approach to optogenetically manipulate MGB→BLA neurons specifically. **b.** Confocal image of MGB with MGB→BLA neurons stained. **c.** Schematic of experimental paradigm. The optogenetic LED was activated 2 seconds before the CS+ presentation and turned off 2 seconds after the end of the US presentation for a total of 36 seconds. **d.** Freezing to the CS+ pre-FC (habituation), during the fear conditioning day and post-FC. Control (white) N = 17, Chrimson (red) N = 8 and ArchT (green) N = 9. Boxplots represent median, 2nd, 3rd quartile, minimum and maximum. Cross indicates mean. Kruskal-Wallis test $p < 0.05$ followed by Dunn's multiple comparisons test. * indicates $p < 0.05$.

Having found that manipulation of the MGB→BLA neurons leads to changes in the animal behavior during an auditory fear conditioning paradigm it was of interest to explore how these manipulations affect the MGB neuronal activity upon fear conditioning.

7.3. Manipulation of MGB→BLA neurons leads to changes in US adaptation

To further understand the role of these neurons and their role in the fear circuit, we performed an all-optical imaging approach. This allowed us to simultaneously image MGB neurons whilst also optogenetically manipulate MGB→BLA neurons (**Fig. 31a-c**). Contrary to the bilateral manipulation, this unilateral approach did not change the freezing levels of the animals across the fear learning and extinction paradigm (**Fig. 31d**). Given that MGB→BLA neurons represent only a fraction of the total MGB neuronal population ($11 \pm 2\%$ in total MGB, N = 4 mice, see also **Fig. 25c**), manipulation of these neurons during the CS-US pairing did not affect the mean CS+ and US responses of the total imaged MGB population (**Fig. 31e**). Neither did it affect the proportion of CS, US or mixed selectivity responsive cells (**Fig. 31f**).

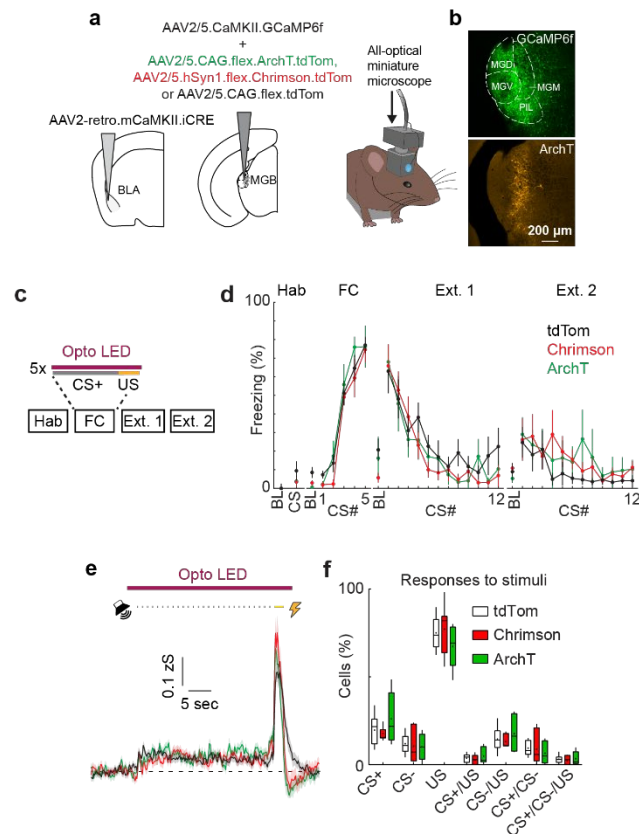


Fig. 31: All-optical activity recording of MGB and manipulation of MGB→BLA neurons.

a. Schematic of viral approach. A retrograde cre was injected in BLA. A cre-dependent opsin or control fluorophore was injected in MGB and GCaMP was injected in MGB allowing for simultaneous recording of MGB neurons and optogenetics manipulation of MGB→BLA neurons. **b.** Confocal images of cre-dependent ArchT in MGB→BLA neurons and GCaMP in all MGB neurons. **c.** Schematic of fear conditioning and extinction paradigm. MGB→BLA neurons were manipulated during the CS-US pairings with the opto LED starting 2 seconds prior to the CS+ and finishing 2 seconds after the end of the US. **d.** Percentage of time spent freezing during 2 minutes baseline (BL) or during CS+ presentations. TdTomato control (tdTom, black, N = 9 mice), Chrimson (red, N = 7 mice) and ArchT (green, N = 6 mice). **e.** Mean MGB population activity \pm s.e.m in response to CS+ and US stimuli upon optogenetic light presentation of tdTomato (black, N = 9 mice), Chrimson (red, N = 7 mice) and ArchT (green, N = 6 mice). **f.** Proportion of CS+, CS-, US and mixed selectivity CS \pm /US responsive neurons for tdTomato control (tdTom, white, N = 9 mice), Chrimson (red, N = 7 mice) and ArchT (green, N = 6 mice). Boxplots represent median, 2nd, 3rd quartile, minimum and maximum. Cross indicates mean. 2-way ANOVA $p > 0.05$.

To further understand how inhibition of MGB→BLA neurons could prevent consolidation of the learned behavior, we looked more specifically at the learning and the US responses. We found that by manipulating the MGB→BLA neurons, there were changes in the adaptation to the US on the fear conditioning day (**Fig. 32a**). Indeed, under normal circumstances, with repeated CS-US presentations, there is adaptation to the US with the response becoming weaker with every US presentation (**Fig. 32, TdTom control**). To quantify this, the response of an activated cell was normalized to the strongest response found in the fear conditioning paradigm (**Fig. 32b**). For the control this meant that the 1st US response had a normalized response of 0.61 (\pm 0.08) and the last US response had a normalized response of 0.16 (\pm 0.07). When the

MGB→BLA neurons are inhibited, this adaptation is reduced (**Fig. 32, ArchT**) as the first US response had a normalized response of 0.61 (± 0.11) and the last US response was 0.41 (± 0.1) and to the opposite when these cells are activated this adaptation is enhanced. (**Fig. 32, Chrimson**) as the initial US response was of 0.72 (± 0.11) and the last US response was of 0.16 (± 0.07).

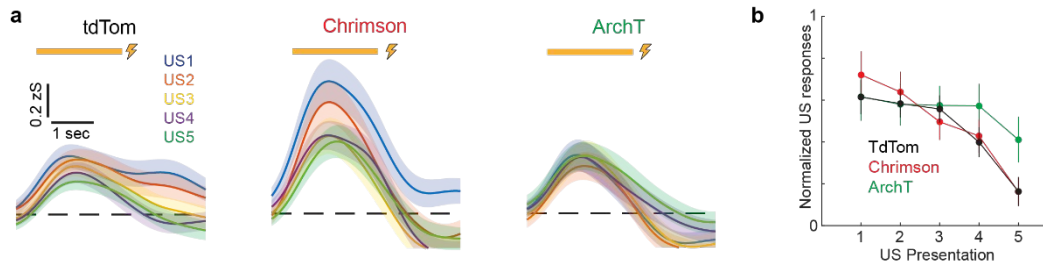


Fig. 32: Manipulation of MGB→BLA neurons leads to changes in US adaptation.

a. Average traces \pm S.E.M. of US responsive cells for individual US presentations (1st US: blue, 2nd US: Orange, 3rd US: Yellow, 4th US: Purple and 5th US: Green). From left to right, tdTomato control (tdTom, $n = 582$ cells from $N = 9$ mice), Chrimson ($n = 393$ cells from $N = 7$ mice) and ArchT ($n = 380$ cells from $N = 6$ mice). **b.** Quantification of the US response adaptation. US responses for each US activated cell were normalized to the strongest US response across the fear conditioning day. tdTomato control (tdTom, black, $n = 341$ cells from $N = 9$ mice), Chrimson (red, $n = 222$ cells from $N = 7$ mice) and ArchT (green, $n = 164$ cells from $N = 6$ mice).

Overall, we found that manipulations of MGB→BLA neurons does not influence the mean response to the CS+ or US of MGB neurons nor the proportion of responsive cells to the different stimuli or combination of stimuli. However, these manipulations lead to changes in US adaptation with inhibition of the MGB→BLA neurons leading to reduced adaptation of the US response whereas activation of the MGB→BLA neurons leads to increased adaptation of the US response. We will next explore whether these changes on the fear conditioning day influence the plasticity across days.

7.4. Manipulation of MGB→BLA neurons leads to aberrant plasticity in MGB

Given that manipulation of MGB→BLA neurons causes changes in adaptation to the US on the fear conditioning day, we looked to see the influence of these cells across the fear conditioning paradigm. We found that there were no significant differences in percentage of CS+ responsive cells across the fear conditioning and extinction paradigm (**Fig. 33a**). To look at how the CS+ responses may change across days we used the same clustering approach previously described.

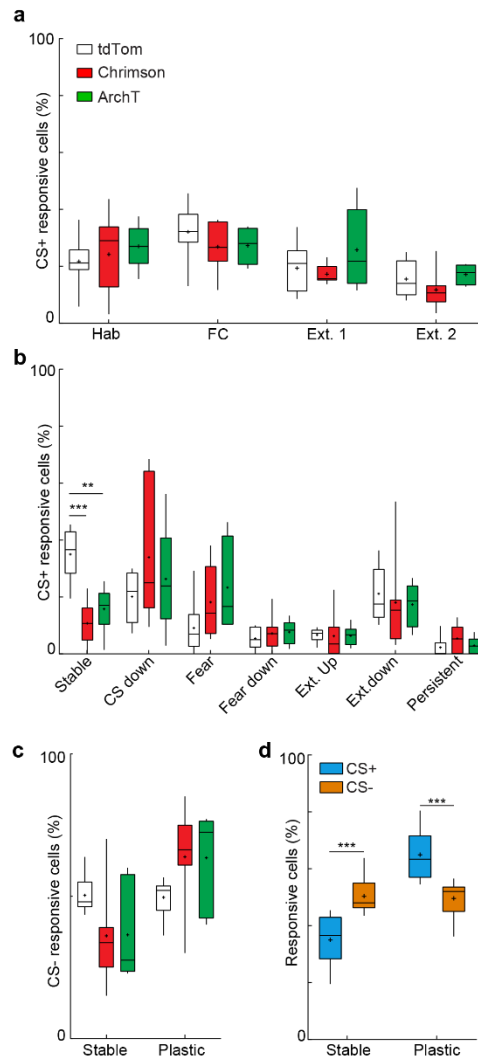


Fig. 33: Manipulation of MGB→BLA neurons causes aberrant plasticity in MGB.

a. Proportion of cells responding to the CS+ across days (tdTom, white, N = 9 mice; Chrimson, red, N = 7 mice and ArchT, green, N = 6 mice; 2-way ANOVA $p > 0.05$). Boxplots represent median, 2nd, 3rd quartile, minimum and maximum. Cross indicates mean. **b.** Quantification of CS+ plasticity subgroups in the tdTomato control (white, N = 9 mice), Chrimson (red, N = 6 mice) and ArchT neurons (green, N = 6 mice). 2-way ANOVA followed by Sidak's post hoc test, $p < 0.005$, ** and *** indicate $p < 0.01$ and 0.001 respectively. Boxplots represent median, 2nd, 3rd quartile, minimum and maximum. Cross indicates mean. **c.** Proportion of CS- responsive cells that are stable or plastic (tdTom, white, N = 9 mice; Chrimson, red, N = 7 mice and ArchT, green, N = 6 mice; 2-way ANOVA $p > 0.05$). Boxplots represent median, 2nd, 3rd quartile, minimum and maximum. Cross indicates mean. **d.** Proportion of cells which are stable or plastic in response to the CS+ or CS- in the tdTomato control group (N = 9 mice). Boxplots represent median, 2nd, 3rd quartile, minimum and maximum. Cross indicates mean. 2-way ANOVA followed by Sidak's post hoc test, $p < 0.005$, *** indicates $p < 0.001$.

Surprisingly, there were significantly fewer stable cells in the Chrimson ($11 \pm 3\%$) and ArchT ($16 \pm 3\%$) groups compared to the control tdTomato group ($35 \pm 3\%$) (**Fig. 33b**). Whilst there was not one plasticity group which was specifically enhanced in either the ArchT and Chrimson groups, these results show that by manipulating the MGB→BLA neurons on the fear conditioning day there is aberrant plasticity in response to the CS+ across days. We next looked to see if this effect was specific to the CS+ or if there was generalization. There was a

small increase in proportion of stable cells in response to the CS- in the control group compared to the other groups however this was not significant (tdTomato: $50 \pm 2\%$, Chrimson: $36 \pm 6\%$ and ArchT: $36 \pm 7\%$, 2-way ANOVA, $p > 0.05$), **Fig. 33c**). We next checked that the animals could differentiate between the associated tone and the control tone. We found that there were significantly more stable cells in responses to the CS- than to the CS+ (**Fig. 33d**). Therefore, suggesting that the effect seen is due to aberrant plasticity after manipulation of the MGB→BLA neurons and not due to the control animals not learning correctly.

These results suggest that manipulation of MGB→BLA neurons leads to aberrant plasticity in MGB. The inhibition of these neurons prevents the adaptation to the US, this could lead to abnormal responses in the fear circuit which prevents the animals from having overnight consolidation of the learned memory and lead to increased plasticity in MGB. The activation of these neurons leads to increased adaptation in response to the US, this could also enhance the responses in the fear circuit and in itself lead to increased plasticity in MGB and perhaps increased freezing to a weaker stimulus. To increase our understanding of this effect, further parts of the fear circuit can be explored. Looking at the CS+ encoding in MGB will also further our understanding.

7.5. Manipulation of MGB→BLA neurons does not alter the CS+ encoding

Manipulation of MGB→BLA neurons causes aberrant plasticity in response to the CS+ in MGB. To try to further understand what is happening in MGB we can explore the CS+ encoding as previously described.

For this, we looked at the CS+ encoding when the animals were in a high fear state (early extinction 1). The proportions of CS+ responsive groups were similar between the different groups (**Fig. 34a**, 2-way ANOVA, $p > 0.05$). The ramp-up cells represented one of the largest groups when the animal was in a high fear state. We therefore observed the proportion of these neurons across days and found a similar proportion of CS+ responsive cells showing ramp-up activity across days in the different groups (**Fig. 34b**, 2-way ANOVA, $p > 0.05$).

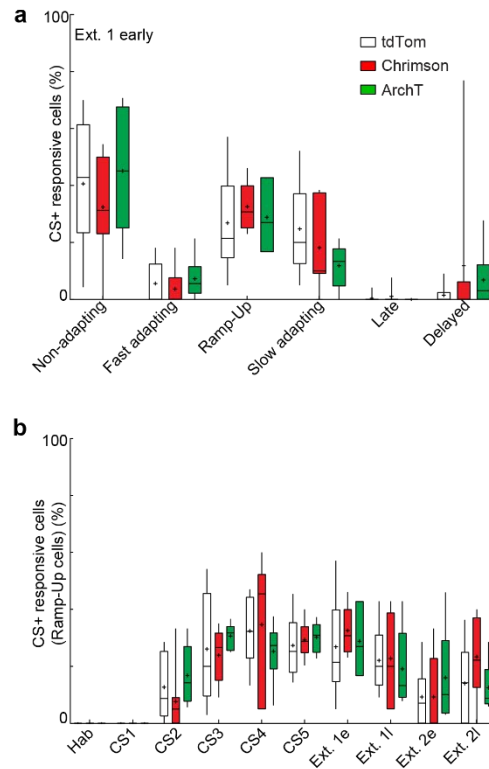


Fig. 34: MGB CS+ encoding is stable despite manipulations of MGB→BLA neurons.

a. Proportion of individual response type groups within CS+ responsive cells/animal on early extinction 1 (tdTom, white, N = 9 mice; Chrimson, red, N = 7 mice and ArchT, green, N = 6 mice; 2-way ANOVA $p > 0.05$). Boxplots represent median, 2nd, 3rd quartile, minimum and maximum. Cross indicates mean.

b. Proportion of ramp-up cells within CS+ responsive cells/animal across days (tdTom, white, N = 9 mice; Chrimson, red, N = 7 mice and ArchT, green, N = 6 mice; 2-way ANOVA $p > 0.05$). Boxplots represent median, 2nd, 3rd quartile, minimum and maximum. Cross indicates mean.

These results show that the CS+ encoding is similar between the different groups when the animal is in a high fear state and across days. Therefore, suggesting that the manipulation of MGB→BLA neurons does not perturb the CS+ encoding which remains stable.

7.6. Discussion

The aim of this chapter was to further understand the role of MGB→BLA neurons within the fear circuit by manipulating them during the fear conditioning paradigm.

Bilateral inhibition of these neurons led to a significant reduction in freezing levels in fear recall therefore suggesting that these cells are necessary for fear learning. This result is similar to another study where they inhibited calretinin positive cells in MGBm⁹². However, they also found that this inhibition led to reduced levels of freezing on the FC day. We found that whilst the vast majority of MGB→BLA neurons were calretinin positive, it was not an exclusive marker

for these neurons. This could explain the difference in results however, the strength of the conditioning protocol and the timing of the footshock could also explain this difference.

There was no bidirectional effect as activation of the MGB→BLA neurons did not lead to enhanced freezing. This could be due to a ceiling effect and it would be interesting to observe the animal's behavior with a milder footshock. Indeed, it has previously been shown that activation of inputs into BLA, from MGB and ACtx, were sufficient to induce learning⁹⁷. It is therefore likely that with a milder footshock the activation of the MGB→BLA neurons would lead to increased freezing compared to a control group.

We next used an all-optical approach allowing us to image total MGB population whilst simultaneously inhibiting or activating MGB→BLA neurons. It was found that inhibiting activity in the MGB→BLA feedforward pathway during fear conditioning led to decreased US adaptation. To the contrary the activation of MGB→BLA neurons led to an increase in US adaptation. These results could suggest that the US adaptation is necessary for learning as the information encoded in the US response is passed on to the CS+ response.

Surprisingly, both the activation and inhibition of this pathway led to enhanced, aberrant across-day single cell plasticity in the total MGB population. We can hypothesize that the modulation of the US adaptation leads to changes in the fear circuit that, via indirect feedback from the amygdala, leads to increased plasticity in MGB. When the MGB→BLA neurons are inhibited the teaching signal from the US is inhibited which leads to a compensatory mechanism in MGB and increased plasticity. When the MGB→BLA neurons are activated, it leads to increased adaptation to the US which therefore leads to increased plasticity in MGB as the information encoded in the US is passed to the CS+ but also the increased activity in the amygdala leads to greater feedback in MGB. This hypothesis can be further explored by looking at different aspects of the fear circuit. In this thesis, we already looked at cortical feedback which did not play a role in this paradigm therefore suggesting that the amygdala feedback to MGB could be coming via the reticular nucleus of the thalamus^{50,94}, which might be crucial to fine-tune single cell plasticity in MGB. This would further support the notion that distributed activity across brain areas and networks is necessary to stabilize neuronal plasticity and facilitate precise memory formation as well as behavioral output.

To further study this, it will be important to understand how this heterogeneous, widely distributed population code is established, then how this is interpreted by different downstream regions and understand how it is related to complex behavioral output. For this, simultaneous multi-site recordings¹⁰⁴, targeted activity-dependent neural manipulations¹⁰⁵ and computational neuroscience tools will be required.

Chapter 8. A plastic medial geniculate body which allows for stable representation of the sensory environment

8.1. Introduction

We have previously shown that on the single cell level MGB shows plasticity across learning. This creates a paradoxical situation whereby MGB can no longer perform its function for sensory coding as the cells are coding for the upcoming danger. We hypothesized that the answer to this paradox comes from the population level coding whereby the single cells code for the learnt behavior whilst the population codes for the sensory inputs. Using miniscope deep brain recordings allowed us to follow large numbers of MGB neurons and therefore look at the population coding of MGB.

8.2. Decoding of MGB population dynamics

We first tested if the CS+ and CS- can be decoded from Ca^{2+} activity based on MGB population activity. First, we trained a three-way quadratic decoder to distinguish between CS+, CS- and baseline activity within the same session (see methods). To balance for different cell population sizes between animals, we randomly sub-selected 40 cells for each animal and averaged decoder accuracy across 50 independent runs. Furthermore, to account for different numbers of CS+ and CS- presentations, we only decoded the first four CS+ and CS- presentations. Within each individual session, the decoders achieved high classification accuracy (**Fig. 35a**, >80% compared to 33% chance level) indicating a distinct representation of the individual CSs by the MGB population. Surprisingly, decoding accuracy was higher in the population of MGB→BLA projectors compared to the total MGB population, except for the fear conditioning day. To test if CS tones can be accurately detected across days from MGB population activity, we next trained sets of two-way decoders to distinguish between baseline and CS+ or CS- responses for each experimental day and tested the trained decoders across days (**Fig 35b**). Strikingly, we found that decoder accuracy is robust across days reaching decoding levels of ca. 70% or higher, for both the CS+ and the CS- (**Fig. 35b, c**). This suggests that on the population level MGB is stable across days for decoding of the auditory sensory environment. This is in contrast to amygdala population coding, where decoding levels for the CS+ drop to chance levels after fear conditioning²², indicating that the amygdala gets hijacked into a high fear state whereas MGB reliably encodes the different CSs. It is also worth noting however that there was a drop in decoder accuracy during the FC day (**Fig. 35a**) which

recovered on the subsequent days. This indicates that there are temporary changes in CS+ encoding during the associative learning.

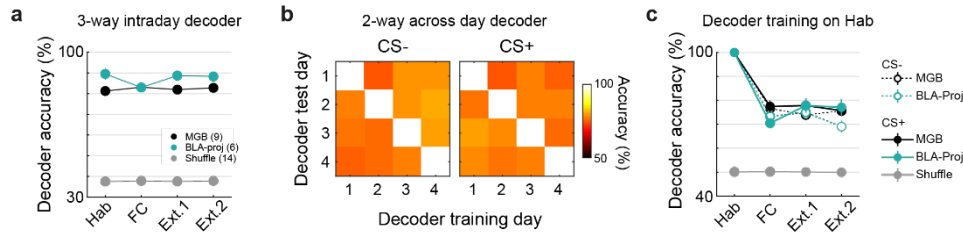


Fig. 35: MGB population dynamics can be stably decoded across days.

a. Intraday three-way decoder of CS+, CS- and baseline population responses in CaMKII-positive (black) and identified amygdala-projecting MGB neurons (turquoise) reached a minimum mean accuracy of 81% across animals. Decoder accuracy dropped to chance levels for decoders trained on randomly label training sets (data presented as mean values \pm s.e.m.). **b.** Intra- and across day accuracy of decoders trained on CS+ or CS- vs. baseline responses, respectively. 1: Hab, 2: FC, 3: Ext. 1, 4: Ext. 2. **c.** Quantification of intra and across day decoder accuracy for decoders trained on habituation day data. Mean decoder accuracy across days is $>70\%$ for CS+ and CS- population responses in CaMKII-positive and identified amygdala-projecting MGB neurons (MGB→BLA $N=6$ mice, MGB $N=9$ mice, data represent mean \pm s.e.m.).

8.3. Population vector distance

8.3.1 Transient plasticity in MGB and MGB→BLA neurons

Next, we compared the population vector distance (PVD) between the evoked population responses to the CS+ and CS- and the evoked population responses to the US (**Fig. 36a-d**). During fear conditioning, we found a decrease of the PVD between the CS+ and the US with consecutive CS-US pairings (**Fig. 36a**) for both the total MGB population as well as for MGB→BLA-projectors, indicating that the CS+ neuronal response was becoming more similar to the US neuronal response.

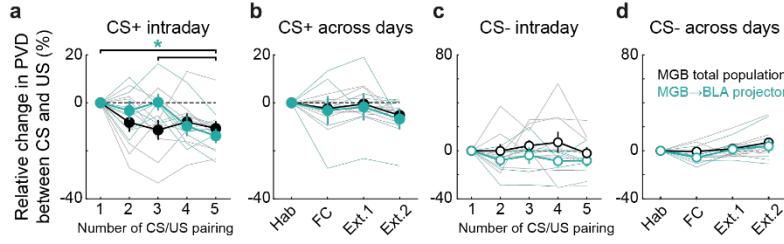


Fig. 36: MGB population vector distance is stable across days.

Relative change in Euclidean population vector distance between the CS+ (d, e) or CS- (f, g) and the US within the fear conditioning session (d, f) or across the individual days of the behavioral paradigm (e, g). Statistics: d: Friedman test across the relative change in CS+ to US PVD of MGB→BLA-projectors ($p < 0.01$), Dunn-Sidak multiple comparisons test 1st and 3rd vs. 5th CS/US pairing, $p < 0.05$. G: Friedman test across the relative change in CS- to US PVD of the total BLA-population ($p < 0.05$), Dunn-Sidak multiple comparisons test FC vs. Ext.2: $p < 0.05$. All other data sets in d-g: $p > 0.05$. MGB population: $N = 9$ mice, MGB→BLA-projectors: $N = 6$ mice (data represent mean \pm s.e.m.).

However, the time courses of the PVD change were different and only the MGB→BLA population reached a significant change in PVD at the end of the session indicating different population dynamics for this subgroup of MGB neurons during associative learning (Friedman test, $p < 0.01$, 1st and 3rd versus 5th pairing: Dunn-Sidak multiple comparisons test, $p < 0.05$). Importantly, no changes were found between the evoked responses to the CS- and US during conditioning. This would suggest that it is a change in the CS+ encoding which leads to the increased similarity to the US and not changes in the US. This was further tested by comparing the PVD between the evoked population responses to the first CS+ response and the subsequent CS+ presentations (Fig. 37a). This showed that indeed there was movement of the CS+ across the FC day. Strikingly and in contrast to previous observations in the amygdala²², the PVD between the CS+ and the US changes were not preserved post conditioning on the extinction days and the population representation recovered to pre-conditioning levels similar to the observations using two-way or three-way decoders (Fig. 35). The same was observed for the across-day population vector distance of the CS+ to itself (Fig. 37b).

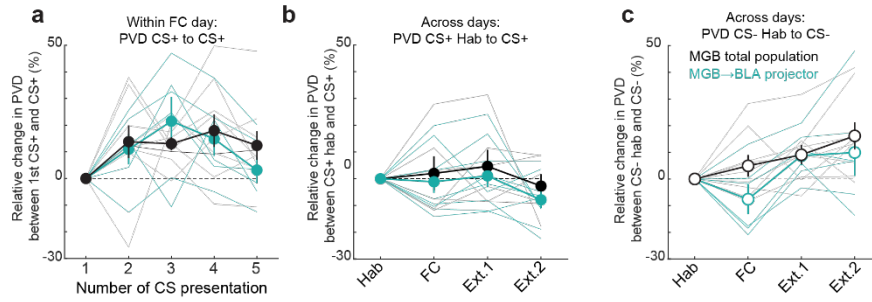


Fig. 37: CS+ to CS+ and CS- to CS- population vector distances.

a. Relative change in PVD between first CS+ and subsequent CS+ presentations during the fear conditioning paradigm (data presented as mean values \pm s.e.m.). **b.** Relative change in PVD between the CS+ on the habituation day and the CS+ presentations on subsequent days (data presented as mean values \pm s.e.m.). **c.** Relative change in PVD between the CS- on the habituation day and CS presentations on subsequent days. MGB total population: N = 9 mice, MGB→BLA projectors: N = 6 mice (data presented as mean values \pm s.e.m.).

However, note that we found a significant difference between the CS- to US PVD of the total MGB population between the conditioning day and the second extinction day (**Fig. 36d**, FC versus Ext. 2: Friedman test, $p < 0.05$, Dunn-Sidak multiple comparisons test, $p < 0.05$). Nevertheless, we did not find a change in the CS- to US PVD between the habituation, fear conditioning and early extinction days indicating that the CS- representation is stable during high fear states in relation to the habituation day and shows no significant drift intraday during fear conditioning. Furthermore, the CS- drifts further away from the habituation CS- which might be reflective of an enhanced safety signal after extinction (**Fig. 37c**).

In addition to the general lack of consolidation of population level changes across fear learning, the strength of PVD-changes between the CS+ and US were not predictive of learned freezing behavior on an animal-by-animal basis (**Fig. 38**).

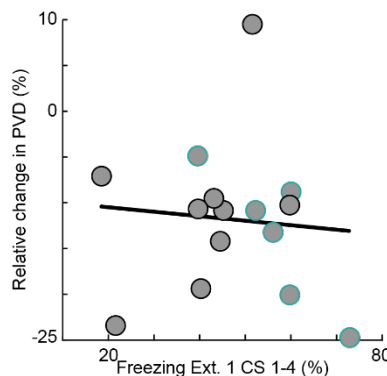


Fig. 38: Correlation of relative change in PVD with fear learning.

Scatter plot of change in population vector distance (Δ PVD) and pre-extinction freezing behavior for N = 15 mice. Black dots: Total MGB population. Cyan dots: MGB→BLA projector population. Line: Linear regression ($R^2 = -0.07$, $p > 0.05$).

8.3.2 Inhibition of cortical feedback does not affect population plasticity

We next investigated whether the chemogenetic inhibition of cortical feedback affected the changes in PVD between the CS and the US (see **Fig. 21**). During the fear conditioning day, the inhibition of cortical feedback did not influence the plasticity of the CS+ (**Fig. 39a**) and the PVD between the control CS- and US was stable in both control and DREADD groups (**Fig. 39c**). The plasticity observed in the CS+ and US PVD was transient as it remained stable across days in both the control and DREADD group (**Fig. 39b**) and the CS- PVD was also stable across days (**Fig. 39d**).

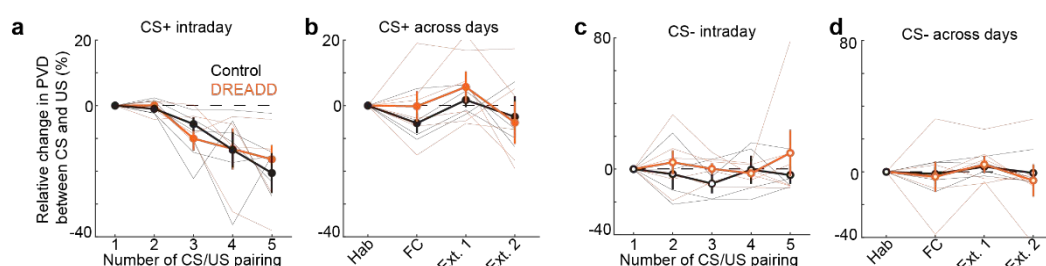


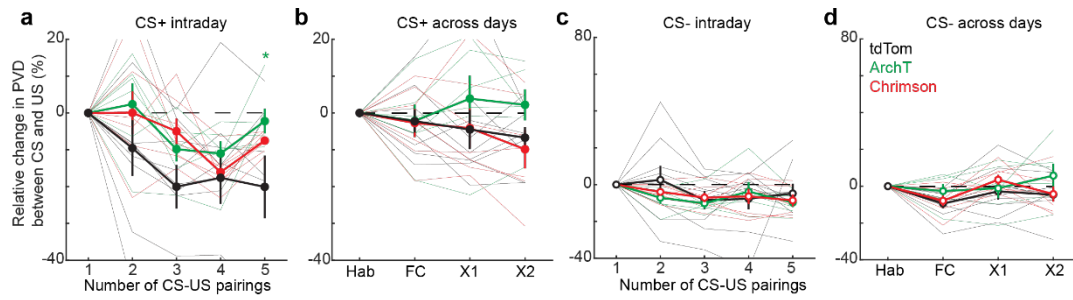
Fig. 39: Inhibition of cortical feedback does not affect MGB PVD between CS and US.

Relative change in Euclidean population vector distance between the CS+ (**a, b**) or CS- (**c, d**) and the US within the fear conditioning session (**a, c**) or across the individual days of the behavioral paradigm (**b, d**). Control, black, $N = 4$ and DREADD, orange, $N = 6$. 2-way ANOVA $p > 0.05$.

The inhibition of cortical feedback did not affect the population coding therefore suggesting that this cortical feedback is not necessary for the population stability in MGB nor for the transient plasticity.

8.3.3 Inhibition of MGB→BLA neurons reduces the transient plasticity

Finally, using an all-optical approach to manipulate MGB→BLA projectors during fear learning (see **Fig. 31**), we find that the inhibition and action of MGB→BLA neurons leads to a reduced shift in the population vector distance between the CS+ and the US on the fear conditioning day (**Fig. 40a**, 5th pairing, relative change control: $-30 \pm 13\%$, ArchT: $-2 \pm 3\%$, Chrimson: $-7 \pm 1\%$ 2-way ANOVA, $p < 0.05$, Sidak multiple comparisons test, $p < 0.05$). The suppression of MGB→BLA neurons and the subsequent decrease in PVD could explain the change in the animals learning (see **Fig. 30**). The activation of MGB→BLA neurons did not cause a significant change in the population plasticity however the 3rd and 5th CS-US pairings did show a weaker change in PVD compared to control. This suggests that there is perhaps a small change in MGB population coding when MGB→BLA neurons are activated.



a. Relative change in PVD between the CS and US for Control, ArchT and Chrimson (2-way ANOVA followed by Sidak's post hoc test, $p < 0.05$, 5th CS+ presentation Control vs. ArchT, $p = 0.0324$, Control $N = 9$ mice, Chrimson $N = 7$ mice, ArchT $N = 6$ mice, data represent mean \pm s.e.m.). **b-d** Relative change in population vector distance between the CS+ (**a**) or CS- (**c-d**) and the US within the fear conditioning session (**c**) or across the individual days of the behavioral paradigm (**b, d**) (MGB \rightarrow BLA ArchT: $N = 6$ mice; tdTom: $N = 9$ mice; Chrimson $N = 7$ mice, data presented as mean values \pm s.e.m.). * indicate p-values smaller than 0.05

It is worth noting that manipulations of MGB \rightarrow BLA activity did not affect the post-conditioning CS-US PVD-change reset and that the CS+ stayed stable relative to the US across days (**Fig. 40b**). These manipulations did not affect the CS- PVD on the fear conditioning day nor across days (**Fig. 40c, d**).

Overall, these results show that the inhibition of MGB \rightarrow BLA neurons reduces the transient population plasticity in MGB. This might be crucial for downstream population plasticity in BLA.

8.4. Discussion

With individual MGB neurons exhibiting plasticity across the associative fear learning paradigm, the question of how this brain region can still stably encode for the sensory environment is essential. The aim of this chapter was to answer this question. Using computational tools, it was possible to analyze the population dynamics of MGB across fear learning.

Firstly, using decoders, it was found that high dimensional representations of CS+ tones are stably encoded in MGB populations across associative fear learning, despite plastic changes in single cell response patterns. Indeed, within a given day of the fear conditioning paradigm, we could train decoders that reliably distinguish between CS+, CS- or baseline activity with high accuracy. Strikingly, we could also train decoders that accurately classified baseline vs. CS+ or CS- presentations across all experimental sessions and along associative fear learning. This is in contrast to the amygdala, where it was possible to train decoders which were accurate across habituation days however they broke down after the fear conditioning

day²². This data suggests that MGB ensembles exhibit stable population level tone representation across days, despite the plasticity of CS responses of individual cells.

This observation is supported when looking at the MGB PVD between the CS+ and US which decreases during the fear conditioning day, yet recovers to baseline levels on the next day after the conditioning session. Therefore, suggesting that MGB population coding of sensory stimuli only transiently change during associative fear learning and reset overnight allowing for stable tone representations on the population level across associative learning. This will be crucial for reliable and unbiased representations of sensory stimuli from the environment.

Once again, this is in stark contrast to the amygdala where it was observed that there was a fear-biased change in population level sensory representations. These changes were stabilized and consolidated after fear learning²². In the amygdala the changes in PVD were predictive of the animal's freezing whereas this is not the case for MGB²². All in all, it suggests that the population code of the amygdala stabilizes "fear hijacking" of the sensory representation, whereas MGB exhibits transient changes in population level encoding, which provides a clean slate for future perception that is unaffected by a valence bias. Nevertheless, the transient population level changes during fear condition in MGB, which are independent of cortical feedback activity, might be crucial to guide long term population level changes in the amygdala or other downstream areas upon associative learning.

Inhibition of MGB→BLA neurons reduces the transient plasticity observed in MGB therefore suggesting that these neurons stabilize the fear circuit. It is hypothesized that this stability is modulated via the TRN as the amygdala provides feedback to MGB via both the auditory cortex and the TRN, but we have shown that the cortical feedback to MGB does not modulate the plasticity. To further understand the fear circuit and the role of these brain areas, it would be of interest to manipulate the TRN neurons whilst recording in MGB. The activation of MGB→BLA neurons did not lead to a significant change in PVD between the CS+ and US. It would be of interest to observe the population level dynamics in MGB when the mice are presented with a milder footshock and the MGB→BLA neurons are activated. It would be hypothesized that this would lead to higher freezing levels compared to a control however this may not be translated in any differences in PVD as, in MGB, there is no correlation between changes in PVD and freezing.

These results show that MGB can balance experience-dependent changes on the single cell level with stable encoding of the sensory environment on the population level.

Chapter 9. General discussion

Associative learning is essential for an animal's survival. Auditory fear conditioning is a paradigm which has been widely used to study associative learning due to its fast learning rates and strong memory formation. A large body of work has placed the amygdala at the center of fear learning. This has led to a strong understanding of how the amygdala's activity dynamics change during the course of fear learning both on the single cell level as well as on the population level^{20–22}. However, it has become apparent that the amygdala is not the sole site of fear learning. Brain areas such as the prefrontal cortex, the auditory cortex as well as many others have exhibited adaptive changes in neuronal activity across fear learning²³. Initially, the auditory thalamus, MGB, received attention for its role as integrative site of CS and US signaling⁵². Electrophysiological recordings in MGB revealed that these neurons receive converging auditory and somatosensory information. It was therefore suggested that MGB might be an ideal site for CS-US integration and neuronal plasticity in auditory fear conditioning. It has been shown that neuronal responses to the auditory CS are enhanced in MGB upon fear learning⁵³. These studies demonstrated that MGB exhibits neuronal response plasticity upstream of response potentiation in the amygdala^{53,72,73,81}.

Despite these studies, the amygdala-centric view has stayed prevalent in the literature with many questions surrounding MGB's response dynamics across auditory fear learning remaining unanswered. How do large populations of MGB neurons encode for the CS and US upon associative learning? How do MGB neurons encode for the CS and US plasticity upon associative learning? Are the amygdala projectors enriched compared to total MGB population? What is MGB's place in the fear circuit? How can MGB coding be plastic, yet ensure stable representations of the sensory environment? This thesis aimed to answer these questions.

Using deep-brain calcium imaging, it was possible to record the neuronal activity of large populations of neurons across an associative fear learning and extinction paradigm. We found that a large proportion of MGB neurons integrate both auditory stimuli as well as the somatosensory footshock. The fact that there was a convergence of the conditioned stimulus and of the unconditioned stimulus on individual MGB neurons led to the hypothesis that MGB was in an ideal position for Hebbian learning and plasticity across the fear conditioning paradigm.

This hypothesis was tested and it was found that the CS+ responses varied across the four-day fear learning paradigm suggesting that there is plasticity in MGB across days. These changes in neuronal responses were not due to a natural drift in MGB but due to the associative learning as there were significantly more stable cells across days in response to the control CS- or in an unpaired group than to the CS+. This plasticity observed in MGB shows that its role goes beyond the textbook model of a simple sensory relay. This observation led to further questions: many studies in the amygdala looked at individual interneuron subtypes and their roles in fear conditioning, what are the roles of individual cell types in MGB? What is the place of MGB in the fear circuit? How can MGB still perform its role as a sensory relay without getting high-jacked into a fear state?

In the rodent, MGB neurons have been found to be primarily excitatory with inhibitory inputs coming mainly from the TRN and IC¹⁰⁶. It is therefore not possible to study individual subtypes of interneurons in MGB. There are different cellular markers with calbindin and calretinin being differentially expressed within MGB subdivisions⁴⁹. One study looked at the role of the calretinin-positive neurons. They found that these cells also exhibited CS-US association and showed plasticity in response to the fear conditioning paradigm⁹². They also mapped the circuitry of these cells, showing that they receive inputs from the IC and they project to the BLA. However, as shown here, calretinin does not seem to be an exclusive marker for the MGB→BLA neurons therefore suggesting that they project to other brain areas. Whilst this thesis did not concentrate on specific cell markers, it did look at the cells in MGB which project to the BLA. It was interesting to note that this cell population did not show enhanced plasticity compared to total MGB neurons therefore suggesting that the experience-dependent changes observed in MGB neuronal activity are distributed to a wider brain network.

Such areas could include the auditory cortex and the striatum. The primary auditory cortex receives inputs from the ventral subdivision of MGB but also from the medial subdivision. The inputs from the ventral subdivision are sharply tuned and respond to fast modulation in sound¹⁰⁷. In other words, these inputs act as a sensory relay. However, by looking specifically at the cells located in MGBv, we found that these cells were just as plastic as cells located in the higher order MGBm. The role of MGBm projections to ACtx and their plasticity has previously been studied¹⁰³. They found that the higher order MGB transmits memory-related information to layer 1 of ACtx, which, in turn, is modulated locally via GABA_b-receptors. Having found that the MGB→BLA neurons send collaterals to layer 1 of ACtx, these results would suggest that the information encoded by ACtx and BLA may not be the same because the modulation of the inputs would differ between the two brain regions. For this reason, it is important to study the role of auditory cortex within fear conditioning.

The role of ACtx within fear conditioning has been well-studied. It was established that neurons in ACtx show enhanced responses to the CS after fear learning¹⁰⁸. It was further shown that these enhanced CS responses were due to the suppression of cortical habituation¹⁰⁹. These physiological changes were on a different temporal scale compared to the BLA and perhaps not reflective of the immediate learning but due to higher cognitive processing of the fear learning¹⁸. This would suggest that the experience-dependent changes observed in MGB are propagated similarly to the BLA and ACtx, perhaps via the same neurons, but due to local modulation of the inputs the brain areas process the information differently. BLA processes the immediate threat whereas the ACtx processes the mnemonic memory and perhaps modulates the attentional gain to the CS stimuli. This hypothesis is further supported by a study showing that inhibition of ACtx does not prevent learning when the CS is either pure tones or noise¹¹⁰.

Whilst it is important to look at the projections of MGB, to fully understand its role in fear learning it is important to study its inputs either feedforward from brainstem areas or feedback from cortical or thalamic areas. Having found that modulation of MGB→BLA neurons leads to increased plasticity in MGB, this would suggest that BLA provides feedback to MGB via an indirect pathway. Here, the role of cortical feedback was investigated. Inhibition of cortical feedback did not affect plasticity in MGB nor modify the animals' behavioral response. This would suggest that MGB feedback from BLA is not via the ACtx but most likely via the TRN. It would be of interest to further study the role of TRN in auditory fear conditioning.

One brain area not investigated in this thesis, but that is at the core of the input drive to MGB, is the IC. IC neurons have previously been shown to be plastic in response to the CS during auditory fear conditioning⁹³. However, a study in bats showed that the unpairing of the CS to the US did not prevent this plasticity therefore suggesting that this plasticity may be due to attention or arousal and not to the learning itself¹¹¹. It is worth noting that these experiments were done using electrophysiology, recording one neuron at a time. It is possible that they only recorded from neurons which have a potentiated response but that is not representative of the overall population. In the experiments performed in this thesis, around 40% of cells were plastic when the CS+ was unpaired from the US therefore it is possible that the IC also shows some plasticity which is due to the learning itself and not due to attention and arousal. To study this, it would be important to look at large populations of IC neurons, similarly to what was performed in this thesis. It would be of particular interest to study the neurons in IC that project to MGB, this will help understand whether MGB inherits plasticity from downstream areas or if it is a site for plasticity itself. We already found that this plasticity is not inherited from the ACtx.

MGB therefore plays a key role within the fear circuit and is more than a sensory relay playing a key role in aversive learning. Is the role of MGB limited to auditory fear conditioning or does it also play a role in other forms of learning? One study explored the role of MGB in a go/no-go auditory discrimination task using fiber photometry¹¹². They found that the sound is encoded in MGB early but that the choice information was also encoded in MGB several hundred of milliseconds after stimulus onset. They also found that MGB exhibited plasticity which correlated with learning. Another study found an increase in thalamo-amygdala synapses strength upon cue-induced rewards¹¹³. All-in-all these studies showed that learning and behavior-related coding in MGB is not unique to fear conditioning but is also present with an appetitive reward.

The role of MGB goes beyond the textbook definition of a sensory relay having shown that it encodes different behaviors related to different forms of learning. This does however lead to the question of how MGB can perform its role as a sensory relay. Whilst it is possible that some cells, such as the stable cells described here, do not encode for any learning or that presynaptic modulation of MGB inputs in auditory cortex could modulate the information presented to the auditory cortex¹⁰³, it was found that the CS representation was stable across days on the population level. This phenomenon has previously been described in cortical areas where it has been shown that on the population level there is stable encoding of sensory stimuli despite single cell response variability^{114,115}. This allows MGB to balance experience-dependent plasticity with consistent ensemble level representations of the sensory environment and for MGB to support stable auditory perception with minimal affective bias.

Understanding the role of MGB during associative learning and its role within the fear circuit is important for understanding and therefore treating disorders where the associative learning is impaired. One such disorder is in PTSD, a disorder where associative learning is debilitating as noises, sounds and/or places are associated with traumatic experiences. The current treatments for PTSD are medications such as antidepressants¹¹⁶ or other types of psychotherapeutic support such exposure therapy¹¹⁷. The neurobiology underlining PTSD is not well understood. However, this thesis places MGB as a brain area of interest in the research on PTSD.

Another disorder where the perception of the world is disrupted is in schizophrenia as patients suffer from hallucinations (“positive” symptoms)¹¹⁸. However, the role of MGB in this disorder has not been well studied. One study did show that MGB sensory computation is implicated in an animal model of schizophrenia, which might lead to the perception phenotype of the mental disorder, such as hallucinations¹¹⁹. Our increased knowledge in the physiological neural circuit-specific computations of MGB will now allow us to probe thalamic function in animal models of schizophrenia (e.g. 22q11DS or ErbB4). Of particular interest will be the cells showing ramping

activity which are believed to encode for timing. Indeed, it has previously been shown in cortico-striatal pathways that temporal control is disrupted in schizophrenia¹²⁰.

Overall, this work has shown that there is a distributed circuit for fear learning and has expanded on the role of MGB within this circuit. It has shown how on the single cell level MGB exhibits plasticity and encodes for the learnt behavior. It has also improved our understanding on how MGB interacts with other brain areas and how these interactions modulate memory formation and learning. Finally, this work has shown that despite the single cell plasticity, MGB can reliably encode for the auditory sensory environment on the population level with minimal affective bias. It has demonstrated how MGB balances experience-dependent plasticity with consistent ensemble level representations of the sensory environment to support stable auditory perception with minimal affective bias.

Chapter 10. Methods

10.1. Animal subjects

8 to 12-week-old male C57Bl/6J, heterozygous ChAT-cre (B6;129S6-Chat^{tm2(cre)}Lowl>/J, JAX#006410) or heterozygous NTSR1-Cre (B6.FVB(Cg)-Tg(Ntsr1-cre)GN220Gsat/Mmucd) mice were used throughout the study. All experiments were done in accordance with institutional guidelines and were approved by the Cantonal Veterinary Office of Basel-Stadt, Switzerland. Animals were housed on a 12-hour light / dark cycle and food and water were provided ad libitum.

10.2. Surgical procedures

Virus was injected with the help of a stereotaxic apparatus (Kopf Instruments) in the medial geniculate body (for imaging experiments 500 nl, AAV2/5.CaMKII.GCaMP6f.WPRE.SV40, Penn Vector Core or AAVDj8.Ef1α.jGCaMP7f.WPRE.bGHp(A), VVF Zurich. For optogenetic experiments 500 nl AAV2/5.CAG.flex.ArchT.GFP, UNC Vector Core, AAV2/5.CaMKII.EGFP.WPRE.hGHp(A), VVF Zürich, AAV2/5.CaMKII.eArchT3.0.2 A.EGFP.WPRE, VVF Zurich or AAV2/5.hSyn.dlox.EGFP.dlox.WPRE, VVF Zurich, for all-optical experiments 500 nl, AAV2/5.CAG.flex.ArchT.tdTomato, UNC Vector Core or AAV2/5.CAG.dlox.tdTomato.dlox.WPRE, VVF Zurich, for tracing experiments 500 nl, AAV2/5.hSyn.flex.axonGCaMP6s94, Addgene; coordinates: AP: -3.28, ML: -1.9, DV: -3.1 mm.), basolateral amygdala (300 nl, AAV2/9.CaMKII.GCaMP6f.WPRE.SV40, Penn Vector Core; rAAV2-retro.EF1a.GCaMP6f.WPRE, Georg Keller, FMI Vector Core, Basel, Switzerland, for tracing experiments 300 nl, rAAV2-retro.hSyn1.mCherry.WPRE.hGHp(A), VVF Zurich; or 50 nl CTB 555, Invitrogen, for optogenetic experiments 300 nl rAAV2-retro.hSyn1.mCherry.icre.WPRE.hGHp(A), VVF Zürich, for all-optical experiments 300 nl AAV2-retro.CaMKII.iCre.WPRE.hGHp(A), VVF Zurich; coordinates AP: -1.7, ML: -3.6, DV: -3.6 mm or in the pedunculo pontine tegmental nucleus for optogenetics 500 nl of AAV2/5.CAG.flex.ArchT.tdTomato, UNC Vector Core AV4567BC, or AAV2/5.shortCAG.lox.ArchT.EGFP.WPRE SV40, VVF Zurich v-461-5, or AAV2/1.Ef1a.DIO.ChrimsonR.tdTomato, Georg Keller FMI Vector Core 326, Basel Switzerland, or AAV2/5.CAG-lox-tdTomato(rev)-lox-WPRE-bGHp(A), VVF Zurich v167-5

coordinates: AP: -4.8, ML: -1.3, DV: -3.4 mm) of 8-12 week old mice with a glass pipette and a pressure ejection system (Picospritzer) under isoflurane anaesthesia (1 – 2%) and buprenorphine (0.1 mg/kg) and ropivacaine (65 mg/kg) analgesia. The rAAV2-retro helper was a gift from Alla Karpova & David Schaffer (Addgene plasmid #81070). Virus for retrograde labelling of MGB neurons was supplemented with blue non-retrograde polymer microspheres (1:2400, Duke Scientific Corp.) to label BLA injection sites. For miniature microscope experiments, one week after virus injection, a gradient refractive index (GRIN) lens (0.5 or 0.6 mm diameter, Inscopix) was implanted during a second surgery (anesthesia and analgesia see above). A 0.8 mm diameter craniotomy was drilled above the MGB and a small track was cut with a 0.7 mm sterile needle. The GRIN lens was then slowly advanced into the brain (coordinates: AP: -3.28, ML: -1.9, DV: -3.0 mm), fixed to the skull with light curable glue (Loctite 4305, Henkel) and the skull was sealed with Scotchbond (3 M), Vetbond (3 M) and dental acrylic (Paladur, Kulzer). A titanium head bar (custom made) was attached to fix the animal during the miniature microscope base plate mounting procedure. For optogenetic experiments, virus (see above) was injected bilaterally in the basolateral amygdala, pedunculopontine tegmental nucleus and medial geniculate body as described above. One week later, optical fibers (0.4 mm, 0.5 NA, Thorlabs) were implanted bilaterally above the medial geniculate body (Coordinates: AP: -3.28, ML: -1.9, DV: -2.9 mm). Optical fibers, the wound and skull were fixed and sealed in a similar manner to GRIN lens implantations. Animals were provided with analgesia (buprenorphine, ropivacaine) and their well-being was monitored throughout the entire experimental period.

10.3. Behavioral paradigms and analysis

Behavioral experiments were performed during the animal's light period. A four or five day auditory fear conditioning paradigm was performed in a habituation / test context (days 1, 3, 4, 5) and a fear conditioning context (day 2). Mice were presented with 5 or 6 intermingled CS+ and CS- during habituation (6 kHz and 12 kHz, intermingled) in a round plexiglass context. CSs were composed of 27 tone pips (200 ms, 75 dB) presented at a rate of 1.1 Hz (Tucker Davis Technologies, TDT 78 or RZ6). Fear conditioning was performed in a ca. 25 cm square plexiglass box and a shock grid floor (Coulbourn, Noldus). The CS+ (6 kHz and 12 kHz, counterbalanced) was terminated by a 2 s 0.65 mA foot shock 1.1 s after the last tone pip. During the extinction sessions (day 3, day 4 and day 5, habituation context), 4 CS- and 12 CS+ were presented. In some experiments, extinction sessions on day 4 or 5 were followed by 4 neutral tone presentations (16 kHz at 70 dB). For optogenetic experiments, animals were habituated to the optical fiber attachment procedure for 3 days before the start of the fear

conditioning paradigm. On the fear conditioning day, optical fibers were attached to the optical fiber implant via a ceramic mating sleeve (Thorlabs). ArchT or Chrimson expressing neurons were continuously inhibited during the five or six CS-US pairings (starting 2 s before CS onset until 2 s after US offset) with a 565 nm LEDs (M565D2, Thorlabs) or with a 625 nm LEDs (M625D3, Thorlabs) for ArchT and Chrimson stimulation respectively. Optical stimulation was controlled with a custom-built stimulation setup consisting of an Arduino board (Arduino Uno REV3, Arduino) and LED drivers (LEDD1B, Thorlabs). For ArchT the stimulation pattern was continuous, for Chrimson it was presented at 20 Hz with an up time of 5 ms and a down time of 45 ms. The light intensity measured at the optical fiber tip was 19 mW and optical fiber implants had a typical attenuation of 30%. Optogenetic experiments were performed and analyzed in a blinded fashion. Behavioral experiments were performed and analyzed using Cineplex 3.4.1 (Tucker Davis Technologies) or Ethovision 14 (Noldus). Behavioral tracking based on the center of mass of the mouse was performed using inbuilt functions of Cineplex and Ethovision. Freezing was initially detected automatically based on periods of absence of movement (threshold: 1 s) and then manually controlled and adjusted for non-freezing episodes (e.g. grooming) *post hoc*.

10.4. Miniature microscope imaging

The miniature microscope (nVista2.0 or nVoke1.0, Inscopix) was fixed to the base plate on the mouse's head before the experiment using head-fixation at the head bar on a flying saucer style running wheel. Mice were initially habituated to this procedure. MGB Ca²⁺ fluorescence was imaged continuously during the behavioral session with the following settings (nVista Software Version: 2.0.4): Framerate: 20 Hz, LED-Power: 50-70%, Gain: 1.0-2.0, Image size: 1024 x 1024 or 1080 x 1080 pxl. LED power and gain were adjusted according to GCaMP expression levels and the same settings were used across days for individual mice. For the all-optical experiments, the OG-LED-Power was presented 2 seconds before the start of the CS+ and finished 2 seconds after the end of the US for a total time of 36 seconds at 10 mW/mm². For ArchT group the opto-stimulation was continuous while for ChrimsonR group was delivered with a 20Hz stimulation pattern.

10.5. Image analysis

Raw image data was analyzed as previously described^{22,101}. Briefly, movies from all behavioral sessions were spatially down sampled (2x), bandpass filtered (Fourier transform) and normalized by the filtered image (ImageJ). The movies were then concatenated and motion corrected using Turboreg (three rounds). Only movies that motion-corrected across days with final spatial dislocations of $< 2 \mu\text{m}$ were used for Ca^{2+} trace extraction. Principal and independent component analysis-based detection of individual regions of interest (ROIs) was performed on downsampled (5 Hz) $\Delta F/F$ movies. ROIs were truncated at 50% peak intensity and limited to a size of 30 pixels (ca. $60 \mu\text{m}$). ROIs were initially oversampled (300 ICs) and then overlaid with the maximum intensity projection of the four-day movie. ROIs that did not match individual neurons were discarded. We typically retained 96 ± 5 ICAs per animal for CaMKII-GCaMP6f, $N = 38$ mice, 65 ± 9 ICAs per animal for rAAV2retro.GCaMP6f, $N = 6$ mice and 95 ± 6 ICAs per animal for AAVDJ8.GCaMP7f $N = 10$ mice. These ICs were then applied to the 20 Hz motion corrected raw fluorescence movie to extract single cell Ca^{2+} traces for further processing.

10.6. Ca^{2+} data analysis

All analysis was based on linearly de-trended and z-scored Ca^{2+} traces of individual neurons. Ca^{2+} traces were baselined to the time periods preceding CS or US onset. To identify CS- and US-responsive neurons and their plasticity types across days, 30 s CS and 2.8 s US responses were analyzed using a combined statistical and supervised cluster analysis approach as previously described¹⁰¹. Briefly, CS and US responses were analyzed by using a combined statistical and supervised cluster analysis. First, CS- and US-responsive cells were identified as significantly responsive if their binned Ca^{2+} fluorescence (CS, 1-s bins, ± 30 -s window around CS onset; US, 1-s bin, ± 14 -s window around US onset) during the stimulus was significantly increased (CS) as well as significantly increased or decreased (US) (Wilcoxon signed-rank test, alpha-level, 0.01) compared with baseline conditions in at least three or two stimulus presentations for the US or CS, respectively (on at least one experimental condition for CS responses). This minimum number of sensory responses allowed a reliable detection of CS and US plasticity profiles instead of merely general responsiveness across all days, without being too sensitive for random Ca^{2+} responses during individual tone presentations. Responses for the CS were collected to tones 1 to 5 in the two habituation sessions and in the first fear extinction session (Ext. early) and to tones 8 to 12 in the second fear extinction session

(Ext. late). Next, we used a supervised clustering approach on the subset of significantly responsive cells to identify different subtypes of CS- and US-responsive neurons. Neuronal responses were collected in time windows of -2 s to 15 s and -10 s to 30 s around US and CS onset, respectively. Principal components analysis was performed on the concatenated responses to the five US stimuli in the FC session to identify the dynamics in the US responses within this session. Responses were then projected on the first four principle components (>60% variance explained), and k-means clustering was performed ($k = 11$, cosine distance). We then manually joined clusters with similar response profiles in relation to the six response types described above. This procedure was replicated for the CS responses after averaging responses to the five selected tones in the habituation and extinction sessions as described above, to identify the different dynamics in CS responses along the conditioning paradigm.

CS+, CS- and baseline responses were decoded from MGB Ca^{2+} activity by fitting three-way (CS+ vs. CS- vs. baseline) or two-way (CS+ vs. baseline or CS- vs. baseline) quadratic discriminant analysis classifiers. We classified CS+ and CS- responses based on the first four presentations to balance for uneven numbers of CS+/- presentations across habituation, fear conditioning and extinction days. Baseline responses were sampled from the 30 s periods preceding the CS+ and CS-. Classifiers were trained on the mean response of five consecutive pip responses within one CS (or the baseline period), such that each training set contained 20 input variables per condition (i.e. 40 for two-way decoders and 60 for three-way decoders). The mean response was calculated based on a 300 ms time window after pip onset and classifiers were trained using a 10-fold cross-validation procedure. Decoder accuracy was calculated as the mean of the diagonal of the confusion matrix. Classifiers were trained for each individual animal and are presented as mean decoding accuracy across animals. To balance for unequal cell numbers between the different animals, we randomly selected 40 neurons from each animal and calculated the mean accuracy from 50 independent runs.

The population vector distance (PVD) between CS and US responses was calculated based on binned (0.275 s bins to accommodate the 1.1 Hz pip frequency) 30 s CS and 4 s US responses. PVD was calculated as the Euclidian distance between each CS bin and the mean binned US or CS response and then averaged for each 30 s CS. Intraday PVD changes were normalized to the PVD of the first CS and across day PVD changes were calculated as the mean intraday PVD change for all CSs and normalized to the mean PVD of the habituation day.

10.7. Sound recordings and analysis

Acoustic signals of the fear conditioning context were recorded with a PCB Precision Condenser Microphone (Model 377C01) microphone and a RZ6 Auditory Processor (Tucker-Davis Technologies) 50 cm above the fear conditioning context at 195 kHz simultaneous to miniature microscope imaging during the fear conditioning session. Sound waves were high-pass filtered at 1 kHz and spectrograms were computed using short-time Fourier transforms (spectrogram function, Signal Processing Toolbox, MATLAB, Mathworks). To detect sound-level correlated neuronal activity, the cross-correlation coefficient between the squared acoustic signal binned in 50 ms and the corresponding Ca^{2+} signal of individual neurons was computed with a maximum lag of 500 ms. Cells were classified as sound-correlated if they exceeded a maximal cross-correlation coefficient of 0.2. Acoustic event onsets were detected based on the peak of the differentiated squared and binned sound wave. Acoustic events were not distinguished between animal movement-related sounds and vocalizations of the animal.

10.8. Histology

After completion of the behavioral experiment, mice were transcardially perfused with ca. 5 ml phosphate buffered saline (PBS, ThermoFisher) followed by 40 ml 4% paraformaldehyde (PFA) in PBS (pH = 7.4). Brains were removed and stored overnight in 4% PFA. 150 μm coronal slices were prepared using a vibratome (Campden Instruments) and immunostained for calretinin using the following solutions and protocol: carrier solution: 1% normal horse serum (NHS, Vector Laboratories) with 0.5% Triton (ThermoFisher) in phosphate buffered saline (PBS, ThermoFisher), blocking solution: 10% NHS with 0.5% Triton in PBS. After several rounds of PBS washes, slices were blocked for two hours at room temperature and incubated in primary antibody in carrier solution (goat anti-calretinin, 1:1000, Swant; rabbit anti-NeuN, 1:3000, Abcam; rabbit anti-GABA, 1:500, SigmaAldrich) overnight at 4 °C. Slices were washed again in PBS and incubated for 2 h at room temperature in secondary antibody in carrier solution (donkey anti-goat 647, 1:1000, ThermoFisher; donkey anti-rabbit 405, 1:1000, Abcam; donkey anti-rabbit 555, 1:1000, ThermoFisher). After four final washes, slices were mounted on slides and cover slipped using 22 x 50 mm, 0.16 - 0.19 mm thick cover glass (FisherScientific). Images were acquired with a LSM710 confocal microscope (Zeiss) and stitched with Zen 2.1 (black, Zeiss). Confocal images were post processed with ImageJ (Version: 2.0). Cells were manually counted using the cell counter plugin (<https://imagej.nih.gov/ij/plugins/cell-counter.html>) for ImageJ.

10.9. Statistical analysis

Statistical analysis was performed using Matlab (Mathworks) and Prism 8 (Graphpad). Unless otherwise indicated, normal distribution of the data was not assumed and non-parametric tests were performed. Values are presented as mean \pm SEM unless stated otherwise. Box and whisker plots indicate median, interquartile range as well as the minimum to maximum value of the distribution. Statistical tests are mentioned in the text or figure legends. *, **, *** indicate p-values smaller than 0.05, 0.01 and 0.001, respectively.

References

1. Sacks H. *Lectures on Conversation*. Vol 1-2. Oxford, UK: Wiley-Blackwell; 1992. doi:10.1002/9781444328301
2. Shanks DR. Connectionist Accounts of the Inverse Base-rate Effect in Categorization. *Conn Sci*. 1992;4(1):3-18. doi:10.1080/09540099208946600
3. Mackintosh NJ. Pavlov and associationism. *Span J Psychol*. 2003;6(2):177-184. doi:10.1017/s1138741600005321
4. Windholz G. Pavlov as a psychologist - A reappraisal. *Pavlov J Biol Sci*. 1987;22(3):103-112. doi:10.1007/BF02734662
5. Clark RE. The classical origins of Pavlov's conditioning. *Integr Physiol Behav Sci*. 2004;39(4):279-294. doi:10.1007/BF02734167
6. Bryant RA. Post-traumatic stress disorder: a state-of-the-art review of evidence and challenges. *World Psychiatry*. 2019;18(3):259-269. doi:10.1002/wps.20656
7. Lord C, Elsabbagh M, Baird G, Veenstra-Vanderweele J. Autism spectrum disorder. *Lancet*. 2018;392(10146):508-520. doi:10.1016/S0140-6736(18)31129-2
8. Tandon R, Gaebel W, Barch DM, et al. Definition and description of schizophrenia in the DSM-5. *Schizophr Res*. 2013;150(1):3-10. doi:10.1016/j.schres.2013.05.028
9. Hintiryan H, Bowman I, Johnson DL, et al. Connectivity Characterization of The Mouse Basolateral Amygdalar Complex. *bioRxiv*. October 2019:807743. doi:10.1101/807743
10. Tsukano H, Hou X, Horie M, et al. Reciprocal connectivity between secondary auditory cortical field and amygdala in mice. *Sci Rep*. 2019;9(1):1-12. doi:10.1038/s41598-019-56092-9
11. Rosenkranz JA, Moore H, Grace AA. The Prefrontal Cortex Regulates Lateral Amygdala Neuronal Plasticity and Responses to Previously Conditioned Stimuli. *J Neurosci*. 2003;23(35):11054-11064. doi:10.1523/jneurosci.23-35-11054.2003
12. Pitkänen A, Pikkarainen M, Nurminen N, Ylinen A. Reciprocal connections between the amygdala and the hippocampal formation, perirhinal cortex, and postrhinal cortex in rat. In: *Annals of the New York Academy of Sciences*. Vol 911. New York Academy of Sciences; 2000:369-391. doi:10.1111/j.1749-6632.2000.tb06738.x
13. Nader K, Majidishad P, Amorapanth P, LeDoux JE. Damage to the lateral and central, but not other, amygdaloid nuclei prevents the acquisition of auditory fear conditioning. *Learn Mem*. 2001;8(3):156-163. doi:10.1101/lm.38101
14. Nader K, Schafe GE, LeDoux JE. Fear memories require protein synthesis in the amygdala for reconsolidation after retrieval. *Nature*. 2000;406(6797):722-726. doi:10.1038/35021052
15. Muller J, Corodimas KP, Fridel Z, LeDoux JE. Functional inactivation of the lateral and basal nuclei of the amygdala by muscimol infusion prevents fear conditioning to an explicit conditioned stimulus and to contextual stimuli. *Behav Neurosci*. 1997;111(4):683-691. doi:10.1037//0735-7044.111.4.683
16. Romanski LM, Clugnet M-C, Bordi F, LeDoux JE. Somatosensory and auditory convergence in the lateral nucleus of the amygdala. *Behav Neurosci*. 1993;107(3):444-450. doi:10.1037//0735-7044.107.3.444

17. Rogan MT, Staubli U V., LeDoux JE. Fear conditioning induces associative long-term potentiation in the amygdala. *Nature*. 1997;390(6660):604-607. doi:10.1038/37601
18. Quirk GJ, Repa JC, LeDoux JE. Fear conditioning enhances short-latency auditory responses of lateral amygdala neurons: Parallel recordings in the freely behaving rat. *Neuron*. 1995;15(5):1029-1039. doi:10.1016/0896-6273(95)90092-6
19. Herry C, Ciocchi S, Senn V, Demmou L, Müller C, Lüthi A. Switching on and off fear by distinct neuronal circuits. *Nature*. 2008;454(7204):600-606. doi:10.1038/nature07166
20. Wolff SBE, Gründemann J, Tovote P, et al. Amygdala interneuron subtypes control fear learning through disinhibition. *Nature*. 2014;509(7501):453-458. doi:10.1038/nature13258
21. Krabbe S, Paradiso E, d'Aquin S, et al. Adaptive disinhibitory gating by VIP interneurons permits associative learning. *Nat Neurosci*. 2019;22(11):1834-1843. doi:10.1038/s41593-019-0508-y
22. Grewe BF, Gründemann J, Kitch LJ, et al. Neural ensemble dynamics underlying a long-term associative memory. *Nature*. 2017;543(7647):670-675. doi:10.1038/nature21682
23. Herry C, Johansen JP. Encoding of fear learning and memory in distributed neuronal circuits. *Nat Neurosci*. 2014;17(12):1644-1654. doi:10.1038/nn.3869
24. Kholodar-Smith DB, Allen TA, Brown TH. Fear Conditioning to Discontinuous Auditory Cues Requires Perirhinal Cortical Function. *Behav Neurosci*. 2008;122(5):1178-1185. doi:10.1037/a0012902
25. Boatman JA, Kim JJ. A thalamo-cortico-amygdala pathway mediates auditory fear conditioning in the intact brain. *Eur J Neurosci*. 2006;24(3):894-900. doi:10.1111/j.1460-9568.2006.04965.x
26. Letzkus JJ, Wolff SBE, Meyer EMM, et al. A disinhibitory microcircuit for associative fear learning in the auditory cortex. *Nature*. 2011;480(7377):331-335. doi:10.1038/nature10674
27. Romanski LM, LeDoux JE. Bilateral destruction of neocortical and perirhinal projection targets of the acoustic thalamus does not disrupt auditory fear conditioning. *Neurosci Lett*. 1992;142(2):228-232. doi:10.1016/0304-3940(92)90379-L
28. Corcoran KA, Quirk GJ. Activity in prelimbic cortex is necessary for the expression of learned, but not innate, fears. *J Neurosci*. 2007;27(4):840-844. doi:10.1523/JNEUROSCI.5327-06.2007
29. Blum S, Hebert AE, Dash PK. A role for the prefrontal cortex in recall of recent and remote memories. *Neuroreport*. 2006;17(3):341-344. doi:10.1097/01.wnr.0000201509.53750.bc
30. Courtin J, Chaudun F, Rozeske RR, et al. Prefrontal parvalbumin interneurons shape neuronal activity to drive fear expression. *Nature*. 2014;505(7481):92-96. doi:10.1038/nature12755
31. Brunzell DH, Kim JJ. Fear conditioning to tone, but not to context, is attenuated by lesions of the insular cortex and posterior extension of the intralaminar complex in rats. *Behav Neurosci*. 2001;115(2):365-375. doi:10.1037/0735-7044.115.2.365
32. Shi T, Feng S, Wei M, Zhou W. Role of the anterior agranular insular cortex in the modulation of fear and anxiety. *Brain Res Bull*. 2020;155:174-183. doi:10.1016/j.brainresbull.2019.12.003

33. de Paiva JPQ, Bueno APA, Dos Santos Corrêa M, Oliveira MGM, Ferreira TL, Fornari R V. The posterior insular cortex is necessary for the consolidation of tone fear conditioning. *Neurobiol Learn Mem.* 2021;179:107402. doi:10.1016/j.nlm.2021.107402
34. Mátyás F, Lee J, Shin HS, Acsády L. The fear circuit of the mouse forebrain: Connections between the mediodorsal thalamus, frontal cortices and basolateral amygdala. *Eur J Neurosci.* 2014;39(11):1810-1823. doi:10.1111/ejn.12610
35. McCullough KM, Morrison FG, Ressler KJ. Bridging the Gap: Towards a cell-type specific understanding of neural circuits underlying fear behaviors. *Neurobiol Learn Mem.* 2016;135:27-39. doi:10.1016/j.nlm.2016.07.025
36. Weinberger NM. The medial geniculate, not the amygdala, as the root of auditory fear conditioning. *Hear Res.* 2011;274(1-2):61-74. doi:10.1016/j.heares.2010.03.093
37. Morest DK. The neuronal architecture of the medial geniculate body of the cat. *J Anat.* 1964;98(4):611-630.
38. De La Mothe LA, Blumell S, Kajikawa Y, Hackett TA. Thalamic connections of the auditory cortex in marmoset monkeys: Core and medial belt regions. *J Comp Neurol.* 2006;496(1):72-96. doi:10.1002/cne.20924
39. Morel A, Imig TJ. Thalamic projections to fields A, AI, P, and VP in the cat auditory cortex. *J Comp Neurol.* 1987;265(1):119-144. doi:10.1002/cne.902650109
40. Calford MB, Aitkin LM. Ascending projections to the medial geniculate body of the cat: Evidence for multiple, parallel auditory pathways through thalamus. *J Neurosci.* 1983;3(11):2365-2380. doi:10.1523/jneurosci.03-11-02365.1983
41. Hackett TA, Barkat TR, O'Brien BMJ, Hensch TK, Polley DB. Linking topography to tonotopy in the mouse auditory thalamocortical circuit. *J Neurosci.* 2011;31(8):2983-2995. doi:10.1523/JNEUROSCI.5333-10.2011
42. Lee CC, Murray Sherman S. Drivers and modulators in the central auditory pathways. *Front Neurosci.* 2010;4(MAY). doi:10.3389/neuro.01.014.2010
43. Lee CC, Winer JA. Connections of cat auditory cortex: I. Thalamocortical system. *J Comp Neurol.* 2008;507(6):1879-1900. doi:10.1002/cne.21611
44. Smith PH, Uhrich DJ, Manning KA. Evaluation of medial division of the medial geniculate (MGM) and posterior intralaminar nucleus (PIN) inputs to the rat auditory cortex, amygdala, and striatum. *J Comp Neurol.* 2019;527(9):1478-1494. doi:10.1002/cne.24644
45. Molinari M, Dell'Anna ME, Rausell E, Leggio MG, Hashikawa T, Jones EG. Auditory thalamocortical pathways defined in monkeys by calcium-binding protein immunoreactivity. *J Comp Neurol.* 1995;362(2):171-194. doi:10.1002/cne.903620203
46. Lee CC. Exploring functions for the non-lemniscal auditory thalamus. *Front Neural Circuits.* 2015;9(November):1-8. doi:10.3389/fncir.2015.00069
47. LeDoux JE, Farb CR, Romanski LM. Overlapping projections to the amygdala and striatum from auditory processing areas of the thalamus and cortex. *Neurosci Lett.* 1991;134(1):139-144. doi:10.1016/0304-3940(91)90526-Y
48. Cai D, Yue Y, Su X, et al. Distinct Anatomical Connectivity Patterns Differentiate Subdivisions of the Nonlemniscal Auditory Thalamus in Mice. *Cereb Cortex.* 2019;29(6):2437-2454. doi:10.1093/cercor/bhy115
49. Lu E, Llano DA, Sherman SM. Different distributions of calbindin and calretinin immunostaining across the medial and dorsal divisions of the mouse medial geniculate body. *Hear Res.* 2009;257(1-2):16-23. doi:10.1016/j.heares.2009.07.009

50. Shosaku A, Sumitomo I. Auditory neurons in the rat thalamic reticular nucleus. *Exp Brain Res*. 1983;49(3):432-442. doi:10.1007/BF00238784
51. Crabtree JW. Functional diversity of thalamic reticular subnetworks. *Front Syst Neurosci*. 2018;12. doi:10.3389/fnsys.2018.00041
52. Bordi F, LeDoux JE. Response properties of single units in areas of rat auditory thalamus that project to the amygdala - II. Cells receiving convergent auditory and somatosensory inputs and cells antidromically activated by amygdala stimulation. *Exp Brain Res*. 1994;98(2):275-286. doi:10.1007/BF00228415
53. Ryugo DK, Weinberger NM. Differential plasticity of morphologically distinct neuron populations in the medial geniculate body of the cat during classical conditioning. *Behav Biol*. 1978;22(3):275-301. doi:10.1016/S0091-6773(78)92351-9
54. Campeau S, Davis M. Involvement of subcortical and cortical afferents to the lateral nucleus of the amygdala in fear conditioning measured with fear-potentiated startle in rats trained concurrently with auditory and visual conditioned stimuli. *J Neurosci*. 1995;15(3 II):2312-2327. doi:10.1523/jneurosci.15-03-02312.1995
55. Han JH, Yiu AP, Cole CJ, Hsiang HL, Neve RL, Josselyn SA. Increasing CREB in the auditory thalamus enhances memory and generalization of auditory conditioned fear. *Learn Mem*. 2008;15(6):443-453. doi:10.1101/lm.993608
56. Parsons RG, Riedner BA, Gafford GM, Helmstetter FJ. The formation of auditory fear memory requires the synthesis of protein and mRNA in the auditory thalamus. *Neuroscience*. 2006;141(3):1163-1170. doi:10.1016/j.neuroscience.2006.04.078
57. Apergis-Schoute AM, Dębiec J, Doyère V, LeDoux JE, Schafe GE. Auditory fear conditioning and long-term potentiation in the lateral amygdala require ERK/MAP kinase signaling in the auditory thalamus: A role for presynaptic plasticity in the fear system. *J Neurosci*. 2005;25(24):5730-5739. doi:10.1523/JNEUROSCI.0096-05.2005
58. Fanselow MS, LeDoux JE. Why we think plasticity underlying pavlovian fear conditioning occurs in the basolateral amygdala. *Neuron*. 1999;23(2):229-232. doi:10.1016/S0896-6273(00)80775-8
59. Maren S, Yap SA, Goosens KA. The amygdala is essential for the development of neuronal plasticity in the medial geniculate nucleus during auditory fear conditioning in rats. *J Neurosci*. 2001;21(6):RC135-RC135. doi:10.1523/jneurosci.21-06-j0001.2001
60. Calford MB. The parcellation of the medial geniculate body of the cat defined by the auditory response properties of single units. *J Neurosci*. 1983;3(11):2350-2364. doi:10.1523/jneurosci.03-11-02350.1983
61. Bordi F, LeDoux JE. Response properties of single units in areas of rat auditory thalamus that project to the amygdala - I. Acoustic discharge patterns and frequency receptive fields. *Exp Brain Res*. 1994;98(2):261-274. doi:10.1007/BF00228414
62. Anderson LA, Wallace MN, Palmer AR. Identification of subdivisions in the medial geniculate body of the guinea pig. *Hear Res*. 2007;228(1-2):156-167. doi:10.1016/j.heares.2007.02.005
63. Rouiller EM, Rodrigues-Dagaëff C, Simm G, De Ribaupierre Y, Villa A, De Ribaupierre F. Functional organization of the medial division of the medial geniculate body of the cat: Tonotopic organization, spatial distribution of response properties and cortical connections. *Hear Res*. 1989;39(1-2):127-142. doi:10.1016/0378-5955(89)90086-5
64. Bartlett EL, Wang X. Correlation of neural response properties with auditory thalamus subdivisions in the awake marmoset. *J Neurophysiol*. 2011;105(6):2647-2667. doi:10.1152/jn.00238.2010

65. Sadagopan S, Wang X. Level invariant representation of sounds by populations of neurons in primary auditory cortex. *J Neurosci.* 2008;28(13):3415-3426. doi:10.1523/JNEUROSCI.2743-07.2008
66. Anderson LA, Linden JF. Physiological differences between histologically defined subdivisions in the mouse auditory thalamus. *Hear Res.* 2011;274(1-2):48-60. doi:10.1016/j.heares.2010.12.016
67. Edeline JM, Manunta Y, Nodal FR, Bajo VM. Do auditory responses recorded from awake animals reflect the anatomical parcellation of the auditory thalamus? *Hear Res.* 1999;131(1-2):135-152. doi:10.1016/S0378-5955(99)00026-X
68. Clarey JC, Barone P, Irons WA, Samson FK, Imig TJ. Comparison of noise and tone azimuth tuning of neurons in cat primary auditory cortex and medial geniculate body. *J Neurophysiol.* 1995;74(3):961-980. doi:10.1152/jn.1995.74.3.961
69. Tollin DJ, Populin LC, Moore JM, Ruhland JL, Yin TCT. Sound-localization performance in the cat: The effect of restraining the head. *J Neurophysiol.* 2005;93(3):1223-1234. doi:10.1152/jn.00747.2004
70. Kelly JB, Judge PW. Effects of medial geniculate lesions on sound localization by the rat. *J Neurophysiol.* 1985;53(2):361-372. doi:10.1152/jn.1985.53.2.361
71. Wepsic JG. Multimodal sensory activation of cells in the magnocellular medial geniculate nucleus. *Exp Neurol.* 1966;15(3):299-318. doi:10.1016/0014-4886(66)90053-7
72. Edeline J-M, Weinberger NM. Subcortical adaptive filtering in the auditory system: Associative receptive field plasticity in the dorsal medial geniculate body. *Behav Neurosci.* 1991;105(1):154-175. doi:10.1037//0735-7044.105.1.154
73. Edeline J-M, Weinberger NM. Thalamic short-term plasticity in the auditory system: Associative retuning of receptive fields in the ventral medial geniculate body. *Behav Neurosci.* 1991;105(5):618-639. doi:10.1037//0735-7044.105.5.618
74. Komura Y, Tamura R, Uwano T, Nishijo H, Ono T. Auditory thalamus integrates visual inputs into behavioral gains. *Nat Neurosci.* 2005;8(9):1203-1209. doi:10.1038/nn1528
75. Chen TW, Wardill TJ, Sun Y, et al. Ultrasensitive fluorescent proteins for imaging neuronal activity. *Nature.* 2013;499(7458):295-300. doi:10.1038/nature12354
76. Hackett TA, Clause AR, Takahata T, Hackett NJ, Polley DB. Differential maturation of vesicular glutamate and GABA transporter expression in the mouse auditory forebrain during the first weeks of hearing. *Brain Struct Funct.* 2016;221(5):2619-2673. doi:10.1007/s00429-015-1062-3
77. Grimsley JMS, Hazlett EG, Wenstrup JJ. Coding the meaning of sounds: Contextual modulation of auditory responses in the basolateral amygdala. *J Neurosci.* 2013;33(44):17538-17548. doi:10.1523/JNEUROSCI.2205-13.2013
78. Williams WO, Riskin DK, Mott KM. Ultrasonic sound as an indicator of acute pain in laboratory mice. *J Am Assoc Lab Anim Sci.* 2008;47(1):8-10. /pmc/articles/PMC2652617/. Accessed May 21, 2021.
79. von Kriegstein K, Patterson RD, Griffiths TD. Task-Dependent Modulation of Medial Geniculate Body Is Behaviorally Relevant for Speech Recognition. *Curr Biol.* 2008;18(23):1855-1859. doi:10.1016/j.cub.2008.10.052
80. Creutzfeldt O, Hellweg FC, Schreiner C. Thalamocortical transformation of responses to complex auditory stimuli. *Exp Brain Res.* 1980;39(1):87-104. doi:10.1007/BF00237072

81. Edeline JM, Weinberger NM. Associative retuning in the thalamic source of input to the amygdala and auditory cortex: receptive field plasticity in the medial division of the medial geniculate body. *Behav Neurosci*. 1992;106(1):81-105. doi:10.1037//0735-7044.106.1.81
82. Amano T, Duvarci S, Popa D, Pare D. The fear circuit revisited: contributions of the basal amygdala nuclei to conditioned fear. *J Neurosci*. 2011;31(43):15481-15489. doi:10.1523/JNEUROSCI.3410-11.2011
83. Bruce RA, Weber MA, Volkman RA, et al. Experience-related enhancements in striatal temporal encoding. *Eur J Neurosci*. 2021;54(3):5063-5074. doi:10.1111/EJN.15344
84. Xu M, Zhang S, Dan Y, Poo M. Representation of interval timing by temporally scalable firing patterns in rat prefrontal cortex. *Proc Natl Acad Sci*. 2014;111(1):480-485. doi:10.1073/PNAS.1321314111
85. Catanese J, Jaeger D. Premotor Ramping of Thalamic Neuronal Activity Is Modulated by Nigral Inputs and Contributes to Control the Timing of Action Release. *J Neurosci*. 2021;41(9):1878-1891. doi:10.1523/JNEUROSCI.1204-20.2020
86. Narayanan NS. Ramping activity is a cortical mechanism of temporal control of action. *Curr Opin Behav Sci*. 2016;8:226-230. doi:10.1016/J.COBEHA.2016.02.017
87. Rikhye R V., Gilra A, Halassa MM. Thalamic regulation of switching between cortical representations enables cognitive flexibility. *Nat Neurosci* 2018 2112. 2018;21(12):1753-1763. doi:10.1038/s41593-018-0269-z
88. Jiang L, Kundu S, Lederman JD, et al. Cholinergic Signaling Controls Conditioned Fear Behaviors and Enhances Plasticity of Cortical-Amygdala Circuits. *Neuron*. 2016;90(5):1057-1070. doi:10.1016/J.NEURON.2016.04.028
89. Motts SD, Schofield BR. Cholinergic and non-cholinergic projections from the pedunculo pontine and laterodorsal tegmental nuclei to the medial geniculate body in Guinea pigs. *Front Neuroanat*. 2010;4(OCT). doi:10.3389/FNANA.2010.00137
90. Schofield BR, Motts SD, Mellott JG. Cholinergic cells of the pontomesencephalic tegmentum: Connections with auditory structures from cochlear nucleus to cortex. *Hear Res*. 2011;279(1-2):85-95. doi:10.1016/J.HEARES.2010.12.019
91. Staib M, Abivardi A, Bach DR. Primary auditory cortex representation of fear-conditioned musical sounds. *Hum Brain Mapp*. 2020;41(4):882-891. doi:10.1002/HBM.24846
92. Barsy B, Kocsis K, Magyar A, et al. Associative and plastic thalamic signaling to the lateral amygdala controls fear behavior. *Nat Neurosci*. 2020;23(5):625-637. doi:10.1038/s41593-020-0620-z
93. Lockmann ALV, Mourao FAG, Moraes MFD. Auditory fear conditioning modifies steady-state evoked potentials in the rat inferior colliculus. *J Neurophysiol*. 2017;118(2):1012-1020. doi:10.1152/JN.00293.2017
94. Aizenberg M, Rolón-Martínez S, Pham T, Rao W, Haas JS, Geffen MN. Projection from the Amygdala to the Thalamic Reticular Nucleus Amplifies Cortical Sound Responses. *Cell Rep*. 2019;28(3):605-615.e4. doi:10.1016/J.CELREP.2019.06.050
95. Chen L, Wang X, Ge S, Xiong Q. Medial geniculate body and primary auditory cortex differentially contribute to striatal sound representations. *Nat Commun*. 2019;10(1). doi:10.1038/s41467-019-08350-7

96. Kimura A, Donishi T, Sakoda T, Hazama M, Tamai Y. Auditory thalamic nuclei projections to the temporal cortex in the rat. *Neuroscience*. 2003;117(4):1003-1016. doi:10.1016/S0306-4522(02)00949-1
97. Kwon JT, Nakajima R, Kim HS, Jeong Y, Augustine GJ, Han JH. Optogenetic activation of presynaptic inputs in lateral amygdala forms associative fear memory. *Learn Mem*. 2014;21(11):627-633. doi:10.1101/lm.035816.114
98. Smith PH, Uhrich DJ, Manning KA. Evaluation of medial division of the medial geniculate (MGM) and posterior intralaminar nucleus (PIN) inputs to the rat auditory cortex, amygdala, and striatum. *J Comp Neurol*. 2019;527(9):1478-1494. doi:10.1002/cne.24644
99. LeDoux JE. Emotion circuits in the brain. *Annu Rev Neurosci*. 2000;23:155-184. doi:10.1146/annurev.neuro.23.1.155
100. Doron NN, Ledoux JE, Keck WM. Organization of Projections to the Lateral Amygdala From Auditory and Visual Areas of the Thalamus in the Rat Vol 412. *Wiley*; 1999. doi:10.1002/(SICI)1096-9861(19990927)412:3
101. Gründemann J, Bitterman Y, Lu T, Krabbe S, Grewe B, Schnitzer M, Lüthi A. Amygdala ensembles encode behavioral states. *Science (80-)*. 2019;364(6437). doi:10.1126/science.aav8736
102. Weglage M, Wörnberg E, Lazaridis I, Tzortzi O, Meletis K. Complete representation of action space and value in all striatal pathways. *bioRxiv*. August 2020:2020.03.29.983825. doi:10.1101/2020.03.29.983825
103. Belén Pardi M, Vogenstahl J, Dalmay T, Spanò T, Pu D, Naumann L, Kretschmer F, Sprekeler H, Letskus J. A thalamocortical top-down circuit for associative memory. *Science (80-)*. 2020;370(6518):844-848. doi:10.1126/science.abc2399
104. Jun JJ, Steinmetz NA, Siegle JH, et al. Fully integrated silicon probes for high-density recording of neural activity. *Nature*. 2017;551(7679):232-236. doi:10.1038/nature24636
105. Emiliani V, Cohen AE, Deisseroth K, Häusser M. All-optical interrogation of neural circuits. *J Neurosci*. 2015;35(41):13917-13926. doi:10.1523/JNEUROSCI.2916-15.2015
106. Evangelio M, García-Amado M, Clascá F. Thalamocortical Projection Neuron and Interneuron Numbers in the Visual Thalamic Nuclei of the Adult C57BL/6 Mouse. *Front Neuroanat*. 2018;0:27. doi:10.3389/FNANA.2018.00027
107. Bartlett EL. The organization and physiology of the auditory thalamus and its role in processing acoustic features important for speech perception. *Brain Lang*. 2013;126(1):29-48. doi:10.1016/j.bandl.2013.03.003
108. Weinberger NM, Diamond DM. Physiological plasticity in auditory cortex: Rapid induction by learning. *Prog Neurobiol*. 1987;29(1):1-55. doi:10.1016/0301-0082(87)90014-1
109. Gillet SN, Kato HK, Justen MA, Lai M, Isaacson JS. Fear Learning Regulates Cortical Sensory Representations by Suppressing Habituation. *Front Neural Circuits*. 2018;0:112. doi:10.3389/FNCIR.2017.00112
110. Zhang GW, Sun WJ, Zingg B, et al. A Non-canonical Reticular-Limbic Central Auditory Pathway via Medial Septum Contributes to Fear Conditioning. *Neuron*. 2018;97(2):406-417.e4. doi:10.1016/J.NEURON.2017.12.010

111. Ji W, Suga N. Tone-Specific and Nonspecific Plasticity of Inferior Colliculus Elicited by Pseudo-Conditioning: Role of Acetylcholine and Auditory and Somatosensory Cortices. *https://doi.org/10.1152/jn002222009*. 2009;102(2):941-952. doi:10.1152/JN.00222.2009
112. Gilad A, Maor I, Mizrahi A. Learning-related population dynamics in the auditory thalamus. *Elife*. 2020;9:1-18. doi:10.7554/ELIFE.56307
113. Tye KM, Stuber GD, Ridder B de, Bonci A, Janak PH. Rapid strengthening of thalamo-amygdala synapses mediates cue-reward learning. *Nature*. 2008;453(7199):1253. doi:10.1038/NATURE06963
114. Huber D, Gutnisky DA, Peron S, O'Connor DH, Wiegert JS, Tian L, Oertner TG, Looger LL, Svoboda K. Multiple dynamic representations in the motor cortex during sensorimotor learning. *Nat* 2012 4847395. 2012;484(7395):473-478. doi:10.1038/nature11039
115. Blackwell JM, Taillefumier TO, Natan RG, Carruthers IM, Magnasco MO, Geffen MN. Stable encoding of sounds over a broad range of statistical parameters in the auditory cortex. *Eur J Neurosci*. 2016;43(6):751-764. doi:10.1111/EJN.13144
116. Karpova NN, Pickenhagen A, Lindholm J, Tiraboschi E, Kuleskaya N, Agústsðóttir A, Antila H, Popova D, Akamine Y, Bahi A, Sullivan R, Hen R, Drew LJ, Castrén E. Fear Erasure in Mice Requires Synergy Between Antidepressant Drugs and Extinction Training. *Science (80-)*. 2011;334(6063):1731-1734. doi:10.1126/SCIENCE.1214592
117. Resick PA, Schnicke MK. Cognitive Processing Therapy for Sexual Assault Victims. *J Consult Clin Psychol*. 1992;60(5):748-756. doi:10.1037/0022-006X.60.5.748
118. Javitt DC, Sweet RA. Auditory dysfunction in schizophrenia: integrating clinical and basic features. *Nat Rev Neurosci* 2015 169. 2015;16(9):535-550. doi:10.1038/nrn4002
119. Chun S, Du F, Westmoreland JJ, et al. Thalamic miR-338-3p mediates auditory thalamocortical disruption and its late onset in models of 22q11.2 microdeletion. *Nat Med*. 2017;23(1):39-48. doi:10.1038/nm.4240
120. Ward RD, Kellendonk C, Kandel ER, Balsam PD. Timing as a window on cognition in schizophrenia. *Neuropharmacology*. 2012;62(3):1175-1181. doi:10.1016/J.NEUROPHARM.2011.04.014



Appendix 1: Taylor J.A., Hasegawa M., Benoit C.M. Amorim Freire J., Theodore M., Ganea D.A., Innocenti S.M., Lu T., Gründemann J.. Single cell plasticity and population coding stability in auditory thalamus upon associative learning. Nat Commun 12, 2438 (2021).

ARTICLE

<https://doi.org/10.1038/s41467-021-22421-8>

OPEN

Single cell plasticity and population coding stability in auditory thalamus upon associative learning

James Alexander Taylor¹, Masashi Hasegawa¹, Chloé Maëlle Benoit ¹, Joana Amorim Freire¹,
Marine Theodore¹, Dan Alin Ganea¹, Sabrina Milena Innocenti¹, Tingjia Lu² & Jan Gründemann ^{1,3}✉

Cortical and limbic brain areas are regarded as centres for learning. However, how thalamic sensory relays participate in plasticity upon associative learning, yet support stable long-term sensory coding remains unknown. Using a miniature microscope imaging approach, we monitor the activity of populations of auditory thalamus (medial geniculate body) neurons in freely moving mice upon fear conditioning. We find that single cells exhibit mixed selectivity and heterogeneous plasticity patterns to auditory and aversive stimuli upon learning, which is conserved in amygdala-projecting medial geniculate body neurons. Activity in auditory thalamus to amygdala-projecting neurons stabilizes single cell plasticity in the total medial geniculate body population and is necessary for fear memory consolidation. In contrast to individual cells, population level encoding of auditory stimuli remained stable across days. Our data identifies auditory thalamus as a site for complex neuronal plasticity in fear learning upstream of the amygdala that is in an ideal position to drive plasticity in cortical and limbic brain areas. These findings suggest that medial geniculate body's role goes beyond a sole relay function by balancing experience-dependent, diverse single cell plasticity with consistent ensemble level representations of the sensory environment to support stable auditory perception with minimal affective bias.

¹Department of Biomedicine, University of Basel, Basel, Switzerland. ²Friedrich Miescher Institute for Biomedical Research, Basel, Switzerland. ³Deutsches Zentrum für Neurodegenerative Erkrankungen (DZNE), Bonn, Germany. ✉email: jan.gruendemann@unibas.ch

Associative learning depends on the reliable integration of sensory stimuli from the environment and their association with specific aversive or appetitive outcomes to shape future behaviours. Many cortical and limbic brain areas have been identified as centres for associative learning. However, how thalamic sensory relays like the auditory thalamus (medial geniculate body, MGB), which provide direct sensory input to these areas, participate in plasticity upon associative learning, yet ensure stable long-term sensory coding remains unknown. Auditory fear conditioning, a well-studied classical conditioning paradigm, identified the amygdala as a core brain area for associative learning of stimulus-predicted (conditioned stimulus, CS, e.g., tone) aversive outcomes (unconditioned stimulus, US, e.g., mild foot shock)^{1–4}. At its input site, amygdala response plasticity is thought to be driven by synaptic potentiation in basolateral amygdala (BLA) neurons^{5,6}. However, early work demonstrated that the higher order MGB, a major auditory input hub to the amygdala⁷, is a site of CS-US integration and plasticity upon fear learning^{8–15}. Enhanced responses to conditioned stimuli and increased synaptic drive from presynaptic MGB neurons to the BLA might act as an additional plasticity mechanism for associative fear learning. Nevertheless, the role of MGB in neuronal response plasticity upon fear learning has been controversially discussed^{1,16,17} and recent physiological studies of fear conditioning mostly omitted this site of sensory integration and response potentiation upstream of the amygdala and auditory cortex. It is currently unknown if individual MGB neurons exhibit complex response dynamics upon adaptive associative and defensive behaviours and how this potential heterogeneity is balanced with reliable representations of sensory inputs from the environment. Furthermore, we are currently lacking a concept of the ensemble level activity and dynamics in this widely projecting thalamic auditory relay site, which is crucial to delineate the distributed population code underlying associative learning and adaptive defensive behaviours^{18,19}.

Here we used a combination of deep brain Ca^{2+} imaging, miniature microscopy and fear conditioning in freely moving mice to reveal the response dynamics and plasticity of large populations of auditory thalamus neurons^{20–22}. We find that individual auditory thalamus neurons exhibit mixed selectivity of CS and US responses with highly diverse plasticity patterns during associative learning, while the ensemble representation of auditory stimuli remains stable along learning. These findings suggest that auditory thalamus plays a role beyond a classic relay function by balancing experience-dependent plasticity with stable ensemble level representations of the sensory environment to support stable auditory perception with minimal affective bias.

Results

Deep brain imaging of auditory thalamus during fear conditioning. We established a gradient-index lens deep brain miniature microscope imaging approach of identified auditory thalamus neuronal populations in freely behaving mice (Fig. 1a, b)^{20,22}. Using genetically-encoded Ca^{2+} sensors (Fig. 1c, AAV2/5. CaMKII.GCaMP6f)²³, we tracked large populations of individual MGB neurons across a four-day auditory fear conditioning paradigm in freely moving mice. Similar to previous reports²⁴, we found GABAergic fibres, typically originating in inferior colliculus and the thalamic reticular complex^{25,26}, but virtually no GABAergic somata in MGB (Supplementary Fig. 1)²⁷, indicating that we mainly imaged Ca^{2+} activity of thalamic relay neurons. We were able to follow 93 ± 4 GCaMP6f-expressing neurons per mouse (Fig. 1d, e, $N = 24$ mice) stably within and across sessions (see Methods). MGB neurons exhibited diverse, spontaneous activity patterns in freely moving animals (Fig. 1f) as well as cell-specific responses to pure tone auditory stimuli (Fig. 1g).

Next, we used a classic four-day fear conditioning and fear extinction paradigm²⁸ (Fig. 2a, b), in which mice learn to associate a mild foot-shock unconditioned stimulus (US) with a predictive conditioned stimulus (CS+, 6 or 12 kHz pure tones, 200 ms pips, 27 pips per CS). After fear conditioning, mice exhibited enhanced freezing to the CS+ ($61 \pm 6\%$) when compared to a neutral CS– ($42 \pm 8\%$, $N = 15$, $p < 0.01$, Mann–Whitney test, Fig. 2b; Supplementary Fig. 2a), which extinguished upon repetitive CS+ presentation (Friedman test, $p < 0.001$, followed by Dunn’s multiple comparisons test, Extinction 1 early vs. Extinction 1 late $p < 0.01$, Extinction 1 early vs. Extinction 2 late $p < 0.001$, Extinction 2 early vs. Extinction 2 late $p < 0.05$). During fear conditioning, the total neuronal population (Fig. 2c) as well as individual MGB neurons (Fig. 2d, e) were strongly responsive to both the CS+ and the US. The proportion of US responsive neurons ($75 \pm 5\%$) was significantly higher than the proportion of CS+ ($27 \pm 3\%$) and CS– neurons ($20 \pm 2\%$, $N = 9$ mice, see “Methods” for classification of responsive neurons), while similar proportions of neurons were responsive to the CS+ and the CS– (Fig. 2f; Supplementary Fig. 2b, c, Friedman test, $p < 0.001$ followed by Dunn’s multiple comparisons test CS+ vs. CS– $p > 0.05$, CS+ vs. US $p < 0.05$, CS– vs. US $p < 0.001$). Furthermore, we found mixed selectivity in subpopulations of neurons that were responsive to combinations of tones and foot shocks, yet they were not enriched beyond chance level in the total population (Fig. 2g). These multisensory neurons were spatially intermingled in MGB and not locally clustered (Fig. 2h–j).

To test if US responses are solely driven by movement of the animal or self-induced sounds, e.g., escape runs or low frequency harmonic vocalizations during the aversive foot shock, we correlated the activity of individual MGB neurons with movement speed or the occurrence of sounds in the context. First, a large proportion of MGB neurons exhibited an apparent correlation between movement speed and Ca^{2+} activity during the US. However, this is most likely due to the simultaneous occurrence and conflation of the 2 s aversive foot shock and the behavioural output (escape), given that the activity in the large majority of MGB neurons was not motion or speed correlated during the habituation period (Supplementary Fig. 3). In addition, US responses in MGB cannot be solely explained by the auditory environment, i.e., movement sounds or low frequency harmonic vocalization^{29,30} of the animal during the aversive foot shock, given that US and CS+ responses were typically substantially larger in sound correlated neurons than responses to self-evoked sounds of the animal (Fig. 2k; Supplementary Fig. 4). This indicates that MGB US responses are most likely driven by direct somatosensory input, pain signals or aversive state switches.

In summary, our data demonstrates that auditory thalamus neurons are strongly responsive to both pure auditory tones as well as aversive stimuli. This integration of CS and US inputs underlines that MGB neurons are ideal candidates for sensory plasticity upon associative learning^{9,17}.

Neural response dynamics of MGB neurons upon fear conditioning. MGB neurons, particularly in the medial subdivision, have been shown to potentiate auditory CS responses upon fear learning¹⁷. However, their response diversity and dynamics on the population level upon associative learning remain unknown. To understand the learning-related dynamics of MGB neurons, we followed the activity of large populations of individual MGB neurons across the 4-day fear conditioning paradigm. Using a cluster analysis approach, we classified CS+ responsive neurons according to their response dynamics before and after fear conditioning and fear extinction (Fig. 3a, b). On the habituation day

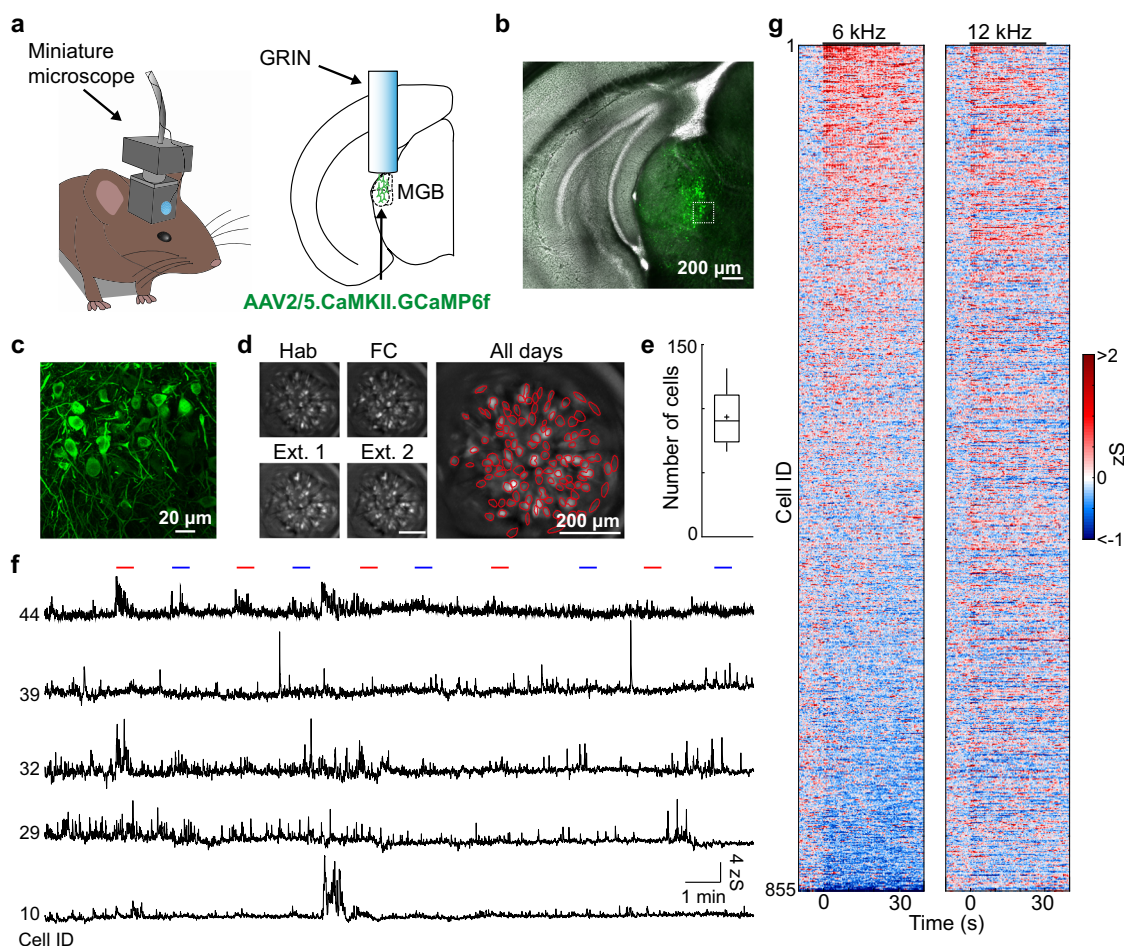


Fig. 1 Imaging neuronal activity of auditory thalamus in freely moving mice. **a** Mouse with a head-mounted miniaturized microscope (left). Location of gradient refractive index (GRIN) lens in the medial geniculate body (MGB, right). **b** Example GCaMP6f expression in MGB. Similarly replicated expression patterns for all animals where GCaMP6f was injected in MGB ($N = 24$ mice). **c** High magnification of GCaMP6f-expressing MGB neurons from **b**. **d** Individual motion corrected fields of view (maximum intensity projection) of one example animal across a four-day fear conditioning paradigm (Hab, FC, Ext. 1, Ext. 2) as well as the maximum intensity projection across all days. Red circles indicate selected individual components. Replicated for all mice ($N = 24$) that underwent calcium imaging. **e** Average number of individual ICs/animal (93 ± 4 neurons, $N = 24$ mice). Boxplots show median, 2nd, 3rd quartile, minimum and maximum. Cross indicates mean. **f** Changes in Ca^{2+} fluorescence of five individual neurons during the habituation session. Lines indicate CS tone presentations (red: 12 kHz, blue: 6 kHz). **g** Tone responses on habituation day 1 of all recorded MGB neurons in fear conditioning experiments ($N = 855$ neurons, $N = 9$ mice).

and on the two extinction days, we identified eight subgroups of CS+ responsive neurons. $7 \pm 1\%$ of cells show stable CS+ responses across days. The remainder could be separated in the following subgroups of plastic neurons: neurons that abolish their complete ($21 \pm 3\%$, CS down cells) or onset ($9 \pm 2\%$, on-down cells) CS+ response after fear conditioning, neurons with enhanced CS+ responses when the animal is in a high fear state ($23 \pm 5\%$, fear cells), neurons that are inhibited when the animal is in a high fear state ($4 \pm 1\%$, fear-down cells) as well as neurons that enhance or decrease their response when the animal extinguished the fear behaviour ($14 \pm 3\%$, extinction-up cells; $8 \pm 2\%$, extinction-down cells). In addition, we identified cells that had stable, enhanced CS+ responses after fear learning ($14 \pm 4\%$, persistent cells, Fig. 3c). Similar subgroups were found for CS− responsive neurons. However, in contrast to the US-paired CS+, the group of CS− stable cells was most prominent across days (Supplementary Fig. 5a–c). In addition, we found similar proportions of CS+ (Supplementary Fig. 2b) and CS− responsive (Supplementary Fig. 2c) neurons during the habituation, fear conditioning and extinction days. However, the proportion of neurons that were plastic and changed their CS responses across

days was significantly higher in the CS+ group ($93 \pm 1\%$) compared to the CS− group ($60 \pm 7\%$, 2-way ANOVA, $p < 0.0001$, followed by Tukey post hoc test, $p < 0.05$), while the proportion of stable neurons was higher in the CS− ($40 \pm 7\%$) compared to the CS+ group ($7 \pm 1\%$, 2-way ANOVA, $p < 0.0001$, followed by Tukey post hoc test, $p < 0.05$, Fig. 3d), indicating that neural response plasticity is learning-specific and more prominent for the paired conditioned stimulus than the control stimulus. To rule out that CS+ plasticity is not just a result of a general drift in tone responsiveness across days, we performed an unpaired conditioning paradigm where the foot shock is not temporally contingent with the tone CS+, such that the mice experience similar sensory stimuli to the fear conditioned animals but do not associate the CS+ with the US and fail to learn to freeze to the CS+ (Supplementary Fig. 6a, b). Unpaired conditioning did not affect the proportions of tone and foot shock responsive neurons in MGB (Supplementary Fig. 6c–h). However, compared to fear conditioned animals, the majority of neurons exhibited stable across-day CS+ tone responses in the unpaired condition ($61 \pm 9\%$), while the proportion of plastic neurons was significantly decreased ($39 \pm 9\%$, $N = 5$ mice, Fig. 3e). This data indicates that

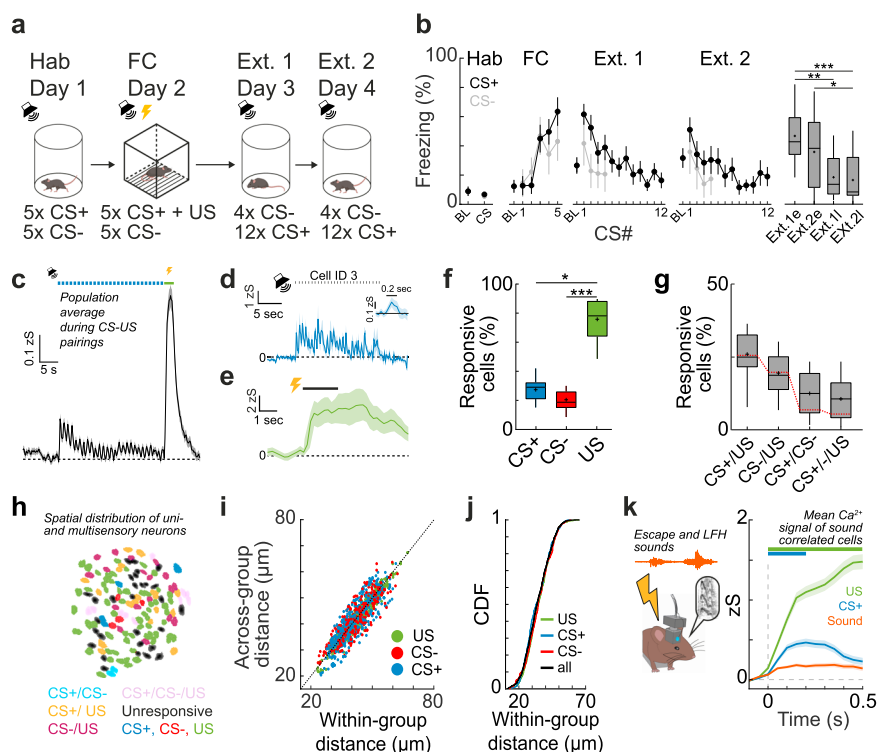


Fig. 2 Mixed selectivity tone CS+ and shock US coding of MGB neurons upon fear conditioning. **a** Details of the 4-day fear conditioning paradigm. **b** Conditioned stimulus (CS) CS+ and CS− freezing (mean ± s.e.m.) during the habituation, fear conditioning as well as extinction days (Ext. 1, Ext. 2. e and l indicate early and late phases of extinction, i.e., the first four or last four CS+ of the session. Friedman test, $p < 0.001$, followed by Dunn's multiple comparisons test, Ext.1e vs Ext.1l $p = 0.0069$, Ext.1e vs Ext.2l $p = 0.0002$, Ext.2e vs Ext.2l $p = 0.0281$, $N = 15$ mice). Boxplots represent median, 2nd, 3rd quartile, minimum and maximum. Cross indicates mean. **c** Population response of one example animal to the CS+ and US (unconditioned stimulus, mean ± s.e.m.). Blue dots indicate CS+ tone pips. Green bar indicates shock US. Example cell response to the CS+ (**d**) and US (**e**). Mean ± s.e.m. of five trials. Dots indicate CS+ tone pips. Inset represents average response to single pips. **f** Proportion of CS+, CS− and US responsive neurons. Friedman test, $p < 0.001$, followed by Dunn's multiple comparisons test: CS+ vs. US, $p = 0.029$; CS− vs. US, $p = 0.0005$ ($N = 9$ mice). Boxplots represent median, 2nd, 3rd quartile, minimum and maximum. Cross indicates mean. **g** Proportion of mixed selectivity CS+ and US coding neurons. Red line indicates chance overlap level ($N = 9$ mice). Boxplots represent median, 2nd, 3rd quartile, minimum and maximum. Cross indicates mean. **h** Example spatial map of unisensory and multisensory mixed selectivity CS and US coding neurons in MGB. **i** Relationship between within response group and across response group pairwise spatial distance between neurons ($N = 855$ cells, $N = 9$ mice). **j** Cumulative distribution function of pairwise distances between all, US-responsive, CS+ and CS− responsive neurons ($N = 855$ cells, $N = 9$ mice). **k** Mean Ca^{2+} activity (± s.e.m.) of sound-correlated neurons during shock evoked sound events e.g., mouse escape sounds and low frequency harmonic vocalizations (LFH, orange), the first CS+ pip (blue) and the US (green) from $N = 550$ CS+/US or $N = 4956$ sound event trials from 110 cells out of $N = 3$ mice. *, **, *** indicate p values smaller than 0.05, 0.01 and 0.001, respectively.

MGB single cell tone responses are by-and-large stable across days, while CS+ response dynamics of individual neurons after fear conditioning are due to associative learning-induced plasticity and not just a general drift of tone-responsiveness in MGB across days. Notably, for the minority of MGB neurons that exhibited CS+ plasticity, the relative proportion of fear cells is significantly decreased (Supplementary Fig. 6f) when compared to fear conditioned animals, indicating that the emergence of this population of neurons with potentiated CS+ responses is specific to auditory fear learning.

All-in-all, this data reveals a broad response diversity of MGB neurons upon fear learning that extends previous observations of fear conditioning potentiated neurons^{15,16,31}. The plastic CS+ subgroups are similar to previously described functional groups in the amygdala^{21,22,28,32}. While fear and extinction neurons are the most prominent groups, they appear alongside other distinct subgroups, indicating that diverse CS+ response plasticity occurs not only in the amygdala, but also upstream in auditory thalamus.

MGB neurons are diversely tuned to auditory frequencies⁹ and individual neurons were reported to change their frequency tuning upon associative learning^{11,12,31}. To estimate changes in auditory frequency tuning in large populations of individual

MGB neurons before and after fear conditioning, we presented 200 ms pips of at least eleven different pure tone frequencies (1–40 kHz) at 65–85 dB to freely moving mice while simultaneously imaging MGB Ca^{2+} activity (Fig. 3f). We found that the mean pip response of the MGB population across all frequencies was nearly doubled after fear conditioning (Fig. 3g). Furthermore, the proportion of tone responsive neurons was increased post conditioning (Fig. 3h, before: $22 \pm 7\%$, after: $37 \pm 6\%$, Wilcoxon signed-rank test, $p < 0.05$, $N = 7$ mice). Besides a general enhancement of pip responses across the whole population and all tones, we found that fear conditioning induces a specific enhancement of selective frequencies compared to the pre-conditioning state (Fig. 3i), which resulted in a shift of the best frequency towards the conditioned stimulus (Fig. 3j, pre FC: |Best frequency - CS+| = 11 ± 0.45 kHz, post FC: |Best frequency - CS+| = 8 ± 0.39 kHz, Wilcoxon signed-rank test, $p < 0.001$, $N = 284$ cells from $N = 7$ mice). This shift was specific for the CS+ and did not occur for the CS− (Fig. 3k, $p > 0.05$, Wilcoxon signed-rank test). This data indicates that auditory fear conditioning affects the auditory frequency tuning of MGB neurons in a stimulus specific manner. However, the absolute shift across the population is small (ca. 3 kHz), suggesting that

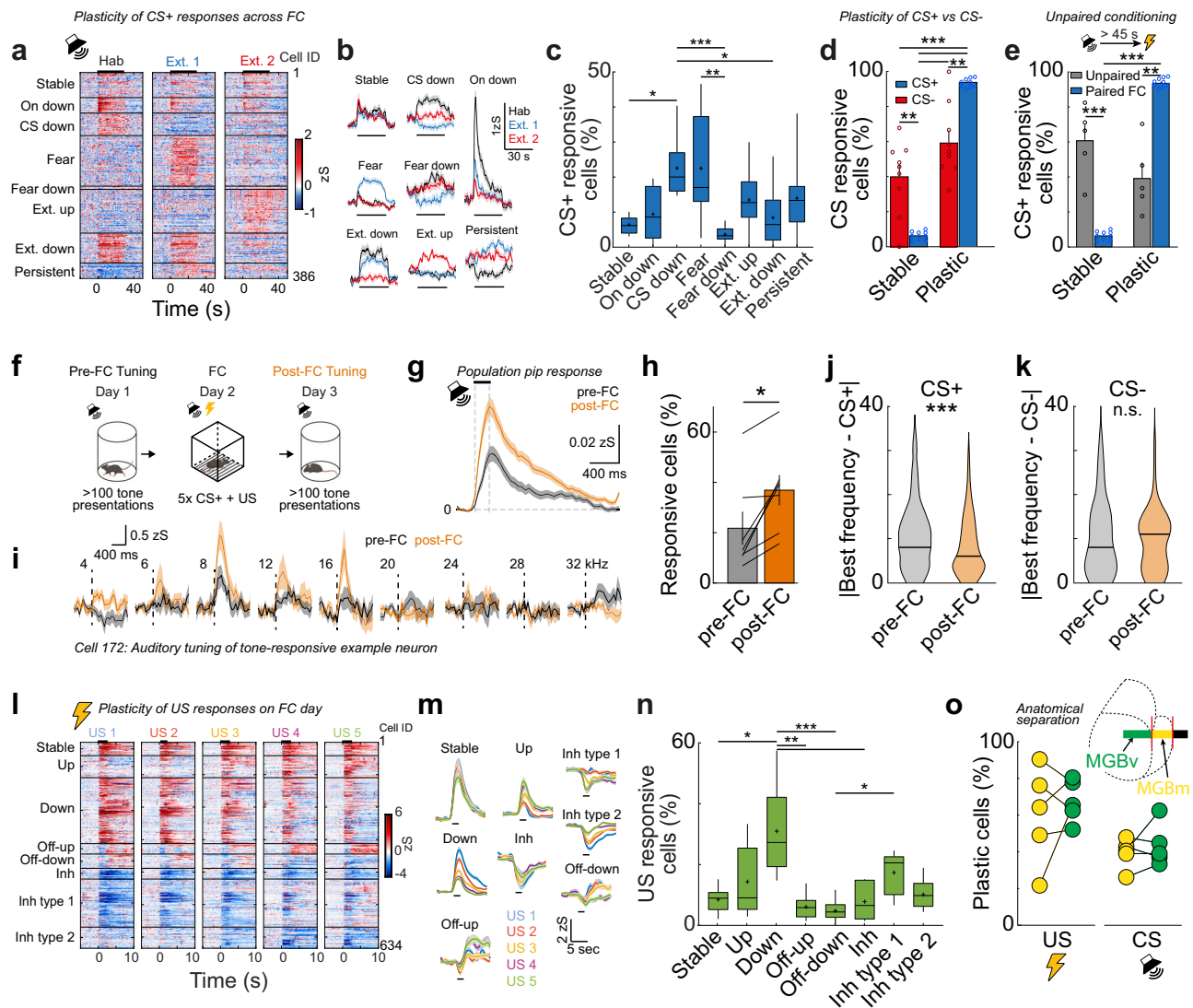


Fig. 3 Single cell response plasticity in MGB upon fear learning. **a** Heat map of single cell CS+ responses on the habituation, extinction 1 and extinction 2 days. Cells were clustered into groups depending on their CS+ response pattern ($N = 386$ cells, $N = 9$ mice). **b** Average traces \pm s.e.m. of neuronal clusters in (a). **c** Proportion of individual plasticity groups within CS+ responsive cells/animal (Kruskal-Wallis test, $p < 0.05$, followed by Dunn's multiple comparisons test; Stable vs cs down, $p = 0.013$, cs down vs fear down, $p = 0.0003$, cs down vs extinction down, $p = 0.035$, fear vs fear down $p = 0.0041$; $N = 9$ mice). Boxplots represent median, 2nd, 3rd quartile, minimum and maximum. Cross indicates mean. **d** Proportion of CS+ and CS- stable and plastic neurons (2-way ANOVA followed by Sidak multiple comparisons test, $p < 0.001$; stable CS- vs. stable CS+, $p = 0.002$; stable CS- vs. plastic CS+, $p < 0.001$; stable CS+ vs. plastic CS-, $p < 0.001$; stable CS+ vs. plastic CS+, $p < 0.001$; plastic CS- vs. plastic CS+, $p = 0.002$, $N = 9$ mice, data presented as mean values \pm s.e.m.). Circles represent individual animals. **e** Proportion of CS+ stable and plastic neurons in a pseudoconditioning paradigm compared to fear conditioned animals (2-way ANOVA followed by Sidak multiple comparisons test, $p < 0.001$; stable unpaired vs plastic unpaired, $p = 0.019$; stable paired vs. plastic paired, $p < 0.001$; stable unpaired vs. stable paired, $p < 0.001$; plastic unpaired vs. plastic paired, $p < 0.001$, Unpaired group $N = 5$ mice, Paired group $N = 9$ mice, data presented as mean values \pm s.e.m.). Circles represent individual animals. **f** Experimental paradigm. Auditory tuning was tested before and after fear conditioning. **g** Population response to individual 200 ms pips before (black) and after (orange) fear conditioning (mean \pm s.e.m., $N = 681$ cells, $N = 7$ mice). **h** Proportion of tone-responsive cells before and after fear conditioning (Two-tailed, Wilcoxon signed-rank test, $p = 0.0156$, $N = 7$ mice, data presented as mean values \pm s.e.m.). Lines represent individual animals. **i** Mean auditory responses \pm s.e.m. of one example neuron before (black) and after (orange) fear conditioning to different tone frequencies (numbers indicate kHz). CS+ : 8 kHz, CS- : 20 kHz. **j** Population statistics for BF tuning towards the CS+ (two-tailed Wilcoxon signed-rank test, $p < 0.001$, $n = 284$ neurons, 7 mice). Horizontal lines represent median. **k** Population statistics for BF tuning towards the CS- (two-tailed Wilcoxon signed-rank test, $p > 0.05$, $N = 284$ neurons, 7 mice). Horizontal lines represent median. **l** Heat maps of single cell US responses to the five US stimulations during the fear conditioning day ($N = 634$ cells, $N = 9$ mice). **m** Average response \pm s.e.m. of plasticity subtypes of US-responsive MGB neurons ($N = 634$ cells, $N = 9$ mice, see also Supplementary Fig. 3). **n** Proportion of individual plasticity groups within US responsive cells/animal (Kruskal-Wallis test, $p < 0.01$ followed by Dunn's multiple comparisons test; Stable vs down, $p = 0.043$; down vs off-up, $p = 0.0006$; down vs. off-down, $p < 0.001$; down vs. inh, $p = 0.0055$; off-down vs inh type 1, $p = 0.018$; $N = 9$ mice). Boxplots represent median, 2nd, 3rd quartile, minimum and maximum. Cross indicates mean. **o** Proportion of US ($N = 5$ mice, $p > 0.05$, Wilcoxon signed-rank test) and CS plastic cells ($N = 5$ mice, $p > 0.05$, two-tailed Wilcoxon signed-rank test) in the ventral (MGBv) and medial (MGBm) subdivisions of MGB. Insert: Schematic of GRIN lens location above the different MGB subdivisions. *, **, *** indicate P values smaller than 0.05, 0.01 and 0.001, respectively.

MGB preserves a broad tuning range for reliable sensory representation, despite a stronger representation of the CS+.

In addition to plasticity of CS tone representations, we found that US responsive neurons can be subdivided into stable ($8 \pm 1\%$) and plastic cells ($92 \pm 1\%$) during fear conditioning. The majority of US responsive cells was plastic and exhibited dynamic intra-session representations of the US (Mann–Whitney test, $p < 0.001$). Using a similar cluster analysis approach, we identified neurons that demonstrated intra-session potentiation or depression and subtypes of inhibited as well as off-responsive neurons that potentially signal relief from the shock (Fig. 3l–n). However, despite its prominent diversity, the US response type was not predictive of CS plasticity in MGB neurons. US response and plasticity type did not overlap with CS response and plasticity type above chance levels (Supplementary Fig. 7), indicating that US inputs per se do not drive plasticity in MGB neurons. Nevertheless, adaptive US responses in MGB could act as an upstream teaching signal in addition to local circuit mechanisms³³, which direct plasticity in downstream areas like the amygdala.

MGB is subdivided into a first order, auditory cortex-projecting nucleus (MGBv) as well as higher order nuclei (MGBd, MGBm), which send axons to cortical and limbic brain areas, e.g., the amygdala (Doron and LeDoux, 1999). To test if MGB CS and US plasticity types are different between first order and higher order nuclei, we subdivided the cells depending on their location in the GRIN lens field of view between MGBv and MGBm after anatomical verification of the lens front location for all mice where MGBv and MGBm were simultaneously imaged ($N = 5$ mice, Supplementary Fig. 8a, b). Similar to the total population of MGB neurons, large fractions of MGBv and MGBm neurons exhibited plasticity to the US or CS+ (Fig. 3o). Nevertheless, plastic cells were not significantly different between either subdivision (Fig. 3o) and the diversity of plasticity subtypes was similar in the first order (MGBv) vs. higher order (MGBm) area of auditory thalamus (Supplementary Fig. 8c–e).

Overall, we found that responses of individual MGB neurons to the CS and US are plastic upon fear conditioning. In addition to previously reported potentiated auditory neurons, we find highly diverse subtypes of CS or US plastic neurons that go beyond FC-driven response potentiation and are distributed similarly across both first order and higher order MGB subdivisions. US response subtypes were not predictive of CS plasticity, nor were the proportions of subgroups or their enrichment predictive of behavioural outcomes on an animal-by-animal basis (Supplementary Table 1), indicating that MGB neurons might play diverse roles in guiding memory formation during associative learning.

Amygdala-projecting MGB neurons are plastic upon associative fear learning. Higher order MGBm neurons project to different output targets including primary and secondary auditory cortex, striatum and the basolateral amygdala^{34–37}. Enrichment of plastic neurons in the MGB → BLA pathway might be crucial for fear learning, given BLA's key role in aversive memory formation³⁸. Similar to previous reports³⁹, we found BLA-projecting MGB neurons to be typically located in higher order MGB areas and particularly enriched in the medial subdivision of MGB (Fig. 4a, b, MGBm, 70 ± 7 vs. $23 \pm 6\%$ dorsal, MGBd or $7 \pm 3\%$ ventral, MGBv). By-and-large, 30% of MGBm and 10% of MGBd neurons were amygdala-projecting (Fig. 4c). In contrast, only a small fraction of MGBv neurons (2%) were retrogradely traced from the amygdala. Furthermore, $85 \pm 2\%$ of amygdala-projecting MGB neurons (Fig. 4d; Supplementary Fig. 9a, $N = 6$ mice) were positive for the higher-order MGB area marker

calretinin⁴⁰, suggesting that calretinin is a highly prevalent but not exclusive marker of BLA-projecting MGB neurons.

To test the physiological function and neuronal activity of amygdala-projecting MGB neurons in fear learning, we used a retrograde virus approach to specifically express GCaMP6f in MGB → BLA-projectors (see “Methods”, Fig. 4e; Supplementary Fig. 9b). On average, we could identify 69 ± 9 BLA-projecting GCaMP6f-positive MGB neurons per mouse (Fig. 4f, g, $N = 6$ mice). Similar to the total MGB population average response (Fig. 2c), MGB → BLA projectors were activated by the CS+ and the US (Fig. 4h). Across animals, $22 \pm 5\%$, $10 \pm 2\%$ or $68 \pm 7\%$ of neurons were responsive to the CS+, CS– or US, respectively. These proportions are comparable to the total MGB population (Figs. 4i, 2-way ANOVA, $p > 0.05$). Furthermore, we did not find that combinations of CS+, CS– and US coding neurons were enriched above chance levels (Fig. 4j). Using a cluster analysis approach, we found the same subgroups of CS+ plasticity types in the subpopulation of MGB → BLA projecting neurons (Fig. 4k, l) across the conditioning paradigm, including stable cells, onset-down cells, CS-down cells, fear cells, fear-inhibited cells, extinction up cells, extinction down cells as well as persistent cells (Supplementary Fig. 9c–e). The proportions of the CS+ plasticity subgroups were similar to the total population in MGB (2-way ANOVA, $p > 0.05$). Analogous to the CS+ representation across days, we found comparable proportions of US plasticity types in MGB → BLA projectors when compared to the total population (Fig. 4m; Supplementary Fig. 9f, 2-way ANOVA, $p > 0.05$).

This data demonstrates that CS as well as US information is encoded by BLA-projecting MGB neurons, identifying MGB → BLA projectors not only as a source of CS tone inputs but also as a strong source of aversive US signals (see also⁹). However, CS and US plasticity is functionally diverse beyond response potentiation and, compared to the total MGB population, CS and US signalling is not enriched in this specific subpopulation of amygdala-projecting MGB neurons.

Activity in the MGB → BLA pathway is necessary for fear memory consolidation and stabilizes MGB plasticity. To test if activity in MGB → BLA projection neurons is necessary for fear learning^{8,41–44} and MGB plasticity, we specifically expressed the inhibitory opsin ArchT in MGB → BLA projection neurons (Fig. 5a, b, Supplementary Fig. 10a–e). Inhibition of MGB → BLA projectors during CS-US pairing on the conditioning day (Fig. 5c) had no effect on fear acquisition (Fig. 5d, mean freezing during the last two CS+ presentations, GFP: $65 \pm 4\%$, $N = 13$ mice; MGB → BLA ArchT: $60 \pm 6\%$, $N = 9$ mice; $p > 0.05$, Mann–Whitney test, Supplementary Fig. 10f). However, freezing levels were significantly reduced during the fear test 24 h later (Fig. 5e, mean freezing during the first four CS+, GFP: $48 \pm 6\%$, $N = 13$ mice; MGB → BLA ArchT: $22 \pm 5\%$, $N = 9$ mice; $p < 0.01$, Mann–Whitney test), indicating that activity in MGB → BLA projectors is necessary for the consolidation of fear memories. In addition, and similar to amygdala-projecting MGB neurons (Fig. 5a–e), we found that inhibition of neuronal activity in the total MGB population (Supplementary Fig. 10f–i) or in the first order ventral nucleus of MGB (Supplementary Fig. 10j) had no effect on fear acquisition during the conditioning session but suppressed fear memory consolidation.

To test how activity in MGB → BLA neurons during fear learning affects across-day plasticity of the total MGB population, we used an all-optical miniaturized microscope imaging approach (Fig. 5f). We specifically expressed ArchT or tdTomato in MGB → BLA neurons (Fig. 5g) and suppressed their activity during the CS-US pairings on the fear conditioning day (Fig. 5c)

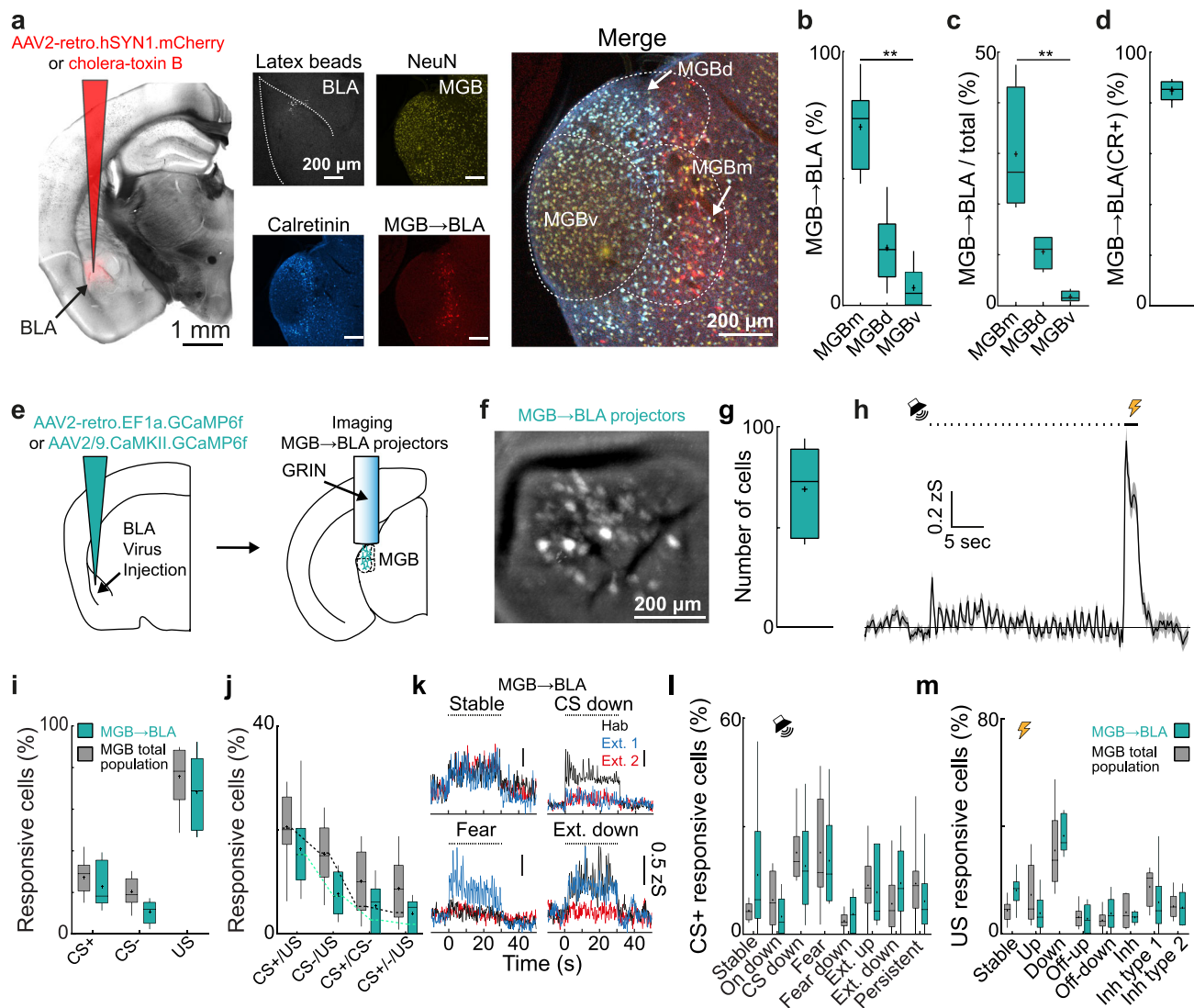


Fig. 4 Functional subclasses of CS and US coding neurons are not enriched in amygdala projecting MGB neurons. **a** Injection of AAV2-retro.hSyn1.mCherry.WPRE.hGHP(A) and latex beads in the basolateral amygdala (BLA). MGB was counterstained for calretinin (cyan) and NeuN (yellow) to quantify the BLA projectors (red). **b** Distribution of BLA-projecting neurons within MGB ($N = 6$ mice, Friedman test $p < 0.001$, followed by Dunn's multiple comparisons test %MGBm vs. %MGBv, $p = 0.0016$). Boxplots represent median, 2nd, 3rd quartile, minimum and maximum. Cross indicates mean. **c** Region-specific proportion of BLA-projecting neurons within MGB subdivisions ($N = 4$ mice, Friedman test, $p < 0.01$, followed by Dunn's multiple comparisons test, %MGBm vs. %MGBv, $p = 0.014$). Boxplots represent median, 2nd, 3rd quartile, minimum and maximum. Cross indicates mean. **d** Proportion of calretinin-positive BLA-projecting neurons ($N = 4$ mice). Boxplots represent median, 2nd, 3rd quartile, minimum and maximum. Cross indicates mean. **e** Schematic of viral strategy and location of GRIN lens in MGB to image neuronal activity of MGB → BLA-projecting neurons. **f** MGB field of view with MGB → BLA-projecting neurons. Replicated in all animals that underwent calcium imaging ($N = 6$ mice). **g** Number of identified individual components per animal (69 ± 9 , $N = 6$ mice). **h** Mean \pm s.e.m population response of one example animal to the CS+ and CS-. Black dots indicate CS + tone pips. Bar indicates shock US. Boxplots represent median, 2nd, 3rd quartile, minimum and maximum. Cross indicates mean. **i** Proportion of CS+, CS- and US responsive neurons for the total MGB population and amygdala-projecting neurons (2-way ANOVA, main effect group, $F_{(1,13)} = 3.3$, $p > 0.05$, $N = 9$ total MGB population mice and $N = 6$ MGB → BLA projection neurons mice, see also Fig. 2f). Boxplots represent median, 2nd, 3rd quartile, minimum and maximum. Cross indicates mean. **j** Proportion of mixed selectivity CS \pm and US coding neurons for the total MGB population and amygdala projecting neurons 2-way ANOVA, $F_{(1,13)} = 3.9$, $p > 0.05$, $N = 9$ mice for the total MGB population and $N = 6$ mice for the population of MGB → BLA projection neurons, see also Fig. 2. Boxplots represent median, 2nd, 3rd quartile, minimum and maximum. Cross indicates mean. **g** Dotted lines indicate chance overlap level. **k** Examples traces of groups of stable, onset down, fear and extinction neurons. **l** Proportion of individual plasticity groups within CS+ responsive cells / animal (2-way ANOVA, $F_{(1,13)} = 1.2$, $p > 0.05$, $N = 9$ mice for the total MGB population and $N = 6$ mice for the population of MGB → BLA projection neurons). Boxplots represent median, 2nd, 3rd quartile, minimum and maximum. Cross indicates mean. **m** Proportion of individual plasticity groups within US responsive cells / animal (2-way ANOVA, $F_{(1,13)} = 0.5$, $p > 0.05$, $N = 9$ mice for the total MGB population and $N = 6$ mice for the population of MGB → BLA projection neurons). Boxplots represent median, 2nd, 3rd quartile, minimum and maximum. Cross indicates mean. ** indicate p values smaller than 0.01.

while simultaneously imaging the activity of the total MGB population (CaMKII-driven GCaMP6f). Given that MGB → BLA neurons represent only a fraction of the total MGB neuronal population (ca. $11 \pm 2\%$ in total MGB, $N = 4$ mice, see also

Fig. 4c), inhibiting MGB → BLA neurons during fear conditioning did not affect the mean CS+ and US response of the total imaged MGB population (Fig. 5h and Supplementary Fig. 11a–e). However, when comparing the CS+ plasticity across fear learning

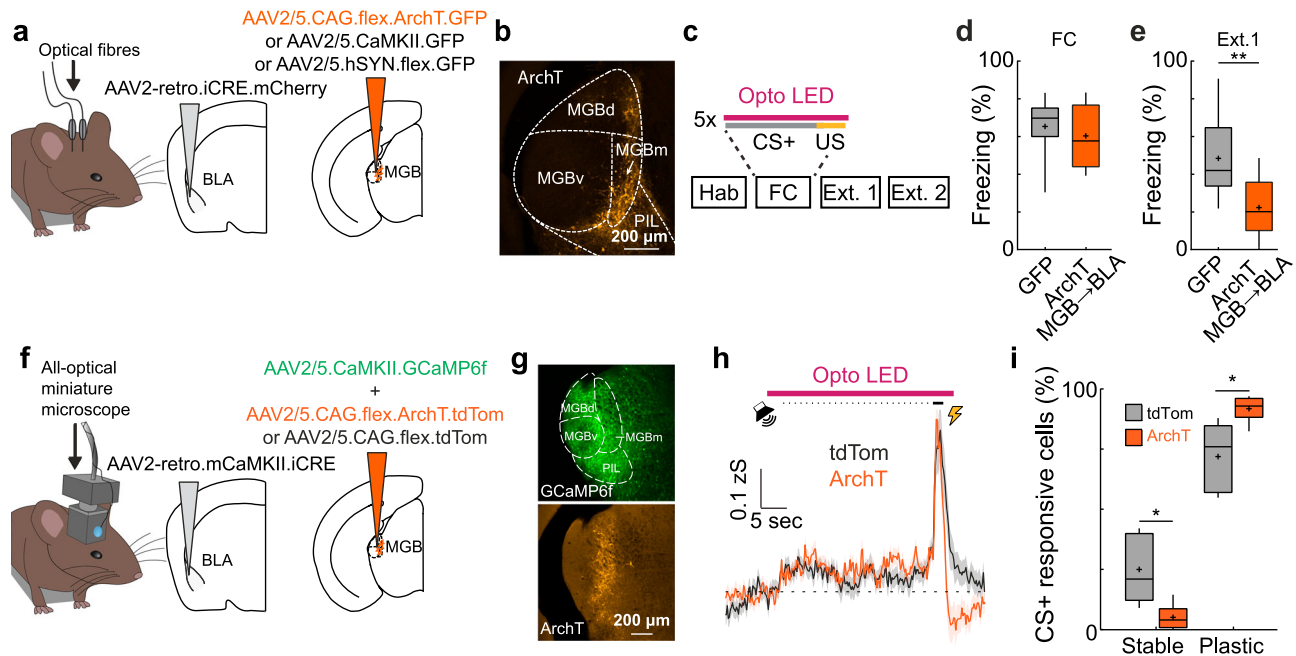


Fig. 5 Inhibition of amygdala projecting MGB neurons prevents memory consolidation and enhances plasticity in MGB. **a** Optogenetic approach to inhibit MGB → BLA projection neurons. **b** Example ArchT expression in MGB → BLA projection neurons. Replicated for all animals that underwent optogenetic inhibition of MGB → BLA neurons ($N = 9$ mice). **c** Experimental paradigm: MGB → BLA neurons are manipulated during the CS+ and US on the fear conditioning day. **d** Freezing of GFP and MGB → BLA ArchT-expressing animals at the end of the fear conditioning paradigm (mean freezing levels to the last two CS+, GFP: $N = 13$ mice, MGB → BLA ArchT: $N = 9$ mice, $p > 0.05$, two-tailed Mann-Whitney test). Boxplots represent median, 2nd, 3rd quartile, minimum and maximum. Cross indicates mean. **e** Freezing of GFP and ArchT-expressing animals upon fear recall during early extinction 1 (Ext. 1, mean freezing during the first four CS+, GFP: $N = 13$ mice, MGB → BLA ArchT: $N = 9$ mice, two-tailed Mann-Whitney test, $p = 0.0056$). Boxplots represent median, 2nd, 3rd quartile, minimum and maximum. Cross indicates mean. **f** All-optical approach to inhibit MGB → BLA projection neurons during simultaneous recording of total MGB population activity. **g** Example GCaMP6f expression in MGB (top) and ArchT expression in MGB → BLA projection neurons (bottom). Replicated for all animals that underwent the all-optical paradigm ($N = 6$ mice). **h** Mean MGB population activity \pm s.e.m in response to CS+ and US stimuli upon optogenetic light presentation of tdTomato (tdTom, black, $N = 5$ mice) and ArchT animals (orange, $N = 6$ mice). **i** Proportion of MGB neurons with stable and plastic CS+ responses after fear conditioning in tdTom ($N = 5$) and ArchT ($N = 6$) mice (2-way ANOVA, $F_{(1, 9)} = 10.09$, $p < 0.05$, Sidak's multiple comparisons test, $p = 0.0104$ each). Boxplots represent median, 2nd, 3rd quartile, minimum and maximum. Cross indicates mean. *, ** indicate p values smaller than 0.05 and 0.01, respectively.

we find that inhibition of MGB → BLA neurons during fear conditioning enhances the proportion of plastic neurons after fear consolidation (Fig. 5i, stable neurons: tdTom = $27 \pm 6\%$, ArchT = $7 \pm 2\%$; plastic: tdTom = $73 \pm 6\%$, ArchT = $93 \pm 2\%$; 2-way ANOVA, $F_{(1, 9)} = 10.09$, $p < 0.05$, Sidak's multiple comparisons test, $p < 0.05$ for stable and plastic neurons; tdTom, $N = 5$, ArchT, $N = 6$ mice). Thus, suppression of activity in MGB → BLA circuits leads to a facilitation of plasticity in MGB—potentially as a compensation mechanism—suggesting that feedforward signalling from MGB to BLA during associative fear learning is crucial to stabilize plasticity in auditory thalamus.

Population coding and representation of the conditioned stimulus across days. Next, we tested if the CS+ and CS− can be decoded from Ca^{2+} activity based on MGB population activity. First, we trained a three-way quadratic decoder to distinguish between CS+, CS− and baseline activity within the same session (see “Methods”). To balance for different cell population sizes between animals, we randomly sub-selected 40 cells for each animal and averaged decoder accuracy across 50 independent runs. Furthermore, to account for different numbers of CS+ and CS− presentations, we only decoded the first four CS+ and CS− presentations. Within each individual session, the decoders achieved high classification accuracy (Fig. 6a, $>80\%$ compared to 33% chance level) indicating a distinct representation of the individual CSs by the MGB population. Surprisingly, decoding

accuracy was higher in the population of MGB → BLA projectors compared to the total MGB population, except for the fear conditioning day. To test if CS tones can be accurately detected across days from MGB population activity, we next trained sets of two-way decoders to distinguish between baseline and CS+ or CS− responses for each experimental day and tested the trained decoders across days (Fig. 6b). Strikingly, we found that decoder accuracy is robust across days reaching decoding levels of ca. 70% or higher, for both the CS+ and the CS− (Fig. 6c). This is in contrast to amygdala population coding, where decoding levels for the CS+ drop to chance levels after fear conditioning²¹, indicating that MGB population representations of CS tones are stable despite associative learning. Furthermore, we found a drop in CS+ encoding in MGB → BLA projectors during the fear conditioning day, which recovered afterwards (Fig. 6c, see also Fig. 6a), indicating temporary changes in CS+ encoding during associative learning.

Finally, we compared the population vector distance (PVD) between the evoked population responses to the CS+ and CS− and the evoked population responses to the US (Fig. 6d–g). During fear conditioning, we found a decrease of the PVD between the CS+ and the US with consecutive CS-US pairings (Fig. 6d) for both the total MGB population as well as for MGB → BLA-projectors. However, the time courses of the PVD change were different and only the MGB → BLA population reached a significant change in PVD at the end of the session indicating different population dynamics for this subgroup of

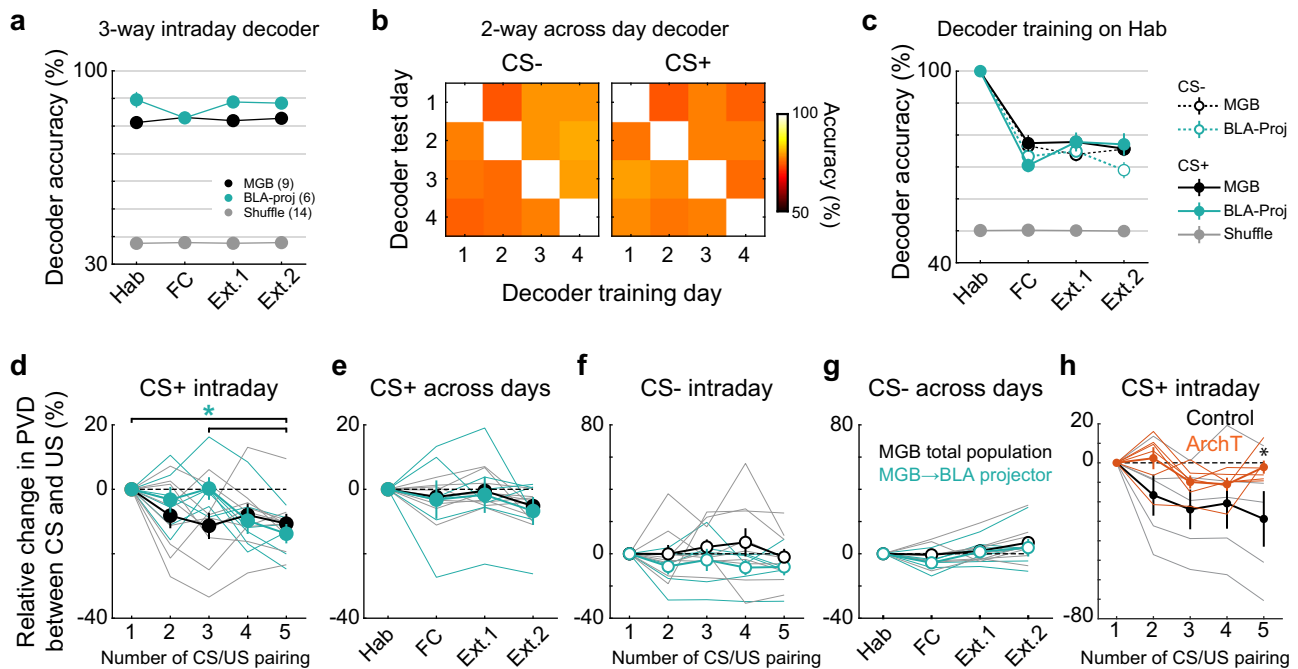


Fig. 6 MGB population dynamics are stable across days. **a** Intraday three-way decoder of CS+, CS– and baseline population responses in CaMKII-positive (black) and identified amygdala-projecting MGB neurons (turquoise) reached a minimum mean accuracy of 81% across animals. Decoder accuracy dropped to chance levels for decoders trained on randomly label training sets (data presented as mean values \pm s.e.m.). **b** Intra- and across day accuracy of decoders trained on CS+ or CS– vs. baseline responses, respectively. 1: Hab, 2: FC, 3: Ext. 1, 4: Ext. 2. **c** Quantification of intra and across day decoder accuracy for decoders trained on habituation day data. Mean decoder accuracy across days is $>70\%$ for CS+ and CS– population responses in CaMKII-positive and identified amygdala-projecting MGB neurons (MGB→BLA $N = 6$ mice, MGB $N = 9$ mice, data represent mean \pm s.e.m.). **d** Relative change in Euclidean population vector distance between the CS+ (**d**, **e**) or CS– (**f**, **g**) and the US within the fear conditioning session (**d**, **f**) or across the individual days of the behavioural paradigm (**e**, **g**). Statistics: **d**: Friedman test across the relative change in CS+ to US PVD of MGB → BLA-projectors ($p < 0.01$), Dunn-Sidak multiple comparisons test 1st and 3rd vs. 5th CS/US pairing, $p < 0.05$. **g**: Friedman test across the relative change in CS– to US PVD of the total BLA-population ($p < 0.05$), Dunn-Sidak multiple comparisons test FC vs. Ext.2: $p < 0.05$. All other data sets in **d**–**g**: $p > 0.05$. MGB population: $N = 9$ mice, MGB → BLA-projectors: $N = 6$ mice (data represent mean \pm s.e.m.). **h** Relative change in PVD between the CS and US for Control and ArchT (2-way ANOVA followed by Sidak's post hoc test, $p < 0.005$, 5th CS+ presentation Control vs. ArchT, $p = 0.0438$, Control $N = 5$ mice, ArchT $N = 6$ mice, data represent mean \pm s.e.m.).

MGB neurons during associative learning (Friedman test, $p < 0.01$, 1st and 3rd versus 5th pairing; Dunn-Sidak multiple comparisons test, $p < 0.05$). Importantly, no changes were found between the evoked responses to the CS– and US during conditioning. In contrast to previous observations in the amygdala²¹, the PVD between the CS+ and the US changes were not preserved post conditioning on the extinction days and the population representation recovered to pre-conditioning levels similar to the observations using two-way or three-way decoders (Fig. 6a, c). The same was observed for the across-day population vector distance of the CS+ to itself (Supplementary Fig. 12). However, note that we found a significant difference between the CS– to US PVD of the total MGB population between the conditioning day and the second extinction day (FC versus Ext. 2: Friedman test, $p < 0.05$, Dunn-Sidak multiple comparisons test, $p < 0.05$). Nevertheless, we did not find a change in the CS– to US PVD between the habituation, fear conditioning and early extinction days indicating that the CS– representation is stable during high fear states in relation to the habituation day and shows no significant drift intraday during fear conditioning. Furthermore, the CS– drifts further away from the US in comparison to the habituation day which might be reflective of an enhanced safety signal after extinction.

In addition to the general lack of consolidation of population level changes across fear learning, the strength of PVD-changes between the CS+ and US were not predictive of learned freezing behaviour on an animal-by-animal basis (Supplementary Fig. 13).

Finally, using an all-optical approach to inhibit MGB → BLA projectors during fear learning (see Fig. 5), we find that the suppression of activity in MGB → BLA leads to a reduced shift in the population vector distance between the CS+ and the US on the fear conditioning day (Fig. 6h, 5th pairing, relative change control: $-30 \pm 13\%$, ArchT: $-2 \pm 3\%$, 2-way ANOVA, $p < 0.05$, Sidak multiple comparisons test, $p < 0.05$), which might be crucial for downstream population plasticity in BLA. However, suppression of MGB → BLA activity did not affect the post-conditioning CS-US PVD-change reset (Supplementary Fig. 11f–h).

Taken together, this data indicates that high dimensional representations of CS+ tones are stably encoded in MGB populations across associative fear learning, despite plastic changes in single cell response patterns. In contrast to the basolateral amygdala²¹, MGB population representations of sensory stimuli only transiently change during associative fear learning and reset overnight, which might be crucial for unbiased representations of stimuli from the environment.

Discussion

By imaging large populations of MGB neurons, we find that auditory thalamus is a site of diverse neuronal plasticity during associative fear learning on the level of single cells as well as the total MGB population. However, changes in MGB population level coding are only transient and do not consolidate overnight, which might be instructive for plastic changes in downstream

structures during learning, yet allows for long-term stability of sensory coding across days.

On the level of individual MGB neurons, we observed associative learning-induced CS+ response potentiation that resembles classic studies which demonstrated that auditory thalamus exhibits enhanced responses to aversive conditioned tones^{14–16,45}. However, recording simultaneously from large populations of individual neurons in MGB during fear conditioning, we find diverse plasticity patterns (at least 7) that are similar or go beyond previously reported plasticity types in cortical⁴⁶ or limbic areas^{21,22,28,32} downstream of MGB as well as calretinin-positive subpopulations of lateral thalamus neurons⁴⁴. Changes in CS responsiveness of individual MGB neurons upon fear learning and extinction were bidirectional, i.e., potentiated or depressed, and depended on the behavioural state of the animal. For example, we find different functional types that are enhanced or depressed particularly in high fear or extinction states. This extends the notion of unidirectional response potentiation in MGB upon associative learning and demonstrates that auditory thalamus neurons exhibit heterogeneous, adaptive signalling of threat-predicting auditory stimuli of the environment. Plasticity in MGB is specific to auditory fear conditioning and not just a general drift of single cell responses across days. However, by-and-large, the proportion of individual plasticity subtypes was not correlated with the strength of post-conditioning freezing or discrimination levels⁴⁷ of the animals (Supplementary Table 1, Supplementary Fig. 13b), suggesting that individual functional neuronal types in MGB are per se not predictive of an animals' behavioural output. Nevertheless, the heterogeneity of the neuronal response plasticity might be necessary to enhance the computational capacity and memory specificity of MGB^{48–51}. Furthermore, precise behavioural outputs might be orchestrated by heterogeneous and complex activity in MGB in coordination with a distributed downstream network. For example, MGB neurons project onto amygdala principal neurons and several amygdala interneuron subclasses^{33,44,52–55}, suggesting that the diversity of MGB plasticity is tuned to the precise MGB → BLA connectivity. This in turn would be crucial for the specific activation of distinct amygdala circuits and amygdala memory engrams to recruit input specific behavioural outputs^{44,56–58}.

Besides auditory stimuli, MGB neurons signal the aversive foot shock (US) during fear conditioning^{9,15}. Indeed, we found that the proportion of foot shock encoding neurons exceeds the number of tone CS+ encoding neurons in auditory thalamus of freely moving animals. The large proportion of US encoding neurons in MGB and the strength of the US signal on the population level could not be explained by movement of the animal or self-vocalization-induced activation of MGB^{59,60}. Aversive US responses are considered to be more prominent in higher order auditory thalamus (MGBm)⁹. Our imaging sites covered both first order (MGBv) and higher-order (MGBm) MGB, and US encoding neurons were equally present in both sites. This demonstrates that multisensory encoding is not an exclusive feature of higher-order areas of MGB in freely moving animals, but can also occur in the first order ventral subdivision that projects to auditory cortex, suggesting that auditory thalamus conveys aversive US information to a broad range of cortical and limbic downstream areas during associative fear learning. Strikingly, US responses were heterogeneous across the population of MGB neurons during fear conditioning. Besides stable US responders, we identified several plasticity types of US responsive neurons, including short term facilitating, depressing or off-responsive neurons. This functional diversity of US neurons indicates that first and higher order auditory thalamus can signal distinct types of instructive information, for example adaptive teaching signals for associative fear learning as well as relief or

safety signals upon termination of the US. Future studies need to address if and how these non-uniform adaptive MGB US signals are relayed to specific circuit elements in downstream areas like the amygdala or auditory cortex^{55–57,61–67}.

CS and US coding neurons are spatially intermingled in auditory thalamus and a large fraction of MGB neurons exhibit mixed selectivity for both, the CS tone and US foot shock. The convergence of diverse CS and US responses in individual MGB neurons renders auditory thalamus an ideal site for neuronal plasticity in associative learning^{9,17}, which is supported by the finding of large numbers of different subgroups of plastic neurons upon fear conditioning. Nevertheless, similar to observations downstream in the basolateral amygdala^{21,22}, the convergence of CS and US responses in MGB neurons was not predictive of the response plasticity of a given neuron. Instead, MGB neurons exhibit manifold functional classes and outcomes of CS/US conversion upon learning (e.g., CS/US responsive cells can become potentiated fear cells or CS down cells), suggesting that heterogeneous fear conditioning-induced auditory response plasticity in MGB is most likely governed by multiple cellular or circuit mechanisms of neuronal plasticity. Indeed, we find subsets of neurons in all groups of CS plastic neurons that were not US responsive during FC (see Supplementary Fig. 7). Converging subthreshold CS and US inputs in dendrites, which cannot be detected by extracellular measurement of somatic neuronal activity during fear conditioning, yet might induce local dendritic plasticity mechanisms^{68–71}, could be a potential source of CS response adaptation. Alternatively, subsets of MGB neurons might not require converging CS and US input¹⁵ to drive functional plasticity upon associative learning, arguing for additional plasticity mechanisms that go beyond classical Hebbian plasticity and coincidence detection on a millisecond timescale⁷², and might additionally involve slower, neuromodulatory mechanisms^{73–75} similar to amygdala circuits^{21,76} or consolidation during sleep¹⁴.

Furthermore, brain-wide distributed interacting circuit mechanisms could play a role in the formation of single cell plasticity upon associative fear learning, not only in MGB but across multiple fear-related brain areas^{16,28,77–82}. The detailed computations within this distributed network¹⁹ and the role of auditory thalamus are poorly understood. Plasticity and adaptive changes in MGB depend on uni- or multi-synapse feedback circuits from distinct brain areas including the amygdala^{16,83} and cortex⁸⁴. Nevertheless, our data supports the notion that learning-induced modifications of neuronal activity in MGB could drive plastic neuronal responses in downstream areas¹⁷. This suggests that at least a part of the heterogeneous response plasticity in amygdala or cortex during associative fear learning could be inherited in a feedforward fashion from adaptive changes in the thalamic relay independent of and in addition to local synaptic and circuit mechanisms^{33,61,63}.

Both, first order auditory cortex-projecting MGBv as well as higher order areas of MGB (including calretinin-positive lateral thalamus → BLA neurons⁴⁴) are necessary for memory consolidation and we found similar proportions of CS and US plastic neurons in both subregions of MGB. Auditory cortex is involved in the formation of fear memories to complex sound stimuli⁴⁶ and plasticity in auditory cortex-projecting MGBv neurons might play an instructive role. Higher order areas of MGB are more broadly-projecting areas of auditory thalamus and target among others auditory cortex, striatum and amygdala^{34,35,37,44,85,86}. Given the amygdala's prominent role in associative fear learning and our finding that activity in the MGB → BLA pathways is crucial for fear memory consolidation (note that we did not find a recently observed effect of MGB → BLA calretinin-positive neurons on fear memory acquisition on the conditioning day⁴⁴, which might due to differences in the strength of the conditioning protocols), we hypothesized that CS and US plastic neurons are

specifically enriched in MGB → BLA projection neurons when compared to the total population including less plastic MGBv neurons^{11,12,31}. Using a retrograde viral approach, we specifically imaged BLA-projecting MGB neurons to distinguish these cells from the general population. Surprisingly, we found that the proportion of plastic neurons was not enhanced in amygdala-projecting neurons and was similar to the proportion of plastic neurons in the total MGB population. This lack of enrichment of neurons with dedicated functions in associative learning suggests that the MGB → BLA pathway is most likely not a labelled line, but that MGB potentially propagates experience-dependent changes of neuronal activity in associative fear learning to a wider brain network, including auditory cortex and striatum³⁴. This is reminiscent of recent findings showing that heterogeneous behaviour-related neural activity of projection neurons of a given brain area is broadcast simultaneously and in parallel to different downstream targets irrespective of the output pathway^{22,87}. Interestingly, this broadcasting might be achieved by the same subsets of individual MGB neurons given that higher order MGB → BLA neurons also project to auditory cortex (Supplementary Fig. 14)^{44,86}. Finally, perturbing activity in the MGB → BLA feedforward pathway during fear conditioning led to enhanced, aberrant across-day single cell plasticity patterns in the total MGB population after fear conditioning. MGB “over-plasticity” could be a compensatory mechanism due to the lack of amygdala activity and polysynaptic amygdala feedback to MGB, e.g., via the reticular nucleus of the thalamus⁸³, which might be crucial to fine-tune single cell plasticity in MGB, further supporting the notion that distributed activity across brain areas and networks is necessary to stabilize neuronal plasticity and facilitate precise memory formation as well as behavioural output^{16,18,19,88}. Future work including simultaneous multi-site recordings⁸⁹, targeted activity-dependent neural manipulations⁹⁰ and computational neuroscience tools will be required to delineate how this heterogeneous, widely distributed population code is established, subsequently interpreted by different downstream regions^{18,19} and related to complex behavioural output.

Locally, on the level of the auditory thalamus, CS responses could be decoded reliably from the population level responses of the total MGB ensemble. Within a given day of the fear conditioning paradigm, we could train decoders that reliably distinguish between CS+, CS− or baseline activity with high accuracy. Strikingly, we could also train decoders that accurately classified baseline vs. CS+ or CS− presentations across all experimental sessions and along associative fear learning. This suggests that MGB ensembles exhibit stable population level tone representation across days, despite the plasticity of CS responses of individual cells during fear conditioning, which can be stable over weeks⁴⁵. This data is supported by the observation that the MGB population vector difference between the CS+ and US decreases during fear conditioning, yet recovers to baseline levels on the next day after the conditioning session. Thus, MGB exhibits stable tone representations on the population level across associative learning, which will be crucial for reliable representations of sensory stimuli from the environment, for example, in light of changing stimulus statistics⁴⁹ in complex environments and plastic single cell responses (see above) or behaviour-driven changes in response amplitudes⁹¹. This is in stark contrast to fear-biased population level changes in sensory representation in the amygdala that are further stabilized and consolidated after learning, and prevent the decoding of tone responses across fear conditioning²¹. While the population code of the amygdala stabilizes “fear hi-jacking” of the sensory representation, MGB exhibits transient changes in population level encoding, which provides a clean slate for future perception that is unaffected by a valence bias. Nevertheless, the transient population level changes

during fear conditioning in MGB, which are dependent on MGB → BLA projection neuron activity, might be crucial to guide long term population level changes in the amygdala or other downstream areas upon associative learning^{21,34,92}.

Taken together, our data indicates that auditory thalamus is ideally positioned to exhibit a complex role in guiding neuronal plasticity and valence assignment during associative learning that goes beyond the classical role of auditory processing and response potentiation during conditioning and potentially extrapolates to a broad set of behavioural functions⁹³. Delineating the neural circuit mechanisms that underlie these highly dynamic representations of uni- and multisensory stimuli in MGB and their experience-dependent plasticity will open new avenues to understand the role of early, pre-cortical sensory relays like auditory thalamus in the formation of sensory percepts and memories that mediate complex behaviours.

Methods

Animals. In total, 8 to 11-week-old C57Bl/6J mice were used throughout the study. Behavioural experiments were performed with male mice. All experiments were done in accordance with institutional guidelines (University of Basel, Tierschutz) and were approved by the Cantonal Veterinary Office of Basel-Stadt, Switzerland. Animals were housed on a 12-h light / dark cycle at an ambient mean temperature and humidity of 22 °C and 55%, respectively. Food and water were provided ad libitum.

Surgeries, virus injection and GRIN lens as well as optical fibre implantation.

Virus was injected with the help of a stereotaxic apparatus (Kopf Instruments) in the medial geniculate body (for imaging experiments 500 nl, AAV2/5.CaMKII.GCaMP6f.WPRE.SV40, Penn Vector Core, for optogenetic experiments 500 nl AAV2/5.CAG.flex.ArchT.GFP, UNC Vector Core, AAV2/5.CaMKII.EGFP.WPRE.hGHP(A), VVF Zürich, AAV2/5.CaMKII.ArchT3.0.2.A.EGFP.WPRE, VVF Zürich or AAV2/5.hSyn.dlox.EGFP.dlox.WPRE, VVF Zürich, for all-optical experiments 500 nl, AAV2/5.CAG.flex.ArchT.tdTomato, UNC Vector Core or AAV2/5.CAG.dlox.tdTomato.dlox.WPRE, VVF Zürich, for tracing experiments 500 nl, AAV2/5.hSyn.flex.axonGCaMP6s⁹⁴, Addgene; coordinates: AP: −3.28, ML: −1.9, DV: −3.1 mm.) or basolateral amygdala (300 nl, AAV2/9.CaMKII.GCaMP6f.WPRE.SV40, Penn Vector Core; rAAV2-retro.EF1a.GCaMP6f.WPRE, Georg Keller, FMI Vector Core, Basel, Switzerland, for tracing experiments 300 nl, rAAV2-retro.hSyn1.mCherry.WPRE.hGHP(A), VVF Zürich; or 50 nl CTB 555, Invitrogen, for optogenetic experiments 300 nl rAAV2-retro.hSyn1.mCherry.icre.WPRE.hGHP(A), VVF Zürich, for all-optical experiments 300 nl AAV2-retro.CaMKII.iCre.WPRE.hGHP(A), VVF Zürich; coordinates AP: −1.7, ML: −3.6, DV: −3.6 mm) of 8–11 week old mice with a glass pipette and a pressure ejection system (Picospritzer) under isoflurane anaesthesia (1 – 2%) and buprenorphine (0.1 mg/kg) and ropivacaine (65 mg/kg) analgesia. The rAAV2-retro helper was a gift from Alla Karpova & David Schaffer (Addgene plasmid #81070). Virus for retrograde labelling of MGB neurons was supplemented with blue non-retrograde polymer microspheres (1:2400, Duke Scientific Corp.) to label BLA injection sites. For miniature microscope experiments, one week after virus injection, a gradient refractive index (GRIN) lens (0.5 or 0.6 mm diameter, Inscopix) was implanted during a second surgery (anaesthesia and analgesia see above). A 0.8 mm diameter craniotomy was drilled above the MGB and a small track was cut with a 0.7 mm sterile needle. The GRIN lens was then slowly advanced into the brain (coordinates: AP: −3.28, ML: −1.9, DV: −3.0 mm), fixed to the skull with light curable glue (Loctite 4305, Henkel) and the skull was sealed with Scotchbond (3 M), Vetbond (3 M) and dental acrylic (Paladur, Kulzer). A titanium head bar (custom made) was attached to fix the animal during the miniature microscope base plate mounting procedure. For optogenetic experiments, virus (see above) was injected bilaterally in the basolateral amygdala and medial geniculate body as described above. One week later, optical fibres (0.4 mm, 0.5 NA, Thorlabs) were implanted bilaterally above the medial geniculate body (Coordinates: AP: −3.28, ML: −1.9, DV: −2.9 mm). Optical fibres, the wound and skull were fixed and sealed in a similar manner to GRIN lens implantations. Animals were provided with analgesia (buprenorphine, ropivacaine) and their well-being was monitored throughout the entire experimental period.

Behavioural paradigms and analysis. Behavioural experiments were performed during the animal’s light period. A four-day auditory fear conditioning paradigm was performed in a habituation / test context (days 1, 3, 4) and a fear conditioning context (day 2). Mice were presented with 5 intermingled CS+ and CS− during habituation (6 kHz and 12 kHz, intermingled) in a round plexiglass context. CSs were composed of 27 tone pips (200 ms, 75 dB) presented at a rate of 1.1 Hz (Tucker-Davis Technologies, TDT 78 or RZ6). Fear conditioning was performed in a ca. 25 cm square plexiglass box and a shock grid floor (Coulbourn, Noldus). The CS+ (6 kHz and 12 kHz, counterbalanced) was terminated by a 2 s 0.65 mA foot shock 1.1 s after the last tone pip. During the extinction sessions (day 3 and day 4, habituation context), 4 CS− and 12 CS+ were presented. For optogenetic experiments, animals were habituated to the optical fibre attachment procedure for

3 days before the start of the fear conditioning paradigm. On the fear conditioning day, optical fibres were attached to the optical fibre implant via a ceramic mating sleeve (Thorlabs). MGB ArchT-expressing neurons were continuously inhibited during the five CS-US pairings (starting 2 s before CS onset until 2 s after US offset) with a 565 nm LEDs (M565D2, Thorlabs). Optical stimulation was controlled with a custom-built stimulation setup consisting of an Arduino board (Arduino Uno REV3, Arduino) and LED drivers (LEDD1B, Thorlabs). The light intensity measured at the optical fibre tip was 19 mW and optical fibre implants had a typical attenuation of 30%. Optogenetic experiments were performed and analyzed in a blinded fashion. Behavioural experiments were performed and analysed using Cineplex 3.4.1 (Plexon Inc) or Ethovision 14 (Noldus). Behavioural tracking based on the centre of mass of the mouse was performed using inbuilt functions of Cineplex and Ethovision. Freezing was initially detected automatically based on periods of absence of movement (threshold: 1 s) and then manually controlled and adjusted for non-freezing episodes (e.g., grooming) post hoc.

Plasticity of auditory tuning of MGB neurons was tested with a three-day paradigm. On day one, the animals were exposed to 165–195 presentations of 200 ms pure tone pips ranging from 1 to 40 kHz at 65, 75 and 85 dB. Pure tones were presented as a series of three pips at a frequency of 0.5 Hz in a round plexiglass context. The different combinations of tone frequency and sound pressure levels were presented as randomized trials (five repetitions per combination) with a minimum intertrial-interval of 11 s. On the consecutive day, the animals underwent a fear conditioning paradigm as described above (counterbalanced CS+ frequencies across animals: 8, 16 or 20 kHz). On the post-learning test day (day three), mice were exposed to the same presentation of pure tone pips as on day 1. MGB neural activity was imaged throughout the four-day fear conditioning and three-day auditory tuning paradigm using a miniature microscope.

Miniature microscope imaging. The miniature microscope (nVista2.0 or nVoke, Inscopix) was fixed to the base plate on the mouse's head before the experiment using head-fixation at the head bar on a flying saucer style running wheel. Mice were initially habituated to this procedure. MGB Ca^{2+} fluorescence was imaged continuously during the behavioural session with the following settings (nVista Software Version: 2.0.4 or nVoke Software Version: 2.1.10): Framerate: 20 Hz, blue LED-Power: 50–70%, Gain: 1.0–2.5, nVoke stimulation LED power: 10 mW/mm². Image size: 1024 × 1024 or 1080 × 1080 pxl. LED power and gain were adjusted according to GCaMP expression levels and the same settings were used across days for individual mice. For all-optical imaging and optogenetic stimulation experiments (nVoke, Inscopix), the stimulation LED was switched on 2 s before the start of the CS and terminated 2 s after the end of the US.

Image analysis. Raw image data was analysed as previously described^{21,22,95}. Briefly, movies from all behavioural sessions were spatially down sampled (2x), bandpass filtered (Fourier transform) and normalized by the filtered image (ImageJ). The movies from all days were then concatenated into a single file and motion corrected using Turboreg (min. three rounds)⁹⁶. Only movies that motion-corrected successfully across days with final spatial dislocations of < 2 µm were used for Ca^{2+} trace extraction. Principal and independent component analysis-based detection of individual regions of interest (ROIs) was performed on down sampled (5 Hz) $\Delta F/F$ movies. ROIs were truncated at 50% peak intensity and limited to a size of 30 pixels (ca. 60 µm). ROIs were initially oversampled (300 ICs) and then overlaid with the maximum intensity projection of the 4-day movie. ROIs that did not match individual neurons were discarded. We typically retained 97 ± 5 ICs per animal for CaMKII-GCaMP6f, $N = 19$ mice, 69 ± 9 ICs per animal for rAAV2-retro.EF1a.GCaMP6f, $N = 6$ mice, 90 ± 2 ICs per animal for tdTomato nVoke experiments, $N = 5$ mice and 94 ± 2 ICs per animal for ArchT nVoke experiments, $N = 6$ mice. These ICs were then applied to the 20 Hz motion corrected raw fluorescence movie to extract single cell Ca^{2+} traces for further processing. The detected ICs from the concatenation method overlap > 99% with a similar individual day detection and post-hoc alignment method and was thus deemed more suitable and efficient (Supplementary Fig. 15).

Ca^{2+} data analysis. All analysis was based on linearly detrended and z-scored Ca^{2+} traces of individual neurons. Ca^{2+} traces were baselined to the time periods preceding CS or US onset. To identify CS- and US-responsive neurons and their plasticity types across days, 30 s CS and 2.8 s US responses were analysed using a combined statistical and supervised cluster analysis approach as previously described²².

Auditory tuning curves were calculated based on the mean Ca^{2+} response during the 250 ms time window after pip onset. Cells were classified as tone-responsive to individual frequency pips if their mean response exceeded 0.5 zS for at least two of the frequencies tested. The best frequency (BF) of a neuron was defined as the frequency that prompted the maximal Ca^{2+} response averaged across trials. The difference in BF to the CS+ for comparison across fear conditioning is calculated on an animal-by-animal basis in absolute values as $\Delta\text{BF} = |\text{BF} - \text{CS+}|$.

CS+, CS- and baseline responses were decoded from MGB Ca^{2+} activity by fitting three-way (CS+ vs. CS- vs. baseline) or two-way (CS+ vs. baseline or CS- vs. baseline) quadratic discriminant analysis classifiers. We classified CS+ and CS- responses based on the first four presentations to balance for uneven numbers of CS+/- presentations across habituation, fear conditioning and extinction days.

Baseline responses were sampled from the 30 s periods preceding the CS+ and CS-. Classifiers were trained on the mean response of five consecutive pip responses within one CS (or the baseline period), such that each training set contained 20 input variables per condition (i.e., 40 for two-way decoders and 60 for three-way decoders). The mean response was calculated based on a 300 ms time window after pip onset and classifiers were trained using a tenfold cross-validation procedure. Decoder accuracy was calculated as the mean of the diagonal of the confusion matrix. Classifiers were trained for each individual animal and are presented as mean decoding accuracy across animals. To balance for unequal cell numbers between the different animals, we randomly selected 40 neurons from each animal and calculated the mean accuracy from 50 independent runs.

The population vector distance (PVD) between CS and US responses was calculated based on binned (0.275 s bins to accommodate the 1.1 Hz pip frequency) 30 s CS and 4 s US responses. PVD was calculated as the Euclidean distance between each CS bin and the mean binned US response and then averaged for each 30 s CS. Intraday PVD changes were normalized to the PVD of the first CS and across day PVD changes were calculated as the mean intraday PVD change for all CSs and normalized to the mean PVD of the habituation day.

Sound recordings and analysis. Acoustic signals of the fear conditioning context were recorded with a PCB Precision Condenser Microphone (Model 377C01) microphone and a RZ6 Auditory Processor (Tucker-Davis Technologies) 50 cm above the fear conditioning context at 195 kHz simultaneous to miniature microscope imaging during the fear conditioning session. Sound waves were high-pass filtered at 1 kHz and spectrograms were computed using short-time Fourier transforms (*spectrogram* function, Signal Processing Toolbox, MATLAB, Mathworks). To detect sound-level correlated neuronal activity, the cross-correlation coefficient between the squared acoustic signal binned in 50 ms and the corresponding Ca^{2+} signal of individual neurons was computed with a maximum lag of 500 ms. Cells were classified as sound-correlated if they exceeded a maximal cross-correlation coefficient of 0.2. Acoustic event onsets were detected based on the peak of the differentiated squared and binned sound wave. Acoustic events were not distinguished between animal movement-related sounds and vocalizations of the animal.

Histology. After completion of the behavioural experiment, mice were transcardially perfused with ca. 5 ml phosphate buffered saline (PBS, ThermoFisher) followed by 40 ml 4% paraformaldehyde (PFA) in PBS (pH = 7.4). Brains were removed and stored overnight in 4% PFA. Of 150 µm coronal slices were prepared using a vibratome (Campden Instruments) and immunostained for calretinin using the following solutions and protocol: carrier solution: 1% normal horse serum (NHS, Vector Laboratories) with 0.5% Triton (ThermoFisher) in phosphate buffered saline (PBS, ThermoFisher), blocking solution: 10% NHS with 0.5% Triton in PBS. After several rounds of PBS washes, slices were blocked for two hours at room temperature and incubated in primary antibody in carrier solution (goat anti-calretinin, 1:1000, Swant; rabbit anti-NeuN, 1:3000, Abcam; rabbit anti-GABA, 1:500, SigmaAldrich) overnight at 4 °C. Slices were washed again in PBS and incubated for 2 h at room temperature in secondary antibody in carrier solution (donkey anti-goat 647, 1:1000, ThermoFisher; donkey anti-rabbit 405, 1:1000, Abcam; donkey anti-rabbit 555, 1:1000, ThermoFisher). After four final washes, slices were mounted on slides and cover slipped using 22 × 50 mm, 0.16–0.19 mm thick cover glass (FisherScientific). Images were acquired with a LSM710 confocal microscope (Zeiss) and stitched with Zen 2.1 (black, Zeiss). Confocal images were post processed with ImageJ (Version: 2.0). Cells were manually counted using the cell counter plugin (<https://imagej.nih.gov/ij/plugins/cell-counter.html>) for ImageJ.

Statistical analysis. Statistical analysis was performed using Matlab (Mathworks) and Prism 8 (Graphpad). Unless otherwise indicated, normal distribution of the data was not assumed and non-parametric tests were performed. Values are presented as mean ± SEM unless stated otherwise. Box and whisker plots indicate median, interquartile range as well as the minimum to maximum value of the distribution. Statistical tests are mentioned in the text or figure legends. *, **, *** indicate *p* values smaller than 0.05, 0.01 and 0.001, respectively.

Reporting summary. Further information on research design is available in the Nature Research Reporting Summary linked to this article.

Data availability

The source data underlying the main figures and Supplementary information are available as Source Data file.

Code availability

Custom code used for analysis in this manuscript is available upon request.

Received: 8 April 2020; Accepted: 1 March 2021;

Published online: 26 April 2021

References

- Fanselow, M. S. & LeDoux, J. E. Why we think plasticity underlying Pavlovian fear conditioning occurs in the basolateral amygdala. *Neuron* **23**, 229–232 (1999).
- Maren, S. & Fanselow, M. S. The amygdala and fear conditioning: has the nut been cracked? *Neuron* **16**, 237–240 (1996).
- Rogan, M. T., Stäubli, U. V. & LeDoux, J. E. Fear conditioning induces associative long-term potentiation in the amygdala. *Nature* **390**, 604–607 (1997).
- Schafe, G. E. et al. Activation of ERK/MAP kinase in the amygdala is required for memory consolidation of pavlovian fear conditioning. *J. Neurosci.* **20**, 8177–8187 (2000).
- Humeau, Y., Shaban, H., Bissière, S. & Lüthi, A. Presynaptic induction of heterosynaptic associative plasticity in the mammalian brain. *Nature* **426**, 841–845 (2003).
- McKernan, M. G. & Shinnick-Gallagher, P. Fear conditioning induces a lasting potentiation of synaptic currents in vitro. *Nature* **390**, 607–611 (1997).
- Rogan, M. T. & LeDoux, J. E. LTP is accompanied by commensurate enhancement of auditory-evoked responses in a fear conditioning circuit. *Neuron* **15**, 127–136 (1995).
- Apergis-Schoute, A. M., Debiec, J., Doyère, V., LeDoux, J. E. & Schafe, G. E. Auditory fear conditioning and long-term potentiation in the lateral amygdala require ERK/MAP kinase signaling in the auditory thalamus: a role for presynaptic plasticity in the fear system. *J. Neurosci.* **25**, 5730–5739 (2005).
- Bordi, F. & LeDoux, J. E. Response properties of single units in areas of rat auditory thalamus that project to the amygdala. I. Acoustic discharge patterns and frequency receptive fields. *Exp. Brain Res.* **98**, 261–274 (1994).
- Bordi, F. & LeDoux, J. E. Response properties of single units in areas of rat auditory thalamus that project to the amygdala. II. Cells receiving convergent auditory and somatosensory inputs and cells antidromically activated by amygdala stimulation. *Exp. Brain Res.* **98**, 275–286 (1994).
- Edeline, J. M. & Weinberger, N. M. Subcortical adaptive filtering in the auditory system: associative receptive field plasticity in the dorsal medial geniculate body. *Behav. Neurosci.* **105**, 154–175 (1991).
- Edeline, J. M. & Weinberger, N. M. Thalamic short-term plasticity in the auditory system: associative returning of receptive fields in the ventral medial geniculate body. *Behav. Neurosci.* **105**, 618–639 (1991).
- Han, J.-H. et al. Increasing CREB in the auditory thalamus enhances memory and generalization of auditory conditioned fear. *Learn. Mem.* **15**, 443–453 (2008).
- Hennevin, E., Maho, C., Hars, B. & Dutrieux, G. Learning-induced plasticity in the medial geniculate nucleus is expressed during paradoxical sleep. *Behav. Neurosci.* **107**, 1018–1030 (1993).
- Ryugo, D. K. & Weinberger, N. M. Differential plasticity of morphologically distinct neuron populations in the medial geniculate body of the cat during classical conditioning. *Behav. Biol.* **22**, 275–301 (1978).
- Maren, S., Yap, S. A. & Goossens, K. A. The amygdala is essential for the development of neuronal plasticity in the medial geniculate nucleus during auditory fear conditioning in rats. *J. Neurosci.* **21**, RC135:1–6 (2001).
- Weinberger, N. M. The medial geniculate, not the amygdala, as the root of auditory fear conditioning. *Hear. Res.* **274**, 61–74 (2011).
- Headley, D. B., Kanta, V., Kyriazi, P. & Paré, D. Embracing complexity in defensive networks. *Neuron* **103**, 189–201 (2019).
- Mobbs, D., Headley, D. B., Ding, W. & Dayan, P. Space, time, and fear: survival computations along defensive circuits. *Trends Cogn. Sci.* **24**, 228–241 (2020).
- Ghosh, K. K. et al. Miniaturized integration of a fluorescence microscope. *Nat. Methods* **8**, 871–878 (2011).
- Grewe, B. F. et al. Neural ensemble dynamics underlying a long-term associative memory. *Nature* **543**, 670–675 (2017).
- Gründemann, J. et al. Amygdala ensembles encode behavioral states. *Science* **364**, 1–9 (2019).
- Chen, T.-W. et al. Ultrasensitive fluorescent proteins for imaging neuronal activity. *Nature* **499**, 295–300 (2013).
- Hackett, T. A., Clause, A. R., Takahata, T., Hackett, N. J. & Polley, D. B. Differential maturation of vesicular glutamate and GABA transporter expression in the mouse auditory forebrain during the first weeks of hearing. *Brain Struct. Funct.* **221**, 2619–2673 (2016).
- Rouiller, E. M., Colomb, E., Capt, M. & de Ribaupierre, F. Projections of the reticular complex of the thalamus onto physiologically characterized regions of the medial geniculate body. *Neurosci. Lett.* **53**, 227–232 (1985).
- Winer, J. A., Marie, Saint, Larue, R. L., Oliver, D. T. & GABAergic, D. L. feedforward projections from the inferior colliculus to the medial geniculate body. *Proc. Natl Acad. Sci.* **93**, 8005–8010 (1996).
- Jager, P. et al. Inhibitory interneurons distribute widely across the mouse thalamus and form ontogenetic spatial clusters. *bioRxiv* (2019) <https://doi.org/10.1101/651745>.
- Herry, C. et al. Switching on and off fear by distinct neuronal circuits. *Nature* **454**, 600–606 (2008).
- Grimsley, J. M. S., Hazlett, E. G. & Wenstrup, J. J. Coding the Meaning of Sounds: Contextual Modulation of Auditory Responses in the Basolateral Amygdala. *J. Neurosci.* **33**, 17538–17548 (2013).
- Williams, W. O., Riskin, D. K. & Mott, K. M. Ultrasonic sound as an indicator of acute pain in laboratory mice. *J. Am. Assoc. Lab. Anim. Sci.* **47**, 8–10 (2008).
- Edeline, J.-M. & Weinberger, N. M. Associative retuning in the thalamic source of input to the amygdala and auditory cortex: Receptive field plasticity in the medial division of the medial geniculate body. *Behav. Neurosci.* **106**, 81–105 (1992).
- Amano, T., Duvarci, S., Popa, D. & Pare, D. The fear circuit revisited: contributions of the basal amygdala nuclei to conditioned fear. *J. Neurosci.* **31**, 15481–15489 (2011).
- Krabbe, S. et al. Adaptive disinhibitory gating by VIP interneurons permits associative learning. *Nat. Neurosci.* **22**, 1834–1843 (2019).
- Chen, L., Wang, X., Ge, S. & Xiong, Q. Medial geniculate body and primary auditory cortex differentially contribute to striatal sound representations. *Nat. Commun.* **10**, 418 (2019).
- Kimura, A., Donishi, T., Sakoda, T., Hazama, M. & Tamai, Y. Auditory thalamic nuclei projections to the temporal cortex in the rat. *Neuroscience* **117**, 1003–1016 (2003).
- Kwon, J.-T. et al. Optogenetic activation of presynaptic inputs in lateral amygdala forms associative fear memory. *Learn. Mem.* **21**, 627–633 (2014).
- Smith, P. H., Uhlrich, D. J. & Manning, K. A. Evaluation of medial division of the medial geniculate (MGM) and posterior intralaminar nucleus (PIN) inputs to the rat auditory cortex, amygdala, and striatum. *J. Comp. Neurol.* **527**, 1478–1494 (2019).
- LeDoux, J. E. Emotion circuits in the brain. *Annu. Rev. Neurosci.* **23**, 155–184 (2000).
- Doron, N. N. & LeDoux, J. E. Organization of projections to the lateral amygdala from auditory and visual areas of the thalamus in the rat. *J. Comp. Neurol.* **412**, 282–409 (1999).
- Lu, E., Llano, D. A. & Sherman, S. M. Different distributions of calbindin and calretinin immunostaining across the medial and dorsal divisions of the mouse medial geniculate body. *Hear. Res.* **257**, 16–23 (2009).
- Antunes, R. & Moita, M. A. Discriminative Auditory Fear Learning Requires Both Tuned and Nontuned Auditory Pathways to the Amygdala. *J. Neurosci.* **30**, 9782–9787 (2010).
- Han, X. et al. A High-light sensitivity optical neural silencer: development and application to optogenetic control of non-human primate cortex. *Front. Syst. Neurosci.* **5**, 1–8 (2011).
- Pereira, A. G., Farias, M. & Moita, M. A. A new thalamo-cortical-amygdala circuit is involved in processing a natural auditory alarm cue. *bioRxiv* (2019) <https://doi.org/10.1101/716910>.
- Barsy, B. et al. Associative and plastic thalamic signaling to the lateral amygdala controls fear behavior. *Nat. Neurosci.* **23**, 625–637 (2020).
- Edeline, J.-M., Neuenschwander-El Massioui, N. & Dutrieux, G. Discriminative long-term retention of rapidly induced multiunit changes in the hippocampus, medial geniculate and auditory cortex. *Behav. Brain Res.* **39**, 145–155 (1990).
- Dalmay, T. et al. A critical role for neocortical processing of threat memory. *Neuron* **104**, 1180–1194.e7 (2019).
- Ghosh, S. & Chattarji, S. Neuronal encoding of the switch from specific to generalized fear. *Nat. Neurosci.* **18**, 112–120 (2015).
- Duarte, R. & Morrison, A. Leveraging heterogeneity for neural computation with fading memory in layer 2/3 cortical microcircuits. *PLOS Comput. Biol.* **15**, e1006781 (2019).
- Blackwell, J. M. et al. Stable encoding of sounds over a broad range of statistical parameters in the auditory cortex. *Eur. J. Neurosci.* **43**, 751–764 (2016).
- Tripathy, S. J., Padmanabhan, K., Gerkin, R. C. & Urban, N. N. Intermediate intrinsic diversity enhances neural population coding. *Proc. Natl Acad. Sci.* **110**, 8248–8253 (2013).
- Sweis, B. M., Mau, W., Rabinowitz, S. & Cai, D. J. Dynamic and heterogeneous neural ensembles contribute to a memory engram. *Curr. Opin. Neurobiol.* **67**, 199–206 (2021).
- Polepalli, J. S., Gooch, H. & Sah, P. Diversity of interneurons in the lateral and basal amygdala. *Npj Sci. Learn.* **5**, 1–9 (2020).
- Wolff, S. B. E. et al. Amygdala interneuron subtypes control fear learning through disinhibition. *Nature* **509**, 453–458 (2014).
- Asede, D. et al. Sensory inputs to intercalated cells provide fear-learning modulated inhibition to the basolateral amygdala. *Neuron* **86**, 541–554 (2015).
- Lucas, E. K., Jegarl, A. M., Morishita, H. & Clem, R. L. Multimodal and site-specific plasticity of amygdala parvalbumin interneurons after fear learning. *Neuron* **91**, 629–643 (2016).
- Kim, J., Pignatelli, M., Xu, S., Itoharu, S. & Tonegawa, S. Antagonistic negative and positive neurons of the basolateral amygdala. *Nat. Neurosci.* **19**, 1636–1646 (2016).
- Namburi, P. et al. A circuit mechanism for differentiating positive and negative associations. *Nature* **520**, 675–678 (2015).
- Gründemann, J. Distributed coding in auditory thalamus and basolateral amygdala upon associative fear learning. *Curr. Opin. Neurobiol.* **67**, 183–189 (2021).

59. Schneider, D. M., Sundararajan, J. & Mooney, R. A cortical filter that learns to suppress the acoustic consequences of movement. *Nature* **561**, 391–395 (2018).
60. Šuta, D., Popelá, J. & Syka, J. Coding of communication calls in the subcortical and cortical structures of the auditory system. *Physiol. Res.* **57** (Suppl 3), S149–S159 (2008).
61. Abs, E. et al. Learning-related plasticity in dendrite-targeting layer 1 interneurons. *Neuron* **100**, 684–699.e6 (2018).
62. Aizenberg, M., Mwilambwe-Tshilobo, L., Briguglio, J. J., Natan, R. G. & Geffen, M. N. Bidirectional regulation of innate and learned behaviors that rely on frequency discrimination by cortical inhibitory neurons. *PLOS Biol.* **13**, e1002308 (2015).
63. Gillet, S. N., Kato, H. K., Justen, M. A., Lai, M. & Isaacson, J. S. Fear learning regulates cortical sensory representations by suppressing habituation. *Front. Neural Circuits* **11**, 112 (2018).
64. Krabbe, S., Gründemann, J. & Lüthi, A. Amygdala inhibitory circuits regulate associative fear conditioning. *Biol. Psychiatry* **83**, 800–809 (2018).
65. Lee, S.-C., Amir, A., Haufler, D. & Pare, D. Differential recruitment of competing valence-related amygdala networks during anxiety. *Neuron* **96**, 81–88.e5 (2017).
66. Letzkus, J. J. et al. A disinhibitory microcircuit for associative fear learning in the auditory cortex. *Nature* **480**, 331–335 (2011).
67. Senn, V. et al. Long-range connectivity defines behavioral specificity of amygdala neurons. *Neuron* **81**, 428–437 (2014).
68. Weber, J. P. et al. Location-dependent synaptic plasticity rules by dendritic spine cooperativity. *Nat. Commun.* **7**, 1–14 (2016).
69. Harvey, C. D. & Svoboda, K. Locally dynamic synaptic learning rules in pyramidal neuron dendrites. *Nature* **450**, 1195–1200 (2007).
70. Humeau, Y. & Lüthi, A. Dendritic calcium spikes induce bi-directional synaptic plasticity in the lateral amygdala. *Neuropharmacology* **52**, 234–243 (2007).
71. Branco, T. & Häusser, M. The single dendritic branch as a fundamental functional unit in the nervous system. *Curr. Opin. Neurobiol.* **20**, 494–502 (2010).
72. Markram, H., Lübke, J., Frotscher, M. & Sakman, B. Regulation of synaptic efficacy by coincidence of postsynaptic APs and EPSPs. *Science* **275**, 213–215 (1997).
73. Brzosko, Z., Mierau, S. B. & Paulsen, O. Neuromodulation of spike-timing-dependent plasticity: past, present, and future. *Neuron* **103**, 563–581 (2019).
74. Izhikevich, E. M. Solving the distal reward problem through linkage of STDP and dopamine signaling. *Cereb. Cortex* **17**, 2443–2452 (2007).
75. Likhtik, E. & Johansen, J. P. Neuromodulation in circuits of aversive emotional learning. *Nat. Neurosci.* **22**, 1586–1597 (2019).
76. Johansen, J. P. et al. Hebbian and neuromodulatory mechanisms interact to trigger associative memory formation. *Proc. Natl Acad. Sci.* **111**, E5584–E5592 (2014).
77. Gehrlach, D. A. et al. Aversive state processing in the posterior insular cortex. *Nat. Neurosci.* **22**, 1424–1437 (2019).
78. Herry, C. & Johansen, J. P. Encoding of fear learning and memory in distributed neuronal circuits. *Nat. Neurosci.* **17**, 1644–1654 (2014).
79. Klavir, O., Genud-Gabai, R. & Paz, R. Functional connectivity between amygdala and cingulate cortex for adaptive aversive learning. *Neuron* **80**, 1290–1300 (2013).
80. Likhtik, E., Stujenske, J. M., Topiwala, M. A., Harris, A. Z. & Gordon, J. A. Prefrontal entrainment of amygdala activity signals safety in learned fear and innate anxiety. *Nat. Neurosci.* **17**, 106–113 (2014).
81. Ozawa, T. et al. A feedback neural circuit for calibrating aversive memory strength. *Nat. Neurosci.* **20**, 90–97 (2017).
82. Penzo, M. A. et al. The paraventricular thalamus controls a central amygdala fear circuit. *Nature* **519**, 455–459 (2015).
83. Aizenberg, M. et al. Projection from the amygdala to the thalamic reticular nucleus amplifies cortical sound responses. *Cell Rep.* **28**, 605–615.e4 (2019).
84. He, J. Corticofugal modulation of the auditory thalamus. *Exp. Brain Res.* **153**, 579–590 (2003).
85. Jones, E. G. Viewpoint: the core and matrix of thalamic organization. *Neuroscience* **85**, 331–345 (1998).
86. Pardi, M. B. et al. A thalamocortical top-down circuit for associative memory. *Science* **370**, 844–848 (2020).
87. Weglage, M., Waernberg, E., Lazaridis, I., Tzortzi, O. & Meletis, K. Complete representation of action space and value in all striatal pathways. *bioRxiv* (2020) <https://doi.org/10.1101/2020.03.29.983825>.
88. Yuste, R. From the neuron doctrine to neural networks. *Nat. Rev. Neurosci.* **16**, 487–497 (2015).
89. Jun, J. J. et al. Fully integrated silicon probes for high-density recording of neural activity. *Nature* **551**, 232–236 (2017).
90. Emiliani, V., Cohen, A. E., Deisseroth, K. & Häusser, M. All-optical interrogation of neural circuits. *J. Neurosci.* **35**, 13917–13926 (2015).
91. Williamson, R. S., Hancock, K. E., Shinn-Cunningham, B. G. & Polley, D. B. Locomotion and task demands differentially modulate thalamic audiovisual processing during active search. *Curr. Biol.* **25**, 1885–1891 (2015).
92. Zhang, X. & Li, B. Population coding of valence in the basolateral amygdala. *Nat. Commun.* **9**, 5195 (2018).
93. Gilad, A., Maor, I. & Mizrahi, A. Learning-related population dynamics in the auditory thalamus. *bioRxiv* (2020) <https://doi.org/10.1101/2020.03.31.017632>.
94. Broussard, G. J. et al. In vivo measurement of afferent activity with axon-specific calcium imaging. *Nat. Neurosci.* **21**, 1272–1280 (2018).
95. Mukamel, E. A., Nimmerjahn, A. & Schnitzer, M. J. Automated analysis of cellular signals from large-scale calcium imaging data. *Neuron* **63**, 747–760 (2009).
96. Thévenaz, P., Ruttimann, U. E. & Unser, M. A pyramid approach to subpixel registration based on intensity. *IEEE Trans. Image Process. Publ. IEEE Signal Process. Soc.* **7**, 27–41 (1998).

Acknowledgements

We thank Georg Keller, Tingjia Lu and Daniela Gerosa Erni for virus production and V. Jayaraman, R. Kerr, D. Kim, L. Looger, K. Svoboda and the HHMI Janelia GENIE Project for making GCaMP6 available, Ed Boyden and MIT for making ArchT available as well as Alla Karpova and David Schaffer who gifted the rAAV2-retro helper (Addgene plasmid # 81070 V). pAAV-hSynapsin1-FLEX-axon-GCaMP6s was a gift from Lin Tian (Addgene viral prep # 112010-AAV5). We thank Raymond Strittmatter and Robert Häring for mechanical workshop and electrical engineering support. We thank Yael Bitterman, Sabine Krabbe, Andreas Lüthi and the Gründemann lab for comments on the manuscript. Funding: Research was supported by the Swiss National Science Foundation (Ambizione Fellowship to J.G., SNF Professorship to J.G.), the European Research Council (Starting Grant, J.G.), the Forschungsfonds Nachwuchsforschende of the University of Basel (M.H.), the Forschungspreis der Schweizerischen Hirnliga (J.G.) and the Department of Biomedicine at the University of Basel. Artworks in parts of some figures were created with BioRender.com. Mouse brain anatomy figures and panels were modified and reprinted from The Mouse Brain in Stereotaxic Coordinates, Paxinos, Franklin, panels 45 and 47, 2001. Mouse cartoons with miniature microscopes from Gründemann et al.²². Reprinted with permission from AAAS.

Author contributions

Conceptualization, J.A.T., M.H. and J.G.; Methodology and imaging experiments, J.A.T., M.H. and J.G.; Experimental support, J.A.F., D.A.G., M.T., C.M.B., S.M.I. and T.L.; Analysis, J.A.T., M.H., C.M.B. and J.G.; Original draft, J.A.T. and J.G.; Revisions, all authors; Supervision and funding, J.G.

Competing interests

The authors declare no competing interests.

Additional information

Supplementary information The online version contains supplementary material available at <https://doi.org/10.1038/s41467-021-22421-8>.

Correspondence and requests for materials should be addressed to J.G.

Peer review information *Nature Communications* thanks the anonymous reviewers for their contribution to the peer review of this work.

Reprints and permission information is available at <http://www.nature.com/reprints>

Publisher's note Springer Nature remains neutral with regard to jurisdictional claims in published maps and institutional affiliations.



Open Access This article is licensed under a Creative Commons Attribution 4.0 International License, which permits use, sharing, adaptation, distribution and reproduction in any medium or format, as long as you give appropriate credit to the original author(s) and the source, provide a link to the Creative Commons license, and indicate if changes were made. The images or other third party material in this article are included in the article's Creative Commons license, unless indicated otherwise in a credit line to the material. If material is not included in the article's Creative Commons license and your intended use is not permitted by statutory regulation or exceeds the permitted use, you will need to obtain permission directly from the copyright holder. To view a copy of this license, visit <http://creativecommons.org/licenses/by/4.0/>.

© The Author(s) 2021